RCA REVIEW
a technical journal

RADIO AND ELECTRONICS
RESEARCH · ENGINEERING

CONTENTS

RCA REVIEW

BOARD OF EDITORS

REPUBLICATION AND TRANSLATION

EXPERIMENTALLY DETERMINED RADIATION CHARACTERISTICS OF CONICAL AND TRIANGULAR ANTENNAS*

BY

GEORGE H. BROWN AND O. M. WOODWARD, JR.

Research Department, RCA Laboratories Division,
Princeton, N. J.

Summary—Measurements of resistance and reactance of conical and triangular sheet antennas operated against ground have been made, with wide variations of both length and flare angle. This data is displayed by means of a series of graphs. Radiation patterns have also been measured for the same types of radiators, and for the same parameters. A comparison of the measured values for conical antennas is made with a small number of published theoretical values.

INTRODUCTION

THE usefulness of large-area radiators for broad-band applications has been amply demonstrated.[1] Antenna designers have utilized various geometrical shapes; cylindrical, conical, triangular, and spheroidal.

Many articles have been published on the theoretical analysis of certain radiator shapes. In particular, the conical radiator has received considerable attention.[2-8] The theoretical treatment involves simplifying assumptions and approximations in order to satisfy the required boundary conditions and to reduce the mathematical difficulties. Calculations following the analysis are indeed laborious. An alternative and

---

* Decimal Classification: R221.

[1] N. E. Lindenblad, "Television Transmitting Antenna for Empire State Building," *RCA Review*, Vol. III, p. 387, April, 1939.

[2] P. D. P. Smith, "The Conical Dipole of Wide Angle," *Jour. Appl. Phys.*, Vol. 19, p. 11, January, 1948.

[3] C. T. Tai, "On the Theory of Biconical Antennas," *Jour. Appl. Phys.*, Vol. 19, p. 1155, December, 1948.

[4] P. D. P. Smith, "Comments on Biconical Antennas," *Jour. Appl. Phys.*, Vol. 20, p. 633, June, 1949.

[5] C. T. Tai, "A Study of the e.m.f. Method," *Jour. Appl. Phys.*, Vol. 20, p. 717, July, 1949.

[6] C. H. Papas and R. King, "Input Impedance of Wide-Angle Conical Antennas Fed by a Coaxial Line," *Proc. I.R.E.*, Vol. 37, p. 1269, November, 1949.

[7] C. H. Papas and R. King, "Radiation from Wide-Angle Conical Antennas Fed by a Coaxial Line," *Proc. I.R.E.*, Vol. 39, p. 49, January, 1951.

[8] S. A. Schelkunoff, "General Theory of Symmetric Biconical Antennas," *Jour. Appl. Phys.*, Vol. 22, pp. 1330-1332, November, 1951.

easier approach to obtain a large amount of engineering data is that of direct experimental measurement.

Although some experimental results have been published by Essen and Oliver,[9] the extent of their coverage is limited.

The data described in this article was obtained during 1945 from experimental impedance and radiation measurements on two types of broad-band radiators, conical and triangular. These particular shapes were chosen for their simplicity of construction as well as for the ease in applying the data to practical feed systems. This work was carried on as a logical step following previously made impedance measurements on cylindrical antennas.[10]

METHOD OF MEASUREMENT

The impedance data was obtained with the use of a conventional slotted transmission line and sliding probe. The probe led to an accurately calibrated superheterodyne receiver which indicated the voltage standing-wave ratio on the line as well as the position of the voltage minimum. From this information the antenna impedance was calculated by the use of transmission-line charts.

Most of the data was secured using a frequency of 500 megacycles. This choice of frequency, having a wave length of approximately two feet, permits the easy manipulation of most of the antenna models, and yet is not so high as to affect the accuracy of the measurements. A few of the very largest cones and triangles, however, were measured at a frequency of 1670 megacycles to facilitate handling the antennas.

In order to provide a minimum-length transmission line to the slotted measuring line and also furnish shielding of the measuring apparatus and operator, only one half of the test dipole was fed against a large image or ground plane (Figure 1). Hence all measured impedance values plotted are one half the values that would be obtained from a balanced dipole.

The ground plane consisted of a conductive disk eight feet in diameter. This size is sufficiently large (approximately four wave lengths) so that the impedance errors due to the use of a finite plane instead of an infinite plane are of second-order effect.

The setup was supported in the clear on high trestles to reduce the effect of the earth, buildings, etc., to a minimum.

---

[9] L. Essen and M. H. Oliver, "Aerial Impedance Measurements," *Wireless Engineer*, Vol. XXII, p. 587, December, 1945.

[10] G. H. Brown and O. M. Woodward, Jr., "Experimentally Determined Impedance Characteristics of Cylindrical Antennas," *Proc. I.R.E.*, Vol. 33, p. 257, April, 1945.
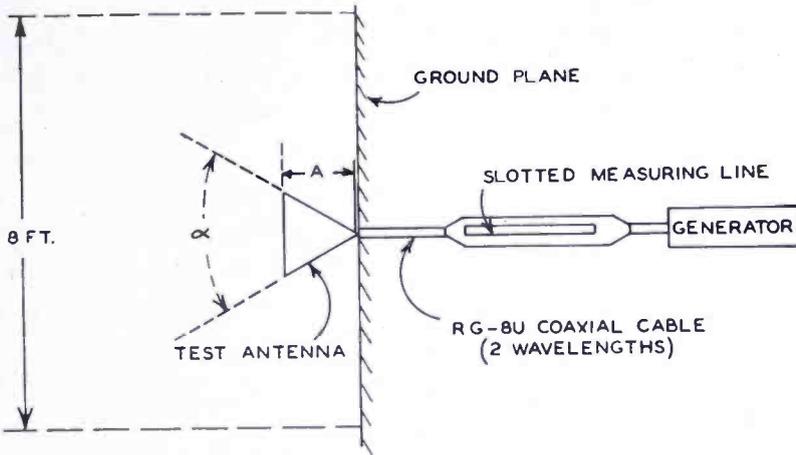
Fig. 1—Arrangement of apparatus in making the impedance measurements.

Figure 2 shows an enlarged view of the unipole feed details. In order to provide a good mechanical means of attachment to the inner conductor of the feed line, the test unipole point was cut off to furnish a truncated mounting base 2.5 electrical degrees in width. The polyethylene insulation of the RG-8U coaxial cable was extended 2.5 electrical degrees beyond the ground screen as shown. All dimensions in electrical degrees are obtained from the product of the physical dimension and the ratio, 360/(wave length). The wave length and the physical dimensions are measured in the same units.
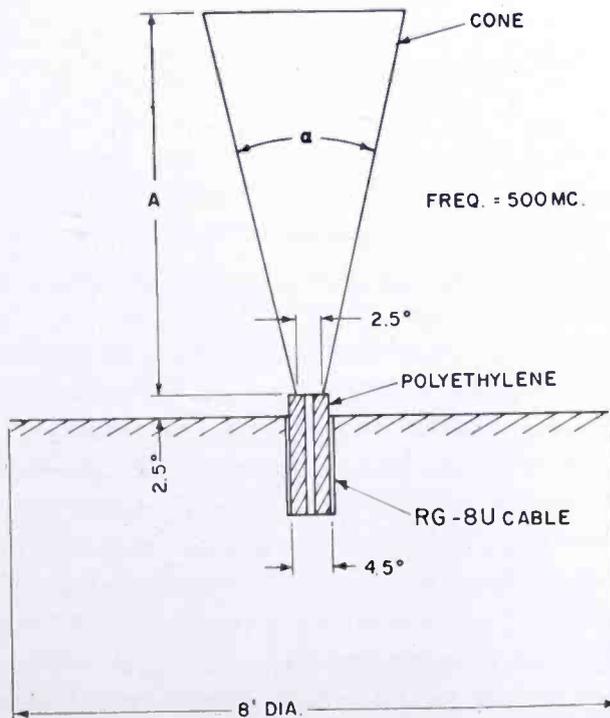
Fig. 2—Enlarged view of the unipole feed.

All impedances are referred to the junction of the coaxial line and the ground plane. Corrections were made on high standing-wave ratios to compensate for the slight loss in the RG-8U feed cable joining the test antenna and the slotted measuring line.

The flare angle of the cones and triangles is designated by the angle α, in degrees. The length of the antenna in electrical degrees, A, is measured from the top to the truncated base.

For the larger test antennas the free end was supported from above by a small polyethylene insulator and long waxed string.

Both the conical and triangular antennas were constructed of copper-plated sheet steel having a thickness of 0.020 inch. The large ends of the cones were not closed. For a given test antenna, measurements were made as the length was cut down.
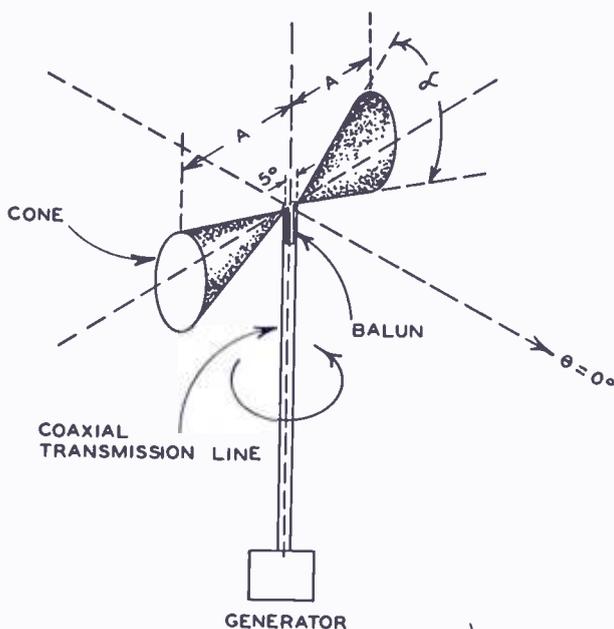
Fig. 3—Arrangement of apparatus in making field pattern measurements.

Field patterns were taken on balanced conical dipoles as shown in Figure 3. The conical dipole was supported with its longitudinal axis horizontal above a motor-driven turntable. A coaxial line from the generator led through the vertical support pipe to a balun, which insures a balanced feed to the test antenna. Long polystyrene rods supported the free ends of the larger dipoles.

The output of a directive receiving antenna located approximately 150 feet away led to a superheterodyne receiver. The receiver output operated an Esterline-Angus recorder.

As the conical dipoles have circular symmetry in the vertical plane, only one field pattern was taken on each test antenna.

Since the flat triangular dipoles do not have such symmetry in the vertical plane, three measurements were necessary to obtain sufficient information on the space radiation.

Referring to Figure 4, field patterns were measured on the triangular dipoles in the XY plane as with the conical dipoles. In addition, field patterns were taken in the XZ plane. The latter was accomplished simply by rotating the triangular dipole 90 degrees on its longitudinal axis and repeating the pattern measurement.

As the only points common to these two patterns lie on the X axis where the radiation is zero, one other measurement is required to
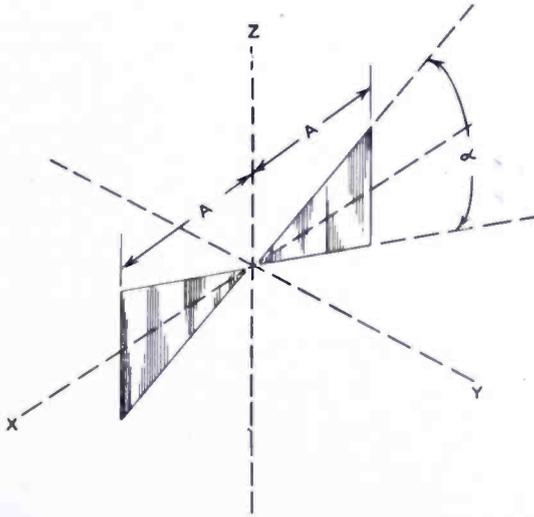
Fig. 4—Geometry of the triangular dipole.

ascertain the relative amplitudes of the two patterns. In order to eliminate any possible ground reflection error, this information was obtained using the impedance measuring setup of Figure 1. The ground plane was mounted horizontally with one half of the test triangle extending vertically above. A vertical receiving antenna with high directivity was placed a great distance away with its center lying in the plane of the ground plane. Currents flowing in the horizontal ground plane produce only horizontally polarized fields at the receiving antenna, hence reception is obtained only from the vertical test antenna.

Relative field strength measurements were taken for two positions of the triangular unipole; one with the vertical receiving antenna lying in the plane of the triangle, and the other with the triangle rotated 90 degrees on its vertical axis.

These measurements, giving the relative field strengths along the Y and Z axes, respectively, supplied the necessary information to correlate the two field patterns taken in the XY and XZ planes.

CONICAL-ANTENNA IMPEDANCE MEASUREMENTS

The measured impedance data taken on the conical unipoles is plotted versus the radiator length in Figures 5 and 6 in terms of the resistance and reactance values. Curves are given for various flare angles up to a value of $\alpha = 90°$. The limiting case of $\alpha = 0°$ represents a cylindrical radiator having a diameter of 2.5 electrical degrees since the feed point was kept fixed at that diameter.
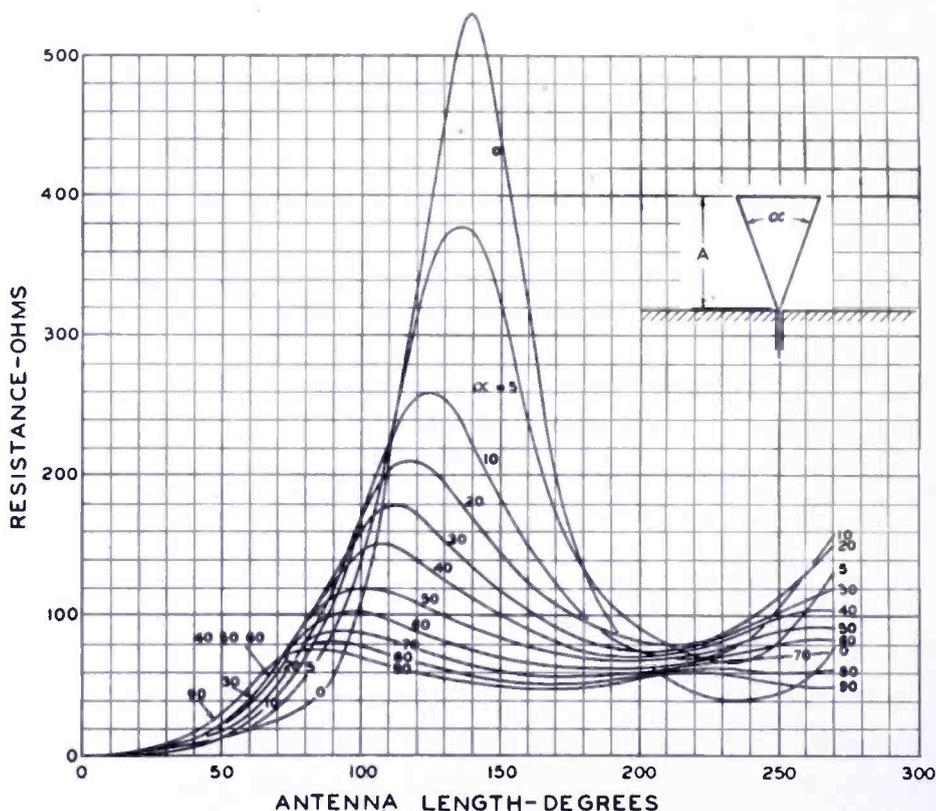
Fig. 5—Measured resistance curves of the conical unipole versus length in electrical degrees for various flare angles.

As the flare angle increases, the amplitude of the resistance and reactance variations decreases. It is seen, for example, that a 90° conical unipole has a resistance of approximately 50 ohms and very low reactance over a very wide frequency range.

The resistance peaks in Figure 5 are replotted in Figure 7 to show the maximum resistance variation versus the flare angle. The radiator length for maximum resistance is also given in Figure 7. These points correspond quite closely to the second resonance values.

Figure 8 shows the antenna lengths for the first resonance plotted against the flare angle.

Some question has arisen in the past as to the effect of closing the

open end of the cone with a plane conducting cover. Time did not permit repeating all measurements with closed ends. However, the impedance of a cone having a flare angle of 60° was determined with its end closed for various lengths. No measurable differences in impedance were detected.

An interesting comparison is given in Figures 9 and 10 between the measured data obtained by the authors and calculated values presented by Papas and King[6] for a 60° flare-angle cone. The cone
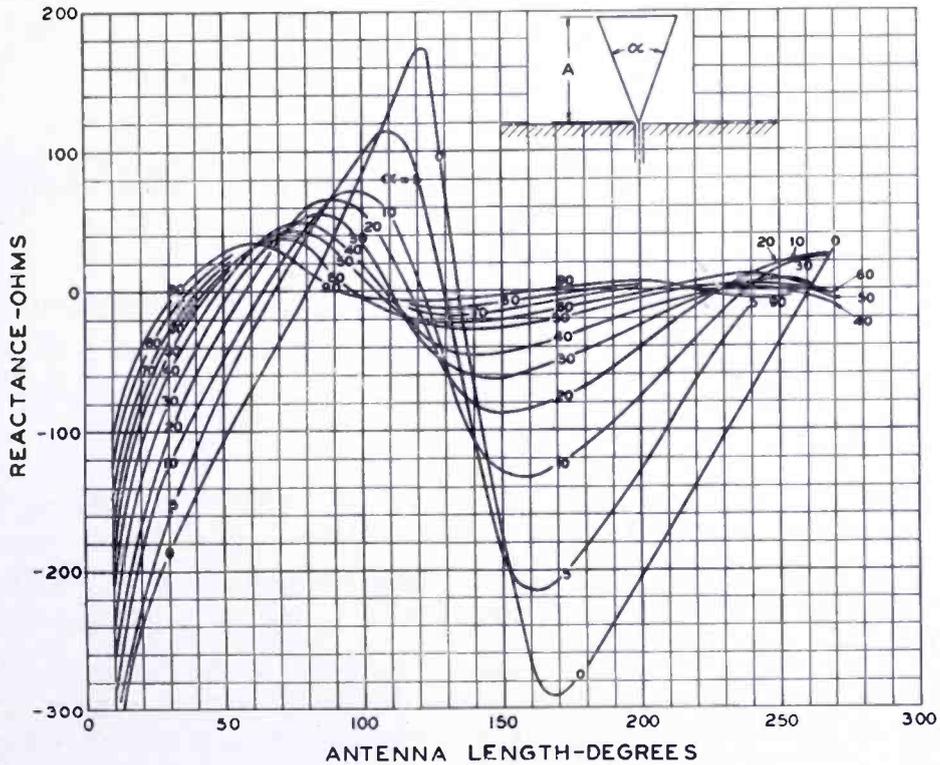
Fig. 6—Measured reactance curves of the conical unipole versus length in electrical degrees for various flare angles.

assumed by Papas and King was capped with a spherical section, while ours was open-ended. Figure 9 shows the comparative results where A is the over-all length of the cone and cap in the theoretical case, while A is the length of the uncapped cone in the measured case. A substantial agreement between the theoretical and experimental values may be noted.

An even better correlation is seen in Figure 10, in which the data of Figure 9 is displayed so that A is the length of the cone proper in both the case of the theoretical values and the measured data.

CONICAL-ANTENNA FIELD-PATTERN MEASUREMENTS

For each value of flare angle, field patterns were measured for
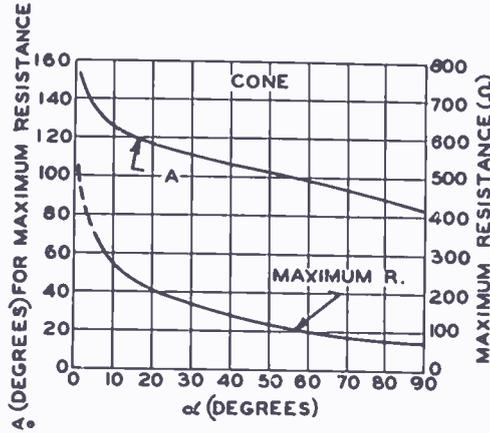
Fig. 7—Maximum conical unipole resistance versus the flare angle in de-
grees, and the unipole length in electrical degrees at which the maximum
resistance occurs versus the flare angle.

half-lengths (A) from 60 to 180 electrical degrees in 30-degree steps,
and from 180 to 270 electrical degrees in 15-degree steps. Closer
intervals of measurement were taken for the longer antennas as the
field configurations change more rapidly in that region.

Since the patterns are symmetrical about the major axes, only one
quadrant is given (Figures 11 to 22). The patterns are plotted in
rectangular coordinates, showing the relative field strength versus
azimuth angle. Also included for comparison are the field patterns
(Figure 11) for a thin wire calculated on the basis of sine-wave
distribution.

It is seen that the sharp nulls of the longer conical dipoles are
gradually filled in as the flare angle is increased to approximately 50°.
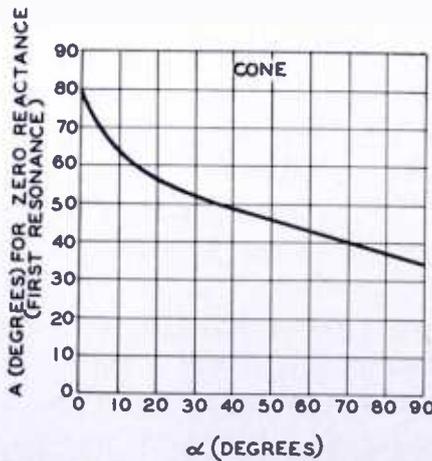
Fig. 8—Conical unipole length in electrical degrees for zero
reactance versus the flare angle.

For larger flare angles, the secondary lobes commence to become prominent again.

For lengths less than 180 electrical degrees, no side lobes appear for any of the measured flare angles.

Field patterns were also repeated on a 60° flare-angle conical dipole
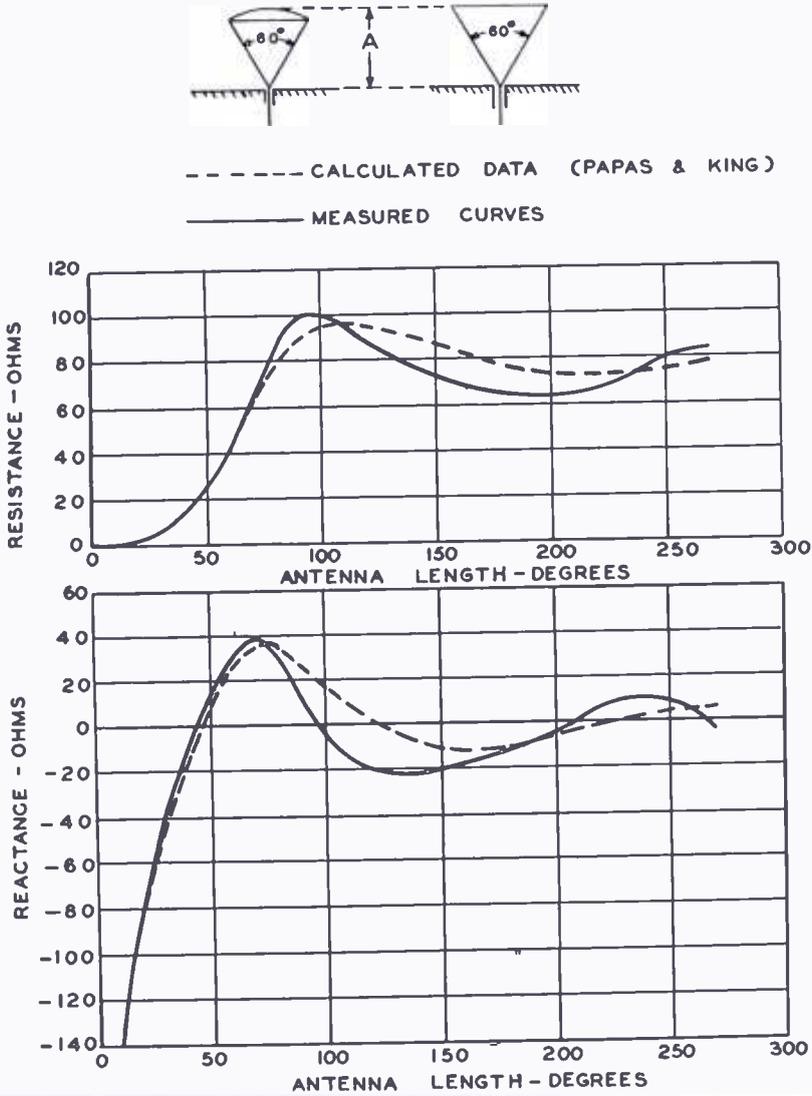
Fig. 9—Comparison of calculated and measured impedance curves for a 60-degree-flare-angle conical unipole.

with closed ends. The patterns were practically identical with those obtained with the ends open.

Calculations by Papas and King[7] on the radiation characteristics of a 60° flare-angle cone for three different antenna lengths are compared with the measured data in Figure 23. A close agreement is observed when the comparison is made on the basis of the over-all

height of the capped cone in the theoretical case with the height of the uncapped cone in the measured instance.

We are then led to the postulate that, in determining the radiation patterns, the addition of the spherical cap effectively lengthens the cone by an amount which is the radius of the spherical cap minus the height of the cone. It does not, however, affect the impedance.
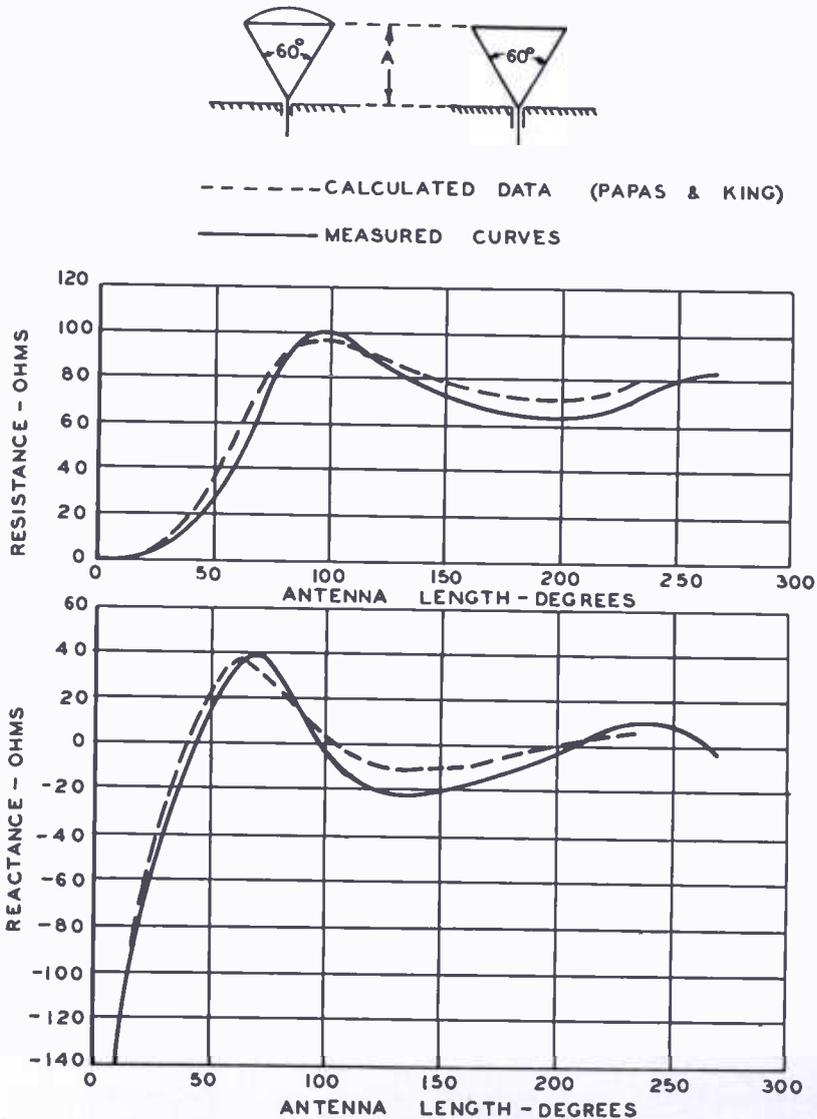
Fig. 10—Comparison of calculated and measured impedance curves for a 60-degree-flare-angle conical unipole.

CONICAL-ANTENNA POWER-GAIN CALCULATIONS

The uniform radiation in the plane normal to the axis of the conical dipoles facilitates the power gain calculations. The radiated energy is an integrated function of the square of the distant field strength
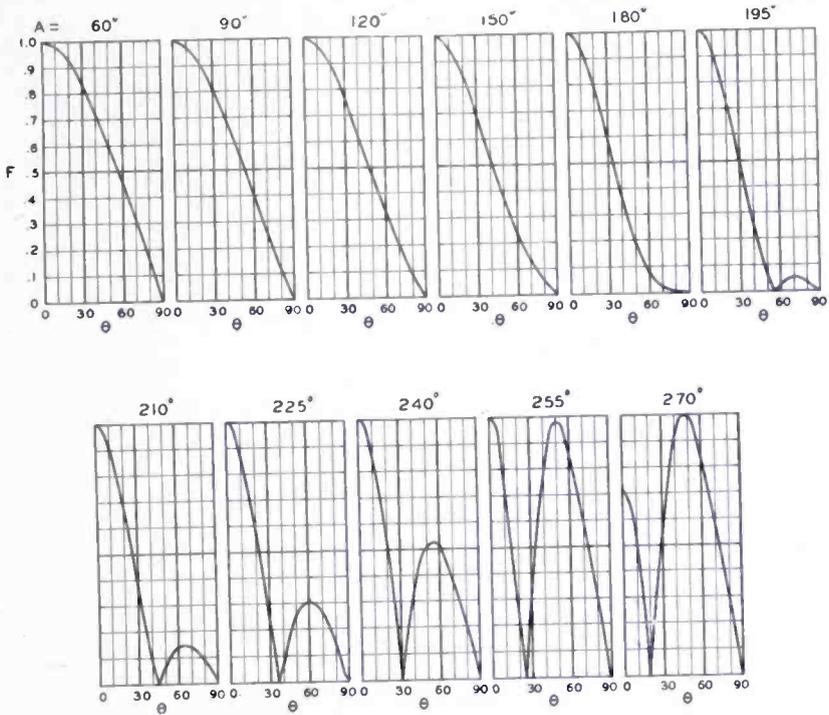
Fig. 11—Calculated field patterns of a thin-wire dipole.
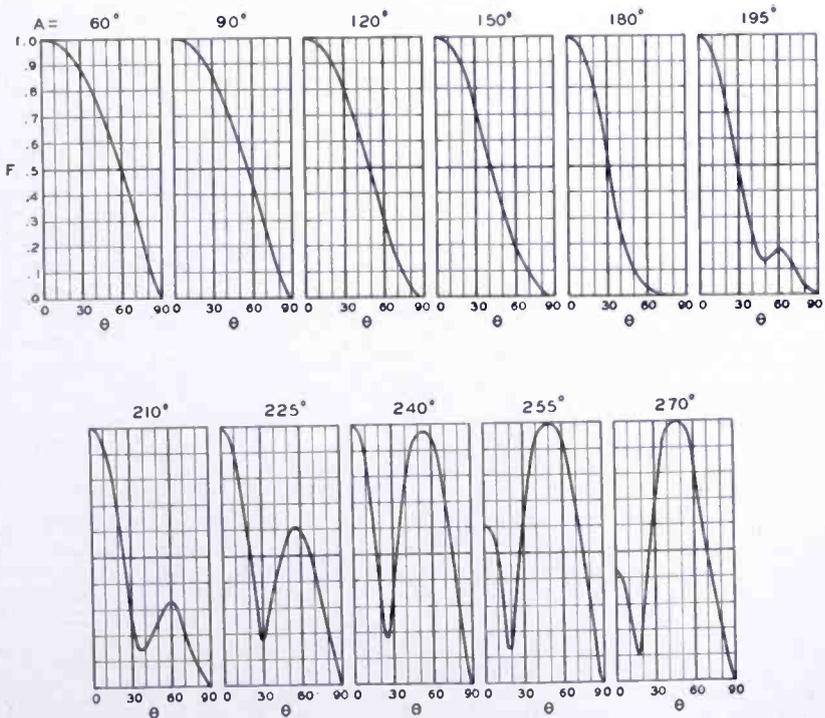
Fig. 12—Measured field patterns of a conical dipole for various
dipole lengths. Flare angle $\alpha = 0$ degrees.
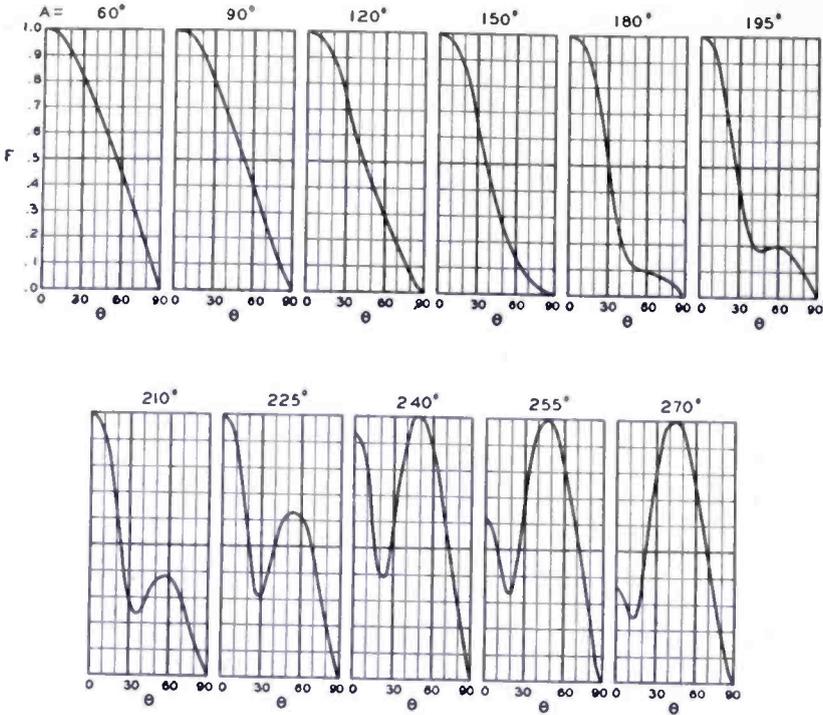
Fig. 13—Measured field patterns of a conical dipole for various dipole lengths. Flare angle $\alpha = 5$ degrees.
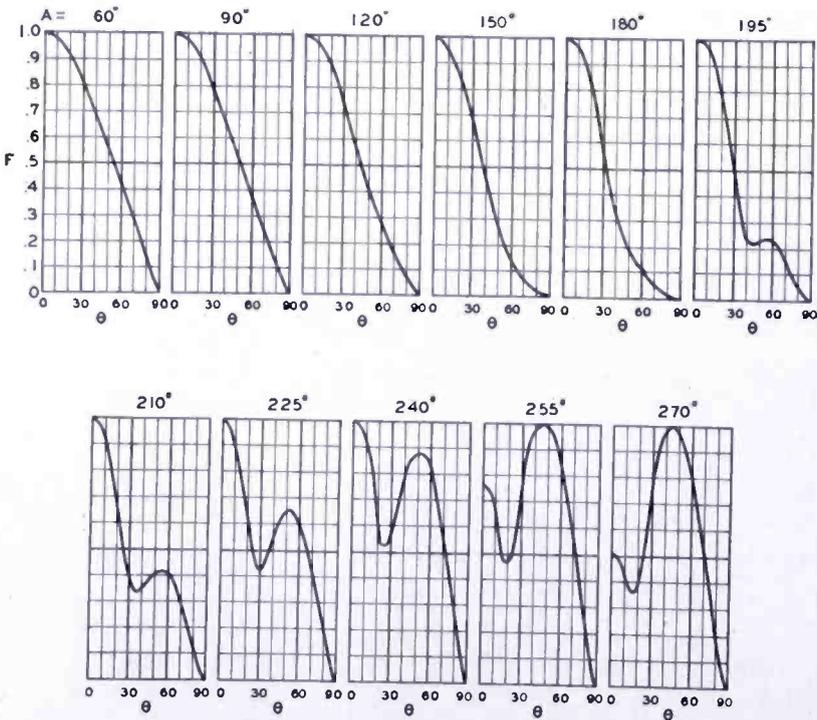
Fig. 14—Measured field patterns of a conical dipole for various dipole lengths. Flare angle $\alpha = 10$ degrees.
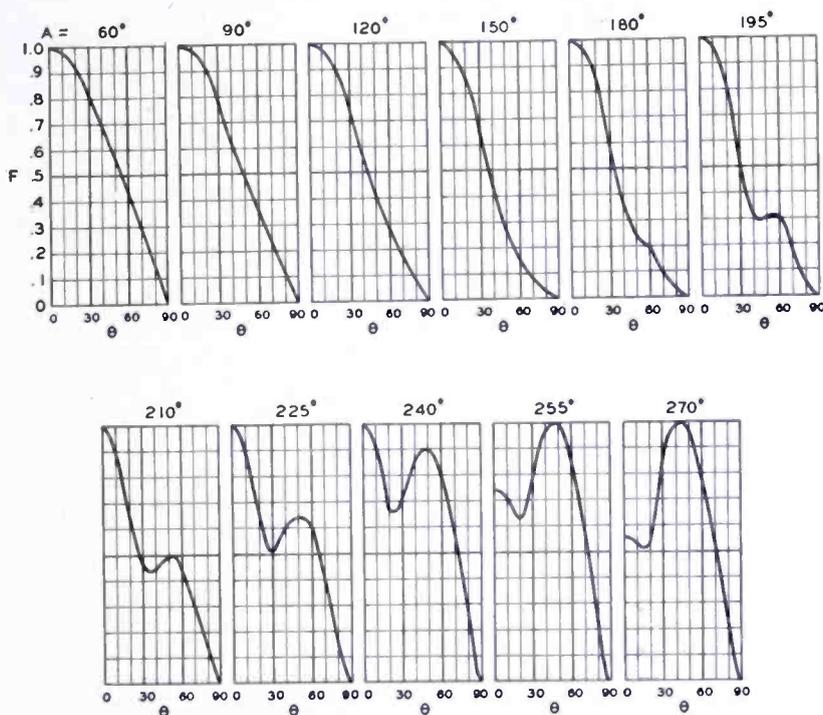
Fig. 15—Measured field patterns of a conical dipole for various dipole lengths. Flare angle $\alpha = 20$ degrees.
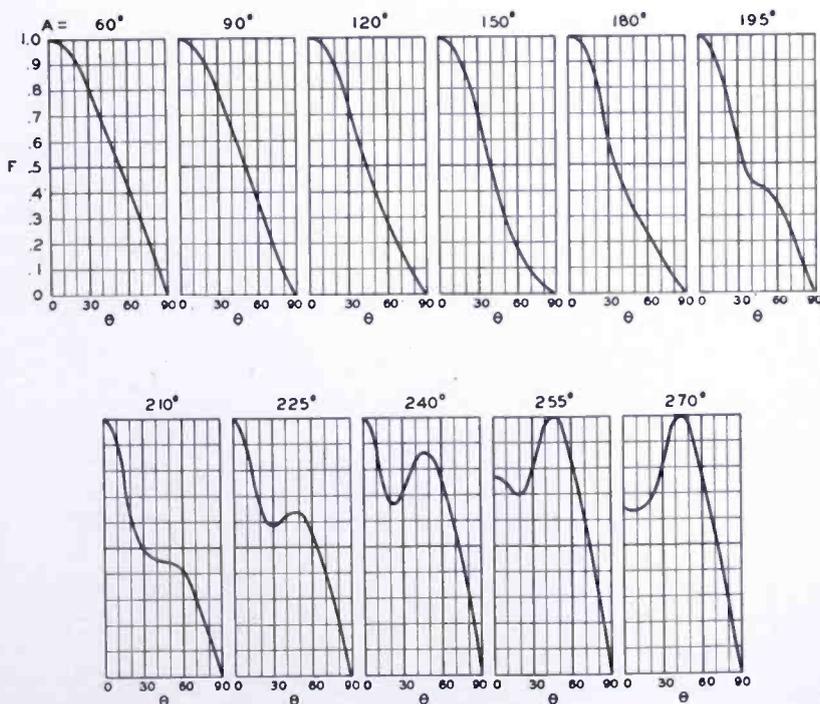
Fig. 16—Measured field patterns of a conical dipole for various dipole lengths. Flare angle $\alpha = 30$ degrees.
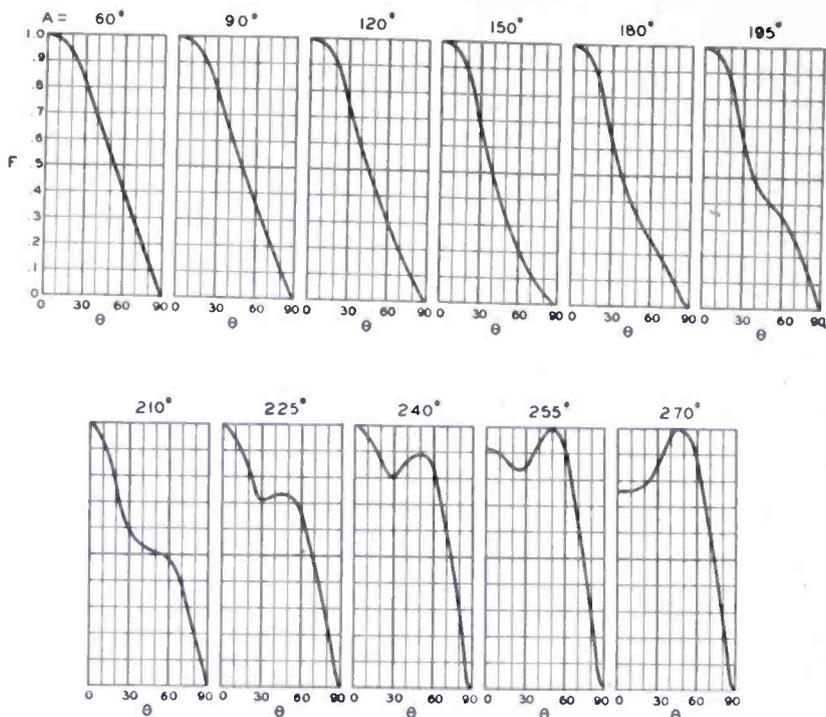
Fig. 17—Measured field patterns of a conical dipole for various
dipole lengths. Flare angle $\alpha = 40$ degrees.
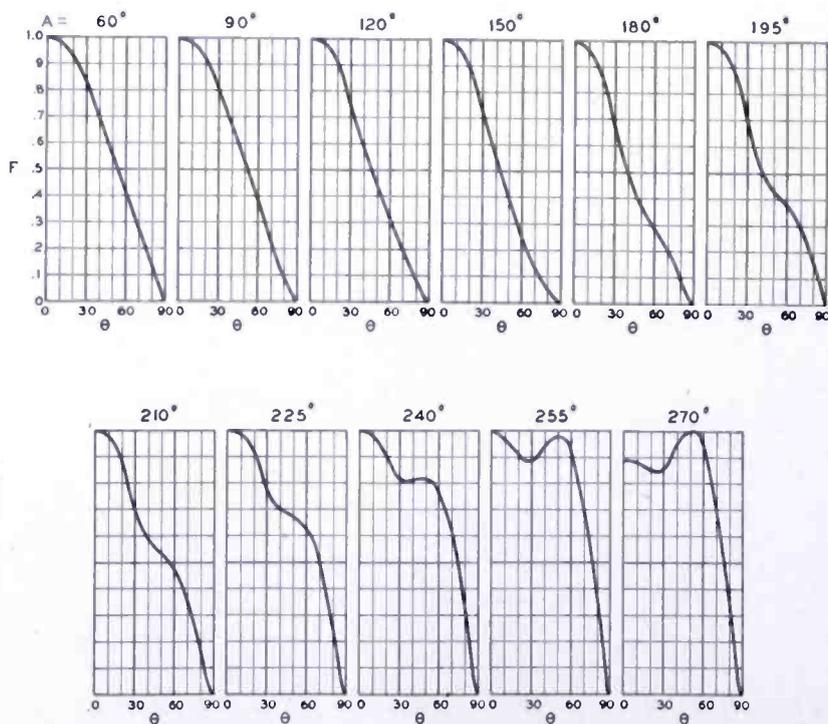
Fig. 18—Measured field patterns of a conical dipole for various
dipole lengths. Flare angle $\alpha = 50$ degrees.
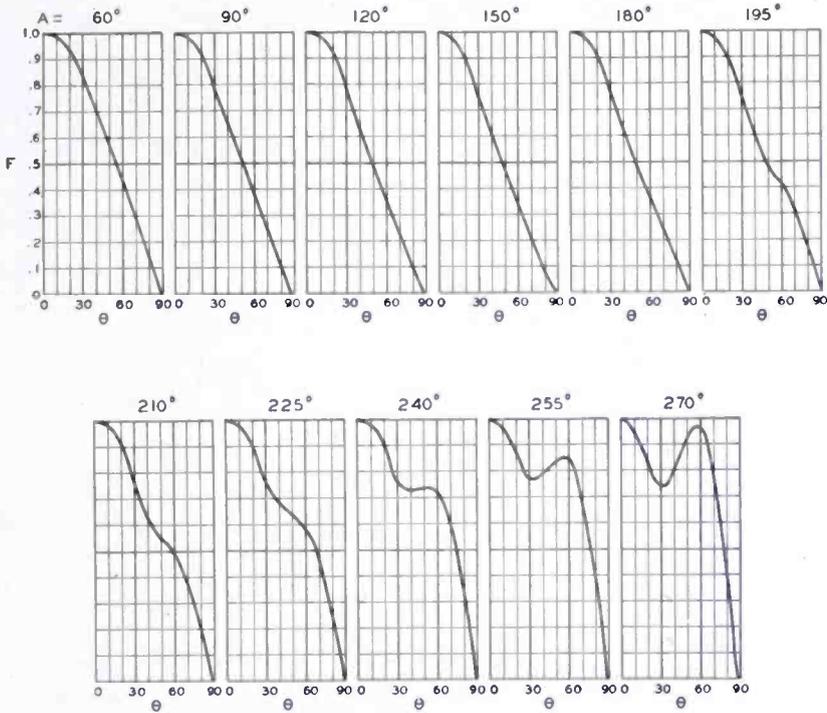
Fig. 19—Measured field patterns of a conical dipole for various
dipole lengths. Flare angle $\alpha = 60$ degrees.
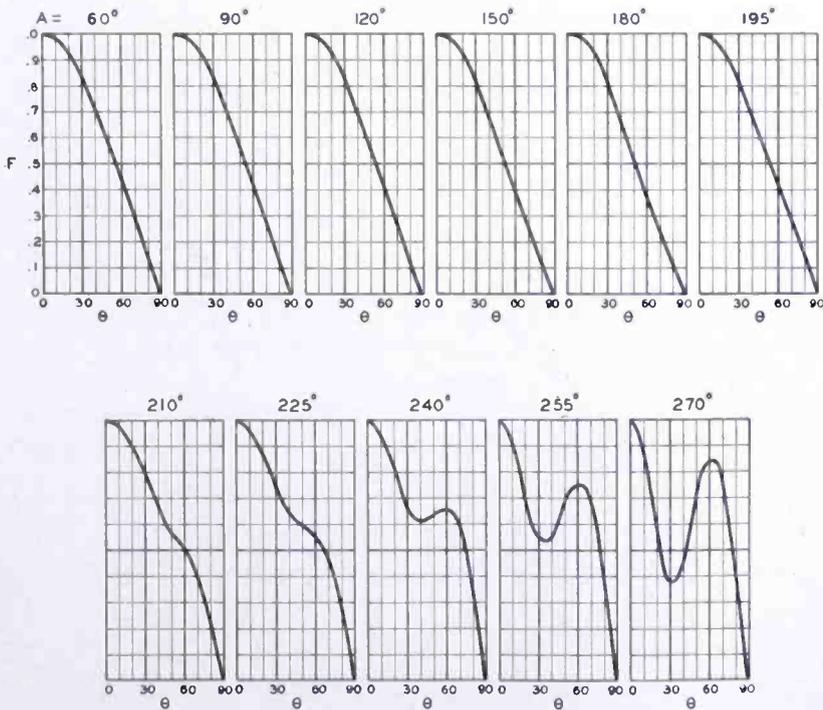
Fig. 20—Measured field patterns of a conical dipole for various
dipole lengths. Flare angle $\alpha = 70$ degrees.
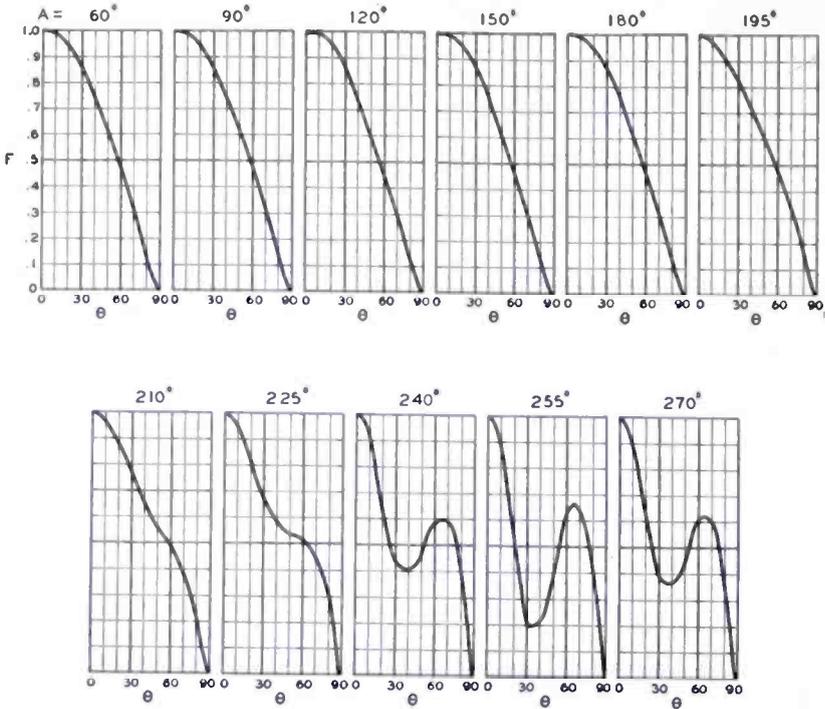
Fig. 21—Measured field patterns of a conical dipole for various dipole lengths. Flare angle $\alpha = 80$ degrees.
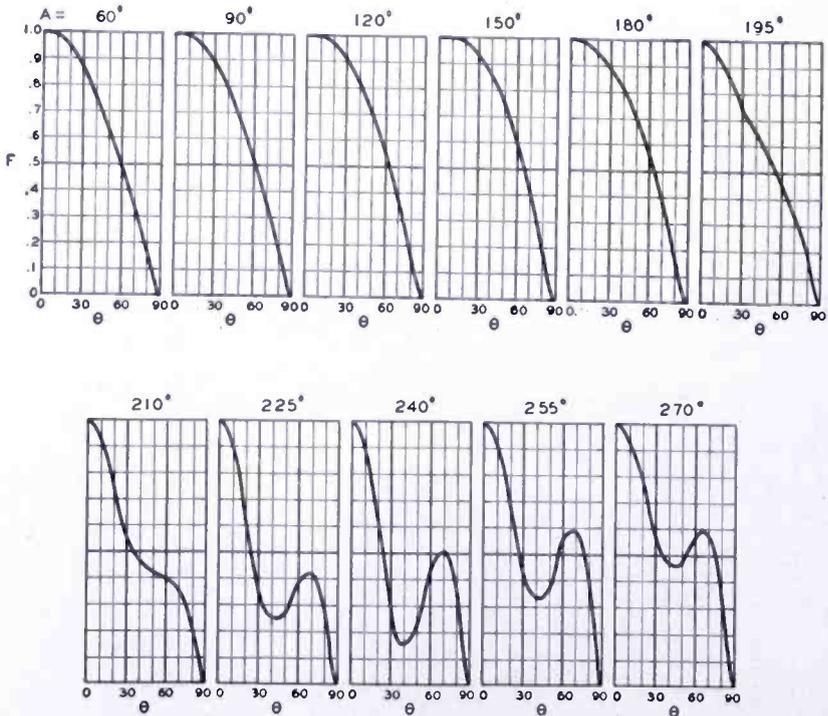
Fig. 22—Measured field patterns of a conical dipole for various dipole lengths. Flare angle $\alpha = 90$ degrees.

times the cosine of the azimuth angle, θ. The measured conical field patterns are replotted on a form shown in Figure 24, in which the coordinates are $F_0{}^2 \cos \theta$ and θ. Hence the relative power integration is mechanically performed by planimetering the area enclosed by the replotted curve. The area under the theoretical field pattern of a half-wave dipole is also measured as a reference. The ratio of the two areas is then the relative maximum power gain of the conical
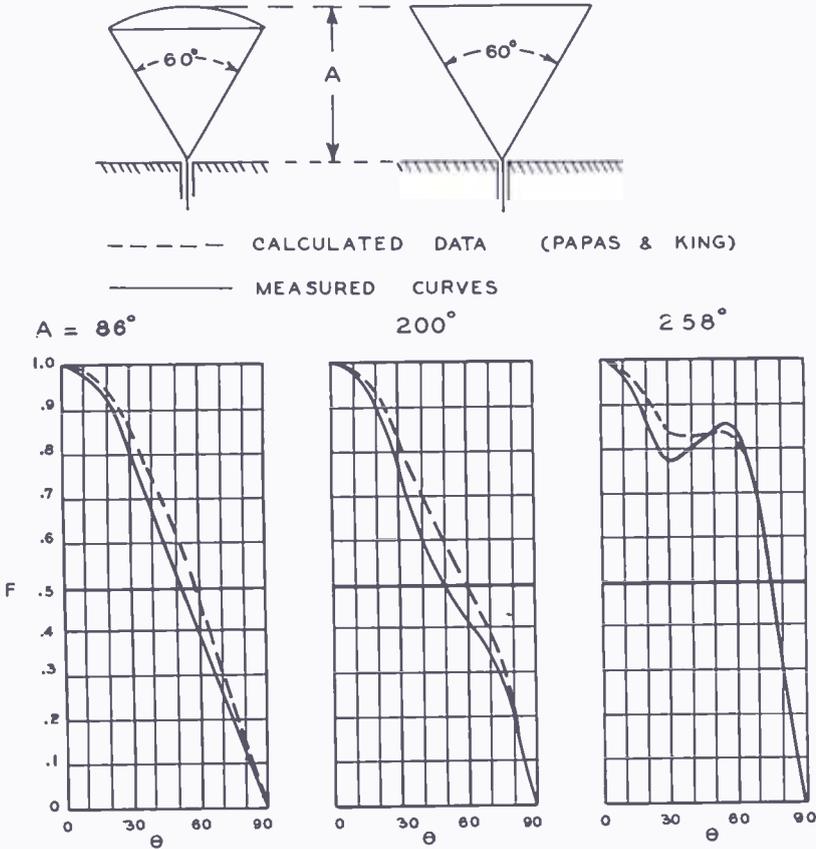
Fig. 23—Comparison of calculated and measured radiation characteristics of a 60-degree-flare-angle conical dipole.

dipole with respect to a theoretical half-wave dipole.

In the example given in Figure 24, the patterns of a 270° conical dipole having a flare angle of 40° and a theoretical half-wave dipole are plotted. The maximum relative power gain is the ratio of the planimetered areas enclosed by the two curves, or

$$P.G._{\text{MAX}} = \frac{2175}{2447} = .89.$$

As the relative field intensity is 0.76 at zero azimuth angle for the

conical dipole, the relative power gain for this broad-side condition is the maximum power gain reduced by the square of the relative field intensity, or

$$P.G._{(\theta=0°)} = .89 \times .76^2 = 0.514.$$

The relative power gain curves at $\theta = 0°$ computed in this manner for all of the measured conical dipoles are given in Figure 25. The different field pattern shapes of the thin-wire dipole (Figure 11) and the cylindrical dipole (Figure 12) result in a considerable departure in power gain for the longer antennas.
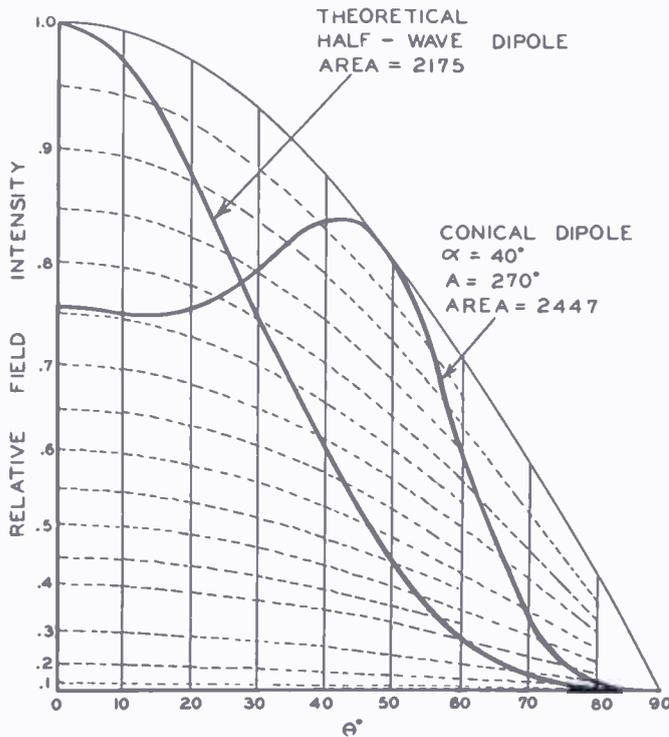
Fig. 24—An example of the relative-power-gain calculation for a 40-degree-flare-angle conical dipole.

An experimental verification that the high power gains for long antennas shown by the theoretical curve of Figure 25 are not realized with practical installations is given in Figure 26. The relative power gains calculated from measured field-strength data by Morrison and Smith[11] on a 400-foot broadcast tower are plotted for two types of tower excitation: base-fed being shown by the crosses and shunt-fed by the circles. The tower diameter was approximately 1½ electrical degrees

---

[11] J. F. Morrison and P. H. Smith, "The Shunt-Excited Antenna," *Proc. I.R.E.*, Vol. 25, p. 690, June, 1937.
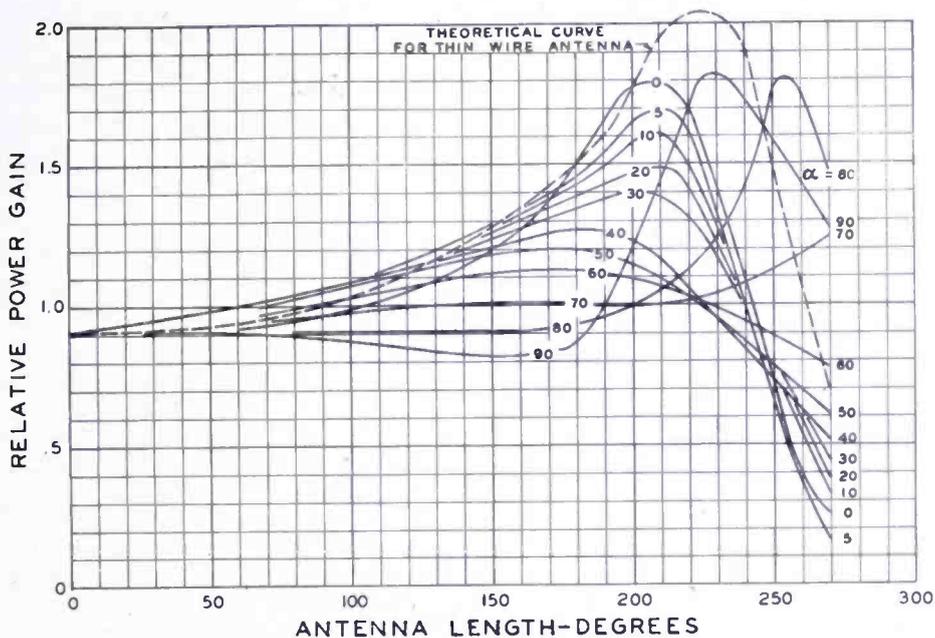
Fig. 25—Calculated power-gain curves of the conical dipoles with respect
to a theoretical half-wave dipole.

for the quarter-wave length. It is seen that the power-gain curve
obtained from our pattern measurements, as well as the Morrison and
Smith data, indicate a peak near 210 degrees and a substantial decrease
at 230 degrees. These results are at considerable variance with the
values obtained by assuming a sine-wave distribution of current.
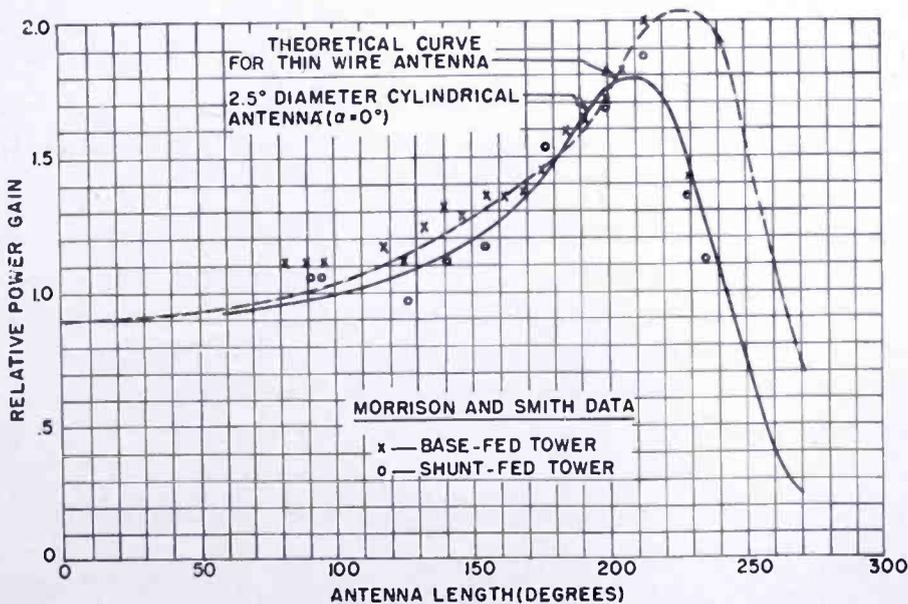
Fig. 26—Comparison of calculated and measured power-gain data.

Triangular-Antenna Impedance Measurements

The measured impedance data taken on the triangular unipoles are plotted in Figures 27 and 28. In general, it is seen that the resistance and reactance fluctuations are greater than with the conical antennas for the same flare angle.

An interesting point may be noted (Figure 28) in that for a length of 140 electrical degrees the reactance is independent of the flare angle of the triangle.
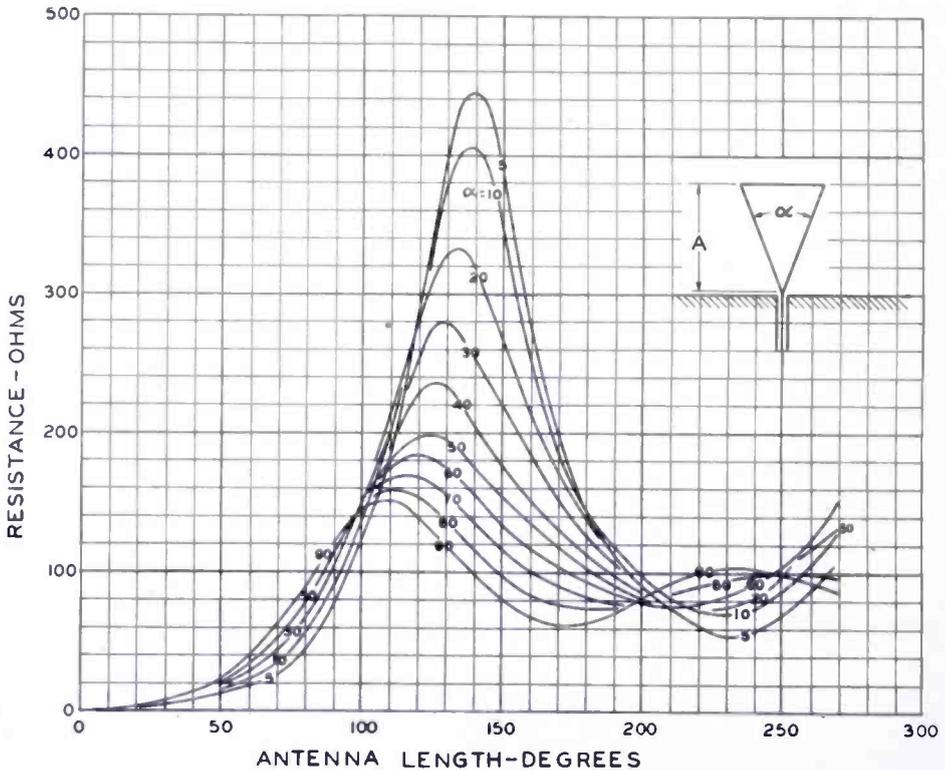
Fig. 27—Measured resistance curves of the triangular unipole versus length in electrical degrees for various flare angles.

The maximum resistance values and corresponding antenna lengths are shown in Figure 29. A comparison of Figures 7 and 29 shows that for a given flare angle the cone peak resistance is considerably lower than the triangle peak resistance.

Figure 30 shows the antenna length for the first resonance plotted versus the flare angle.

Triangular-Antenna Field-Pattern Measurements

The measured relative field patterns for the triangular dipoles are plotted in Figures 31 to 40 in the same manner as for the conical dipoles. Patterns taken in the XY plane are shown as dashed curves and pat-
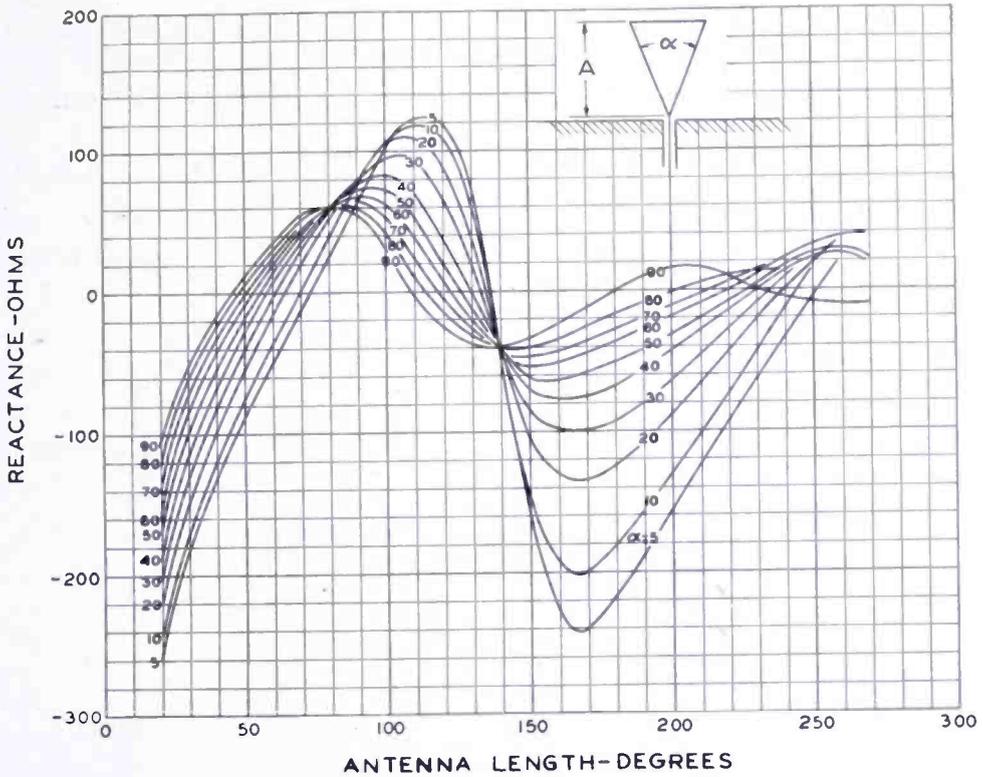
Fig. 28—Measured reactance curves of the triangular unipole versus length in electrical degrees for various flare angles.

terns taken in the XZ plane as solid curves.

The two patterns depart considerably for triangular dipoles of large flare angle and substantial length.
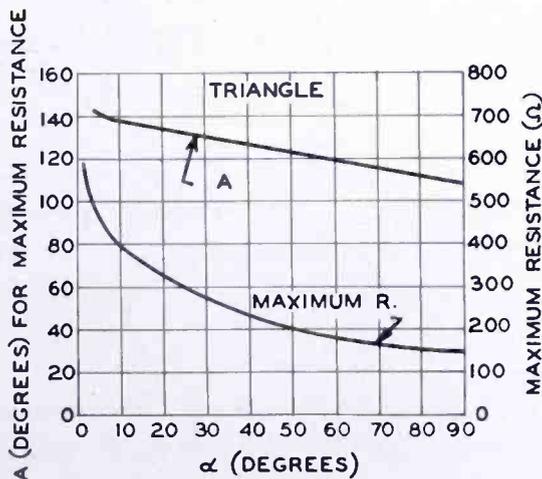
Fig. 29—Maximum triangular unipole resistance versus the flare angle in degrees, and the unipole length in electrical degrees at which the maximum resistance occurs versus the flare angle.

As the triangle field patterns do not always have circular symmetry in one plane, the power-gain measurement described previously could not be used. No other method of determining the power gain was attempted.

Figure 41 shows an application of the measured data to a particular design example. A broad-band dipole was required[12] for receiving use with 300-ohm characteristic impedance line in the ultra-high-frequency range of 480 to 920 megacycles.

The dipole was made in the form of triangular elements supported by an insulating arm. From a study of the impedance data of Figures 27 and 28, a flare angle of 60° and total length of 13½ inches was chosen as a suitable compromise to limit the standing-wave ratio to
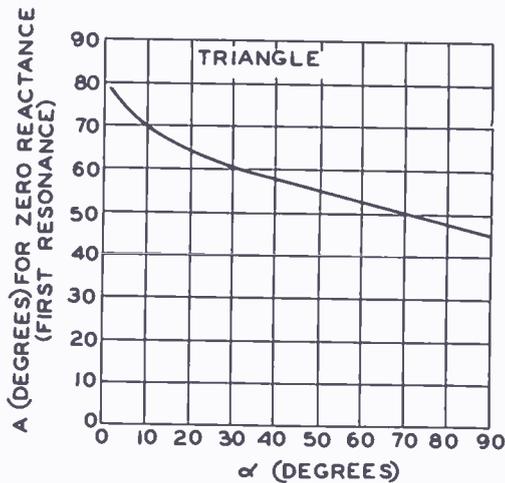
Fig. 30—The triangular unipole length in electrical degrees for zero reactance versus the flare angle.

2:1 or less over the frequency range. The final measured results are shown in Figure 42.

CONCLUSION

Useful design information was obtained experimentally on the radiation characteristics of conical and triangular antennas for wide variations in their physical dimensions. The data is presented graphically in terms of the input resistance and reactance, field patterns, and relative power gain.

A comparison of the measured values for conical antennas is made with a small number of published theoretical values, with excellent agreement.

---

[12] G. H. Brown, "Field Test of Ultra-High-Frequency Television in the Washington Area," *RCA Review*, Vol. IX, p. 572. December, 1948.
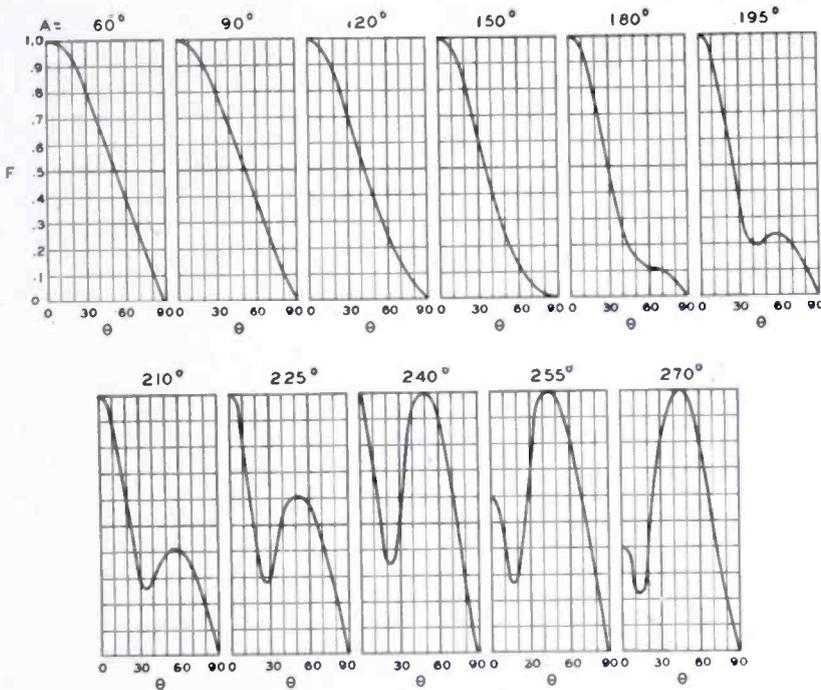
Fig. 31—Measured field patterns of a triangular dipole for various dipole lengths. The patterns are for both the XZ and the XY planes. Flare angle $\alpha = 5$ degrees.
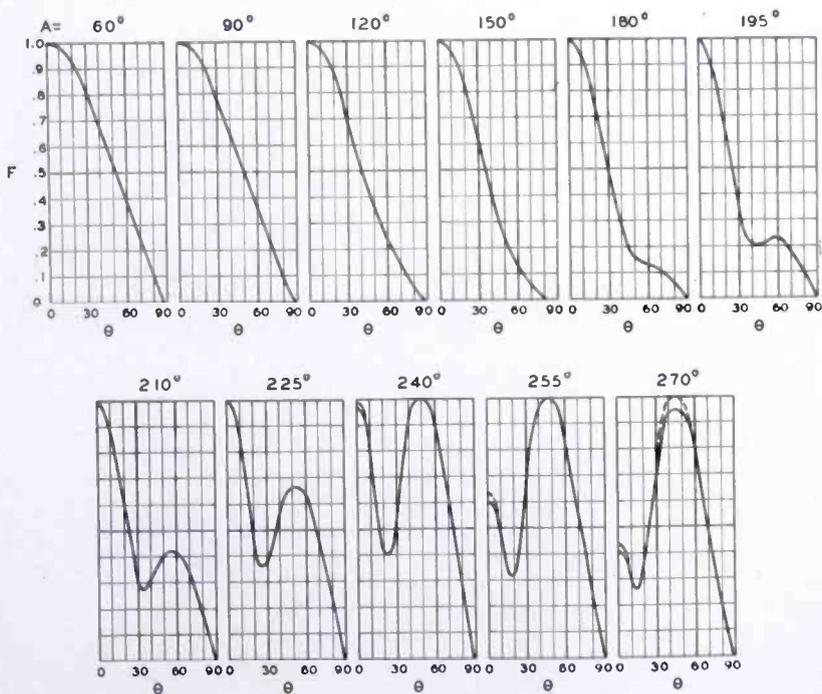
Fig. 32—Measured field patterns of a triangular dipole for various dipole lengths. The patterns in the XZ plane are indicated by the solid curves, and the patterns in the XY plane by the dashed curves. Flare angle $\alpha = 10$ degrees.
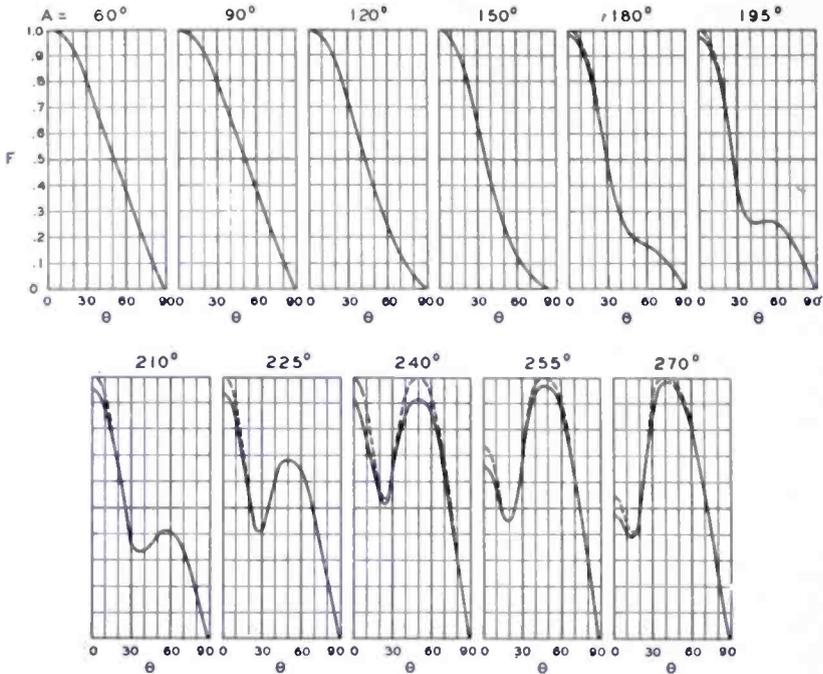
Fig. 33—Measured field patterns of a triangular dipole for various dipole
lengths. The patterns in the XZ plane are indicated by the solid curves,
and the patterns in the XY plane by the dashed curves. Flare angle
$\alpha = 20$ degrees.
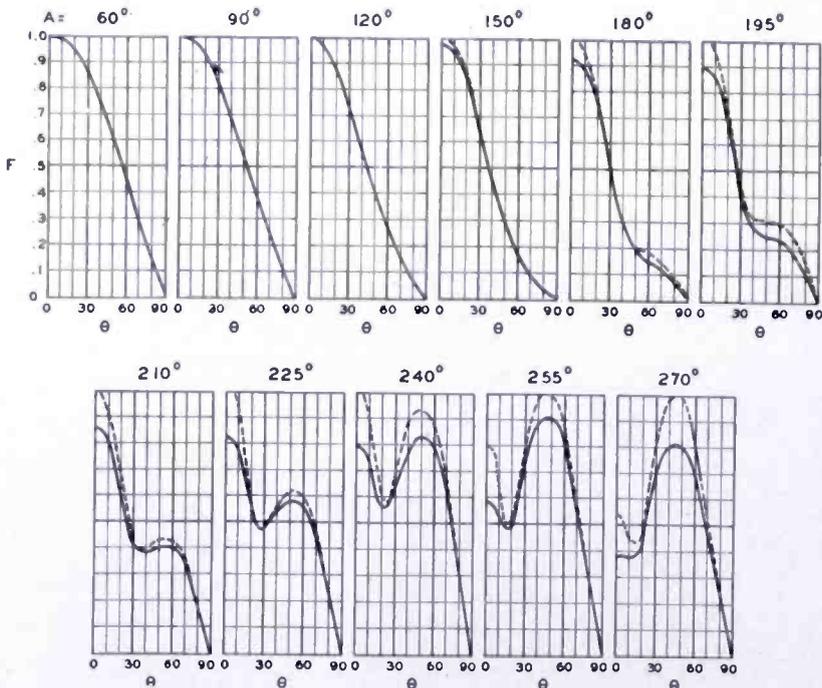
Fig. 34—Measured field patterns of a triangular dipole for various dipole
lengths. The patterns in the XZ plane are indicated by the solid curves,
and the patterns in the XY plane by the dashed curves. Flare angle
$\alpha = 30$ degrees.
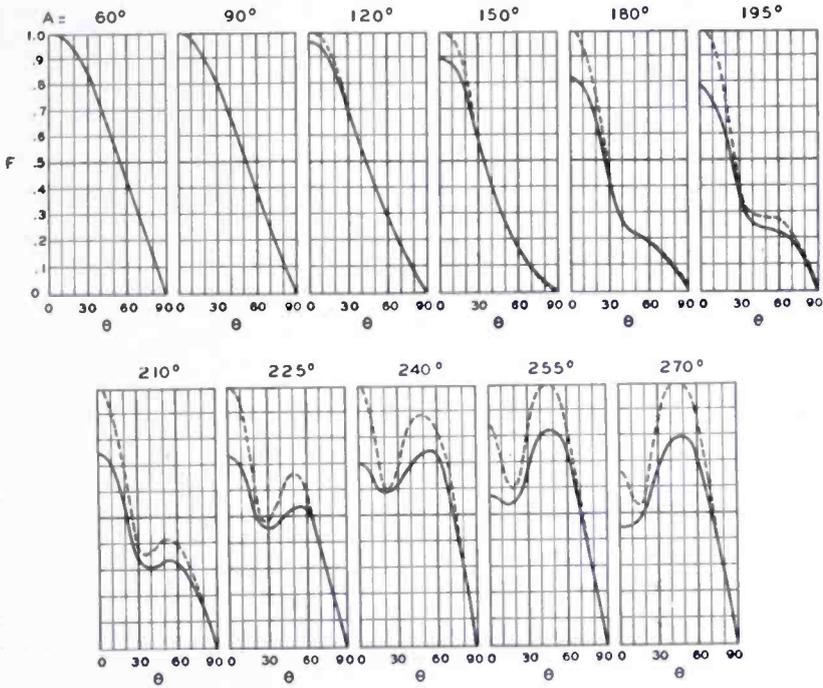
Fig. 35—Measured field patterns of a triangular dipole for various dipole lengths. The patterns in the XZ plane are indicated by the solid curves, and the patterns in the XY plane by the dashed curves. Flare angle $\alpha = 40$ degrees.
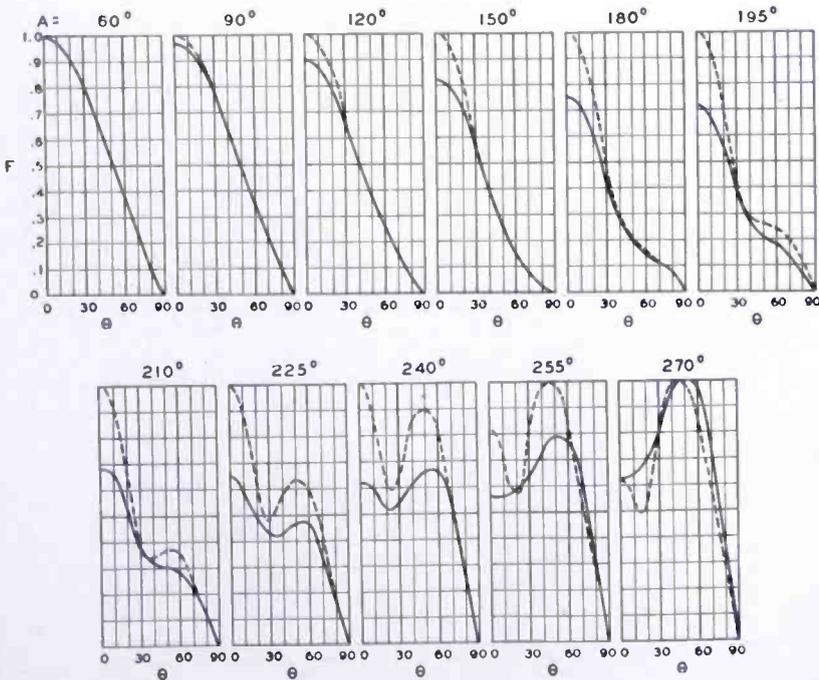
Fig. 36—Measured field patterns of a triangular dipole for various dipole lengths. The patterns in the XZ plane are indicated by the solid curves, and the patterns in the XY plane by the dashed curves. Flare angle $\alpha = 50$ degrees.
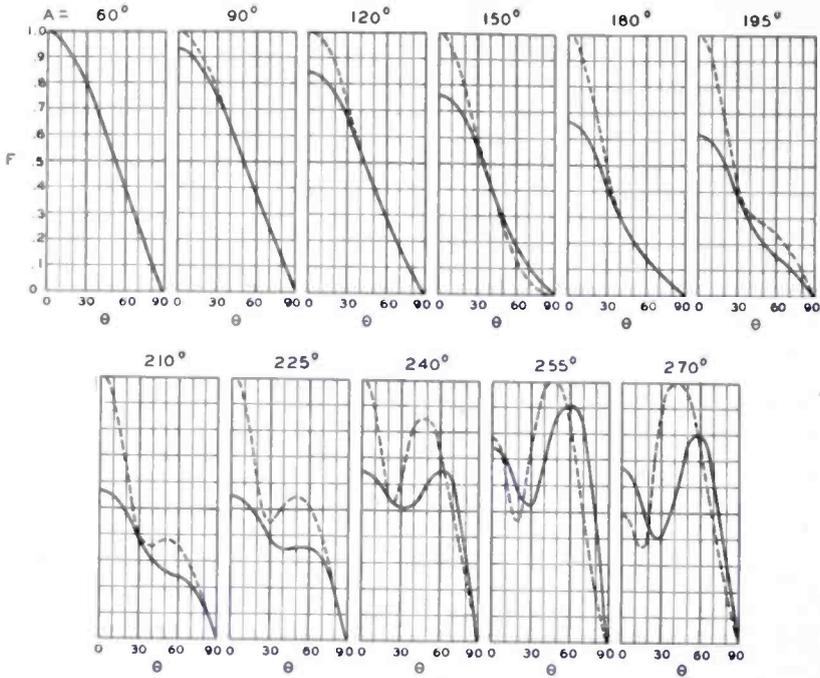
Fig. 37—Measured field patterns of a triangular dipole for various dipole lengths. The patterns in the XZ plane are indicated by the solid curves, and the patterns in the XY plane by the dashed curves. Flare angle α = 60 degrees.
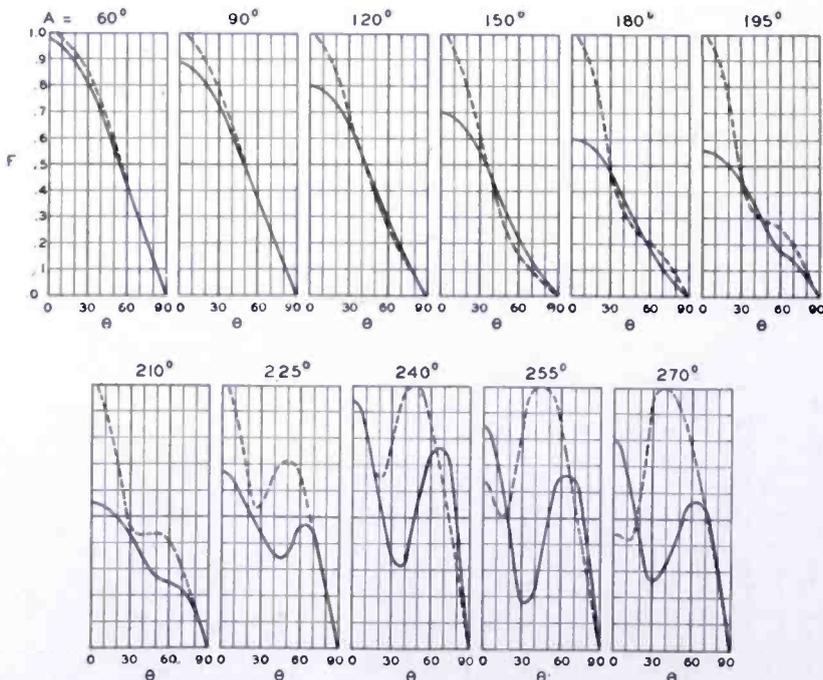
Fig. 38—Measured field patterns of a triangular dipole for various dipole lengths. The patterns in the XZ plane are indicated by the solid curves, and the patterns in the XY plane by the dashed curves. Flare angle α = 70 degrees.
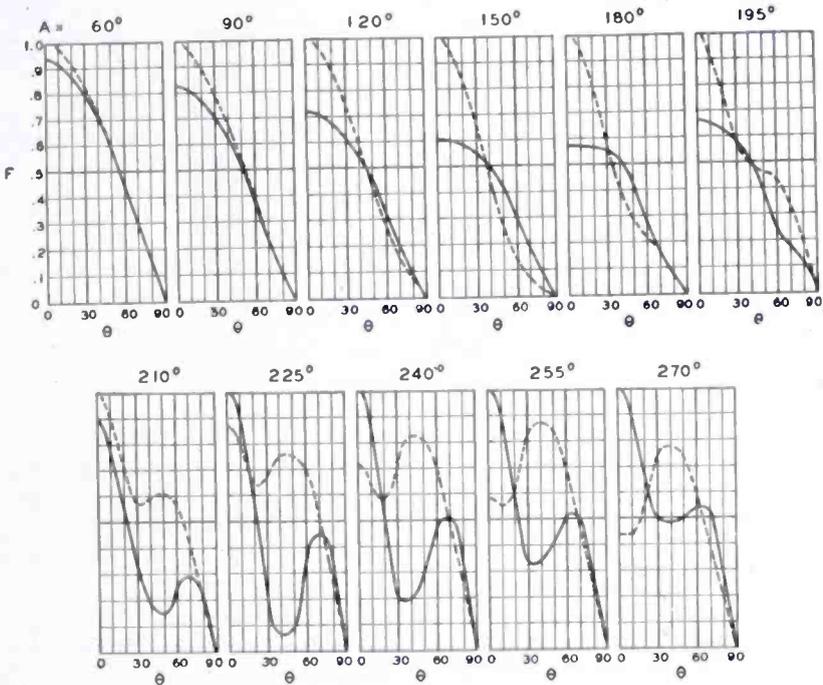
Fig. 39—Measured field patterns of a triangular dipole for various dipole lengths. The patterns in the XZ plane are indicated by the solid curves, and the patterns in the XY plane by the dashed curves. Flare angle $\alpha = 80$ degrees.
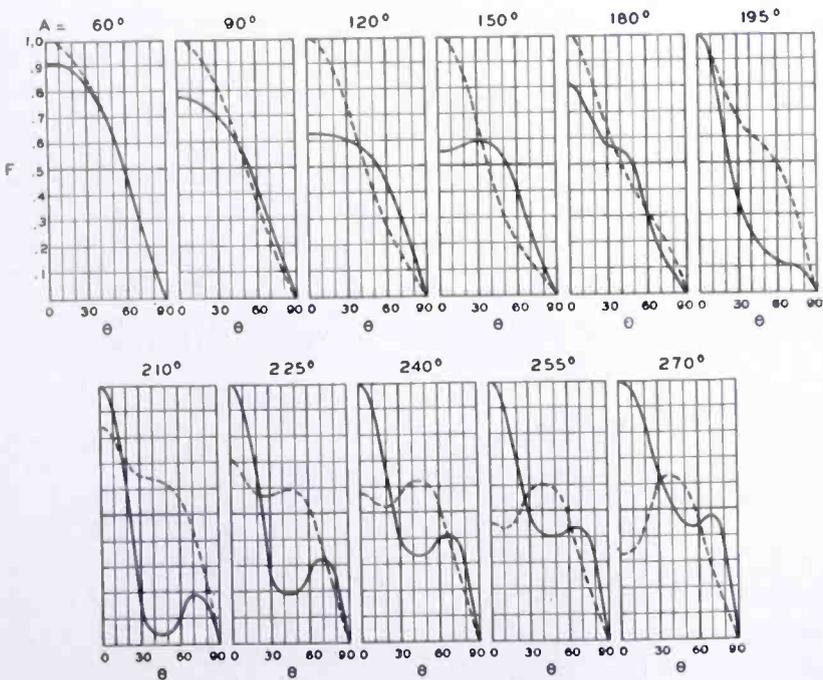
Fig. 40—Measured field patterns of a triangular dipole for various dipole lengths. The patterns in the XZ plane are indicated by the solid curves, and the patterns in the XY plane by the dashed curves. Flare angle $\alpha = 90$ degrees.
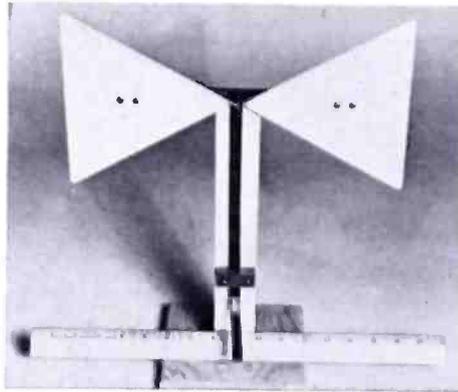
Fig. 41—An application of the measured impedance data to a
practical receiving dipole.
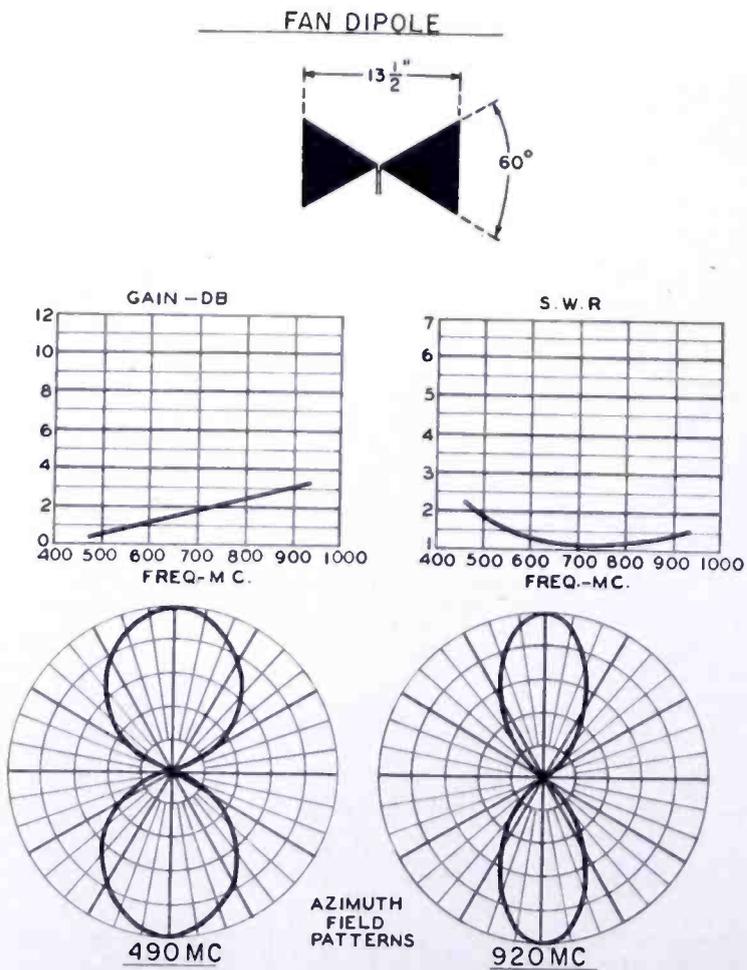
Fig. 42—Measured characteristics of fan dipole.

PHOTOCONDUCTIVITY STUDY OF ACTIVATION OF BARIUM OXIDE*

By

HENRY B. DeVore

Research Department, RCA Laboratories Division,
Princeton, N. J.

Summary—Photoconductivity studies have been made for barium oxide cathodes at various stages of thermionic activation, for the purpose of attempting to establish the donor energy levels. Changes occurring during activation are reflected in the development of the long-wave-length tail of the photoconductivity curve. For states of low activity, this tail has a threshold in the neighborhood of 2.3 electron volts, and, with increasing thermionic activity, a second threshold at about 1.4 electron volts develops. The measurements are interpreted as indicating the development of donors at levels having these depths below the conduction band during the activation. Tentative explanations of the origin of these donors are advanced.

INTRODUCTION

A NUMBER of studies of the optical and photoelectrical characteristics of barium oxide,[1-5] together with conductivity and thermionic emission studies, have led to a reasonably consistent picture of its energy-band structure.[6] The electron affinity χ (Figure 1) has a value in the range of 0.7 to 1.0 electron volt (e.v.). The top of the filled band lies approximately 5 e.v. below vacuum potential. The optical absorption edge at ~ 3.7 e.v. is interpreted as the lowest energy required to transfer an electron from the filled band to an exciton state. As a large increase in photoconductivity occurs at this energy, the exciton may be thermally dissociated at room tempera-

---

* Decimal Classification: 535.3.

[1] W. W. Tyler, "Optical Absorption in Barium Oxide Films," *Phys. Rev.*, Vol. 76, p. 1887, December 15, 1949.

[2] E. A. Taft and J. E. Dickey, "Optical Absorption Edge for BaO as determined by the Method of Ives and Briggs," *Phys. Rev.*, Vol. 78, p. 625, June 1, 1950.

[3] W. W. Tyler and R. L. Sproull, "Optical Absorption and Photoconductivity in Barium Oxide," *Phys. Rev.*, Vol. 83, p. 548, August 1, 1950.

[4] H. B. DeVore and J. W. Dewdney, "Photoconductivity and Photoelectric Emission of Barium Oxide," *Phys. Rev.*, Vol. 83, p. 805, August 15, 1951.

[5] L. Apker, E. Taft, and J. Dickey, "On the Photoelectric Emission and Energy Structure of BaO," *Phys. Rev.*, Vol. 84, p. 508, November 1, 1951.

[6] J. A. Krumhansl, "Energy Levels in BaO," *Phys. Rev.*, Vol. 82, p. 573, May 15, 1951.
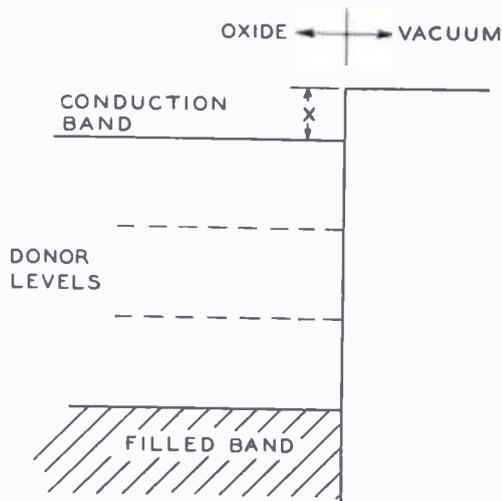
Fig. 1—Energy-level diagram for barium oxide.

tures. Within this framework, it is desirable to locate the positions of the energy states corresponding to the donors which are formed in the process of thermionic activation. For this purpose, a study has been made of the development, during activation, of the low-energy tails of the spectral photoconductivity curves of barium oxide.

EXPERIMENTAL TECHNIQUE

The apparatus used in this study is the same as has been used in our previously reported work on barium oxide photoconductivity[4] and is shown schematically in Figure 2. The specimen is irradiated, at constant intensity throughout the spectrum, with intermittent illumination, using the combination of a high-pressure mercury-arc source,
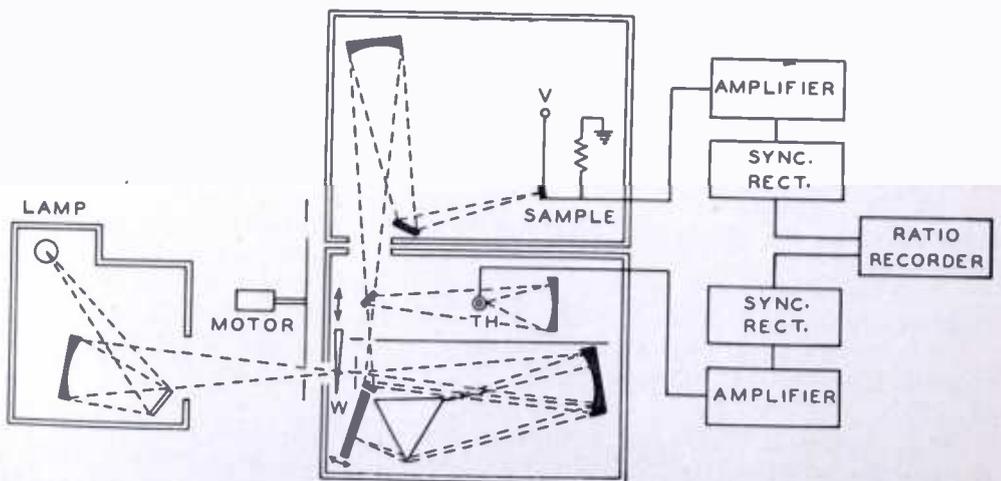
Fig. 2—Arrangement of apparatus for photoconductivity study.

quartz monochromator, light chopper, and absorbing wedge to control the intensity. The photoconductive current is amplified and rectified, as is the output of a thermistor illuminated simultaneously by the monochromator. These two signals are combined in a ratio recorder which is driven synchronously with the monochomator wave-length control, so that a curve is obtained in which photocurrent per unit intensity of radiation is plotted against the wave length of the radiation incident on the specimen. In the present study, the potential applied across the oxide sample was 5-90 volts direct current, rather than alternating current, as employed in the previous work, since the inevitable harmonic content of the alternating current produced a noise level too high to permit satisfactory study of the low-energy tails.

Normally, the monochromator slit widths are set at 0.4 millimeter, and the light intensity maintained at a level which can be held uniform throughout the spectral range 1.0 to 4.0 e.v. With this setting 2×10^{-5} watt of radiation falls on the sample, in an area 5.2 square millimeters. The band width at half maximum intensity is 0.04 e.v. for monochromator settings between 1.2 e.v. and 2.0 e.v., decreasing to 0.02 e.v. at 4.0 e.v. setting. In some of the more recent studies, it has been found that the low-energy tails may be much more satisfactorily displayed by employing a considerably increased radiation intensity. Sufficient intensity to provide irradiation at 7×10^{-4} watt between 1.0 e.v. and 3.0 e.v. was obtained by increasing the slit width to 1.0 millimeter. This increases the half-maximum band width to 0.1 e.v. in the region from 1.2 e.v. to 2.0 e.v., decreasing to 0.07 e.v. at 3.0 e.v. setting. This comparatively large band width of the monochromator gives rise to increased rounding of the inflection regions of the photoconductivity curves

The barium oxide samples were obtained from sprayed cathode coatings of barium carbonate (Mallinckrodt "Ultra Pure") on an electrolytic nickel base, having a platinum probe wire embedded in the coating. The tube structure (Figure 3) was the same as described previously.[4] In this work, the tube was sealed to a vacuum system which had provisions for admitting oxygen for deactivation and methane for activation.

The following processing schedule was employed. After sealing to the vacuum system, a tube was exhausted and baked for several hours at 400°C. When it had cooled, the barium carbonate was reduced to oxide by gradually heating until evolution of gas had substantially ceased. This required about an hour and the final temperature was approximately 900°C. The tube was then cooled, oxygen was admitted to a pressure of 0.1 millimeter of mercury, and the cathode heated at

600°C for several minutes. The cathode was allowed to cool in the oxygen atmosphere to attain a well deactivated state.

During the course of the study, barium oxide cathodes were activated by (1) heating, (2) heating and drawing thermionic emission current, (3) heat treating in a methane atmosphere,[7] and (4) by evaporating barium metal on the surface of the heated oxide. In general, it was found that treatments (1) and (2) led to rather poor thermionic activity, while treatments (3) and (4) yielded well-activated cathodes. Thermionic emission measurements were made by the technique described in reference (7), using the point of 20 per cent departure from the 3/2 power law as a measure of the emission.
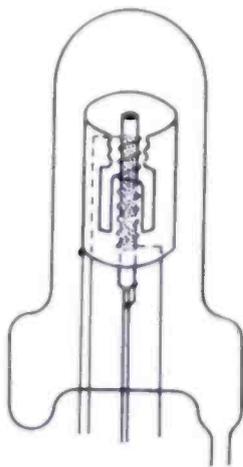
Fig. 3—Experimental tube.

OBSERVATIONS

It has been found that shapes of the barium oxide photoconduction curves are reproducible through several cycles of activation-deactivation, although the magnitudes of the photocurrents tend to increase each time the cycle is repeated. The peak photocurrent (at ~ 3.8 e.v.) was usually larger for activated than for deactivated states, although the magnitude of this increase varied from one specimen to another over very wide ranges. All curves have been normalized to uniform peak height, which has been assigned the arbitrary value 100. This was done in order that the development of the low-energy tails might be exhibited separately from changes due to activation which should affect all parts of the curves, as, for example, changes in mobility or trap density.

---

[7] N. B. Hannay, D. MacNair, and A. H. White, "Semi-Conducting Properties in Oxide Cathodes," *Jour. Appl. Phys.*, Vol. 20, p. 619, July, 1949.
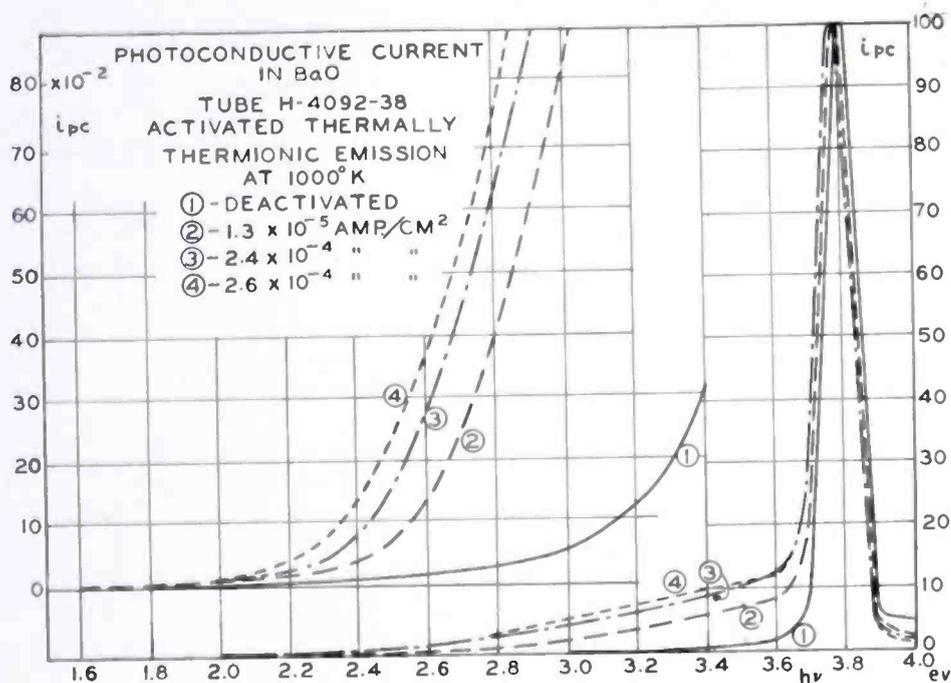
Fig. 4—Photoconductive current in BaO, activated thermally.

A typical series of photoconduction curves, all made for the same cathode in various states of activation, are shown in Figures 4, 5, and 6. The insert curves in Figures 4 to 6, and Figures 4a to 6a, show the low-energy tails, measured at high light intensity, plotted on en-
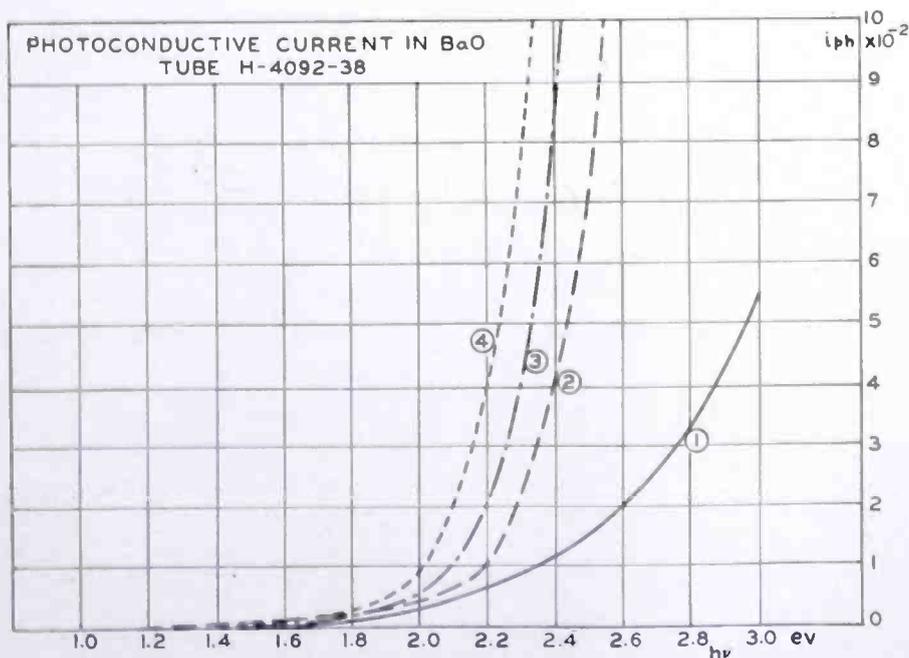
Fig. 4a—Low-energy tails of curves in Figure 4.
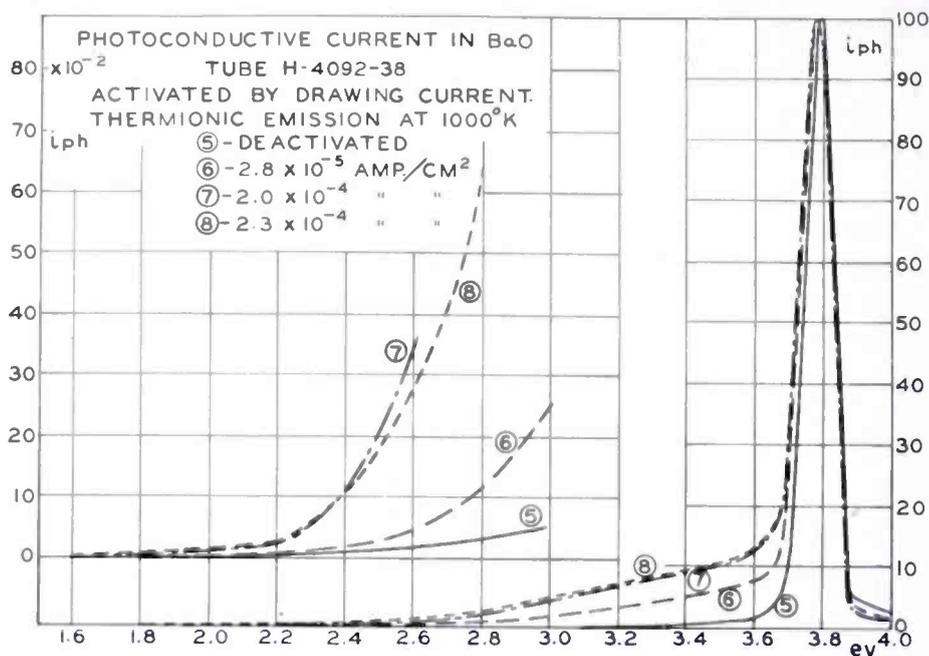
Fig. 5—Photoconductive current in BaO, activated by drawing current.

larged scales to show the detailed form of these curves.

A notable feature, common to all curves, is the absence of any peaks in the low-energy region corresponding to the donors formed during the activation. This result is interpreted as indicating that the transition of an electron from a donor site to the bottom of the conduction
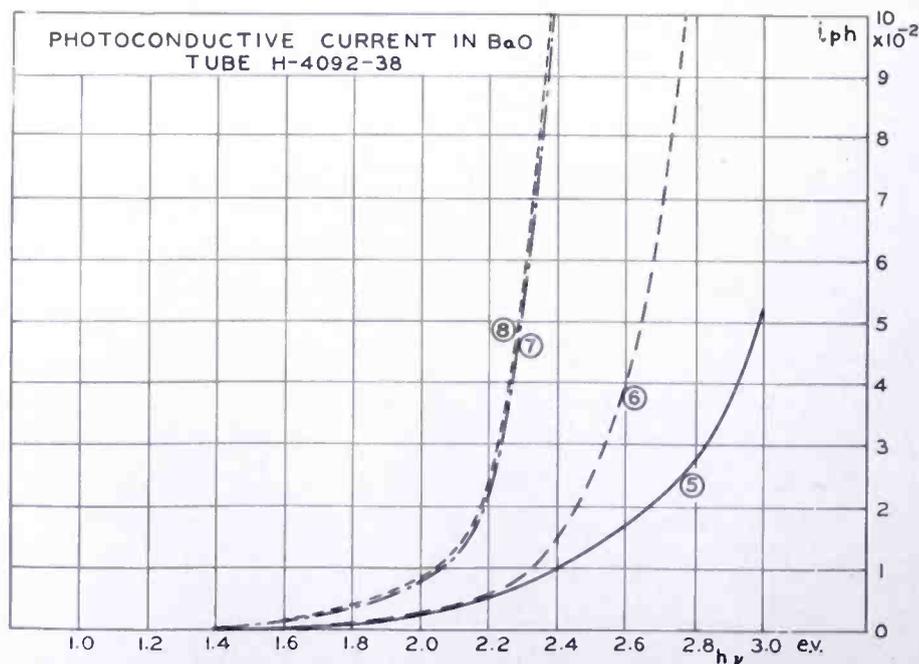
Fig. 5a—Low-energy tails of curves in Figure 5.
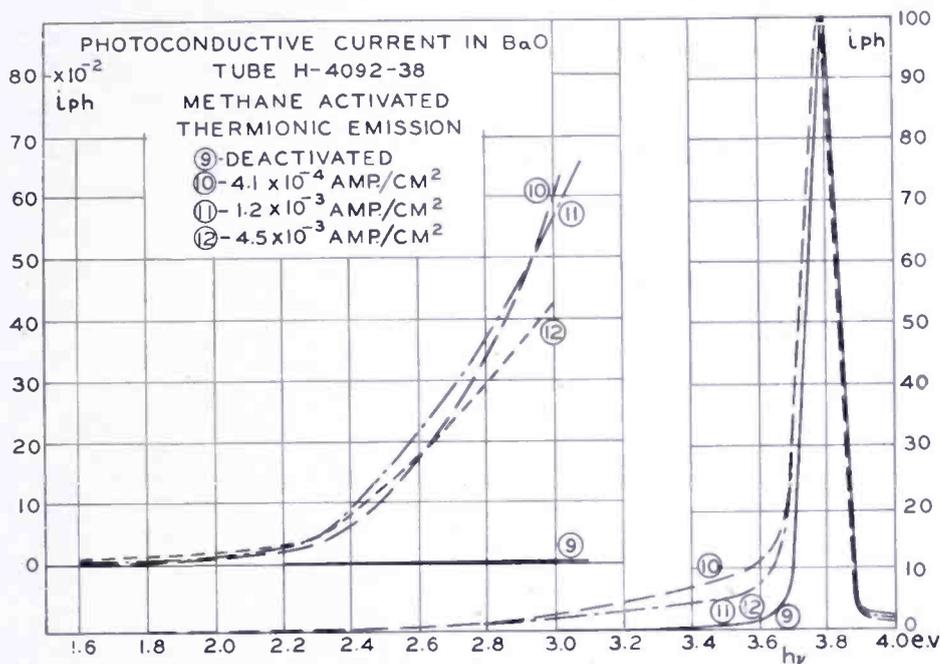
Fig. 6—Photoconductive current in BaO, activated by methane treatment.

band is not more probable than the transition to a higher level in this band. However, the curves obtained for a large number of tests have all shown good consistency in the location of the thresholds. As is shown in the curves, two distinct thresholds appear during activation. The first of these lies at about 2.3 e.v. and the second at about 1.4 e.v.
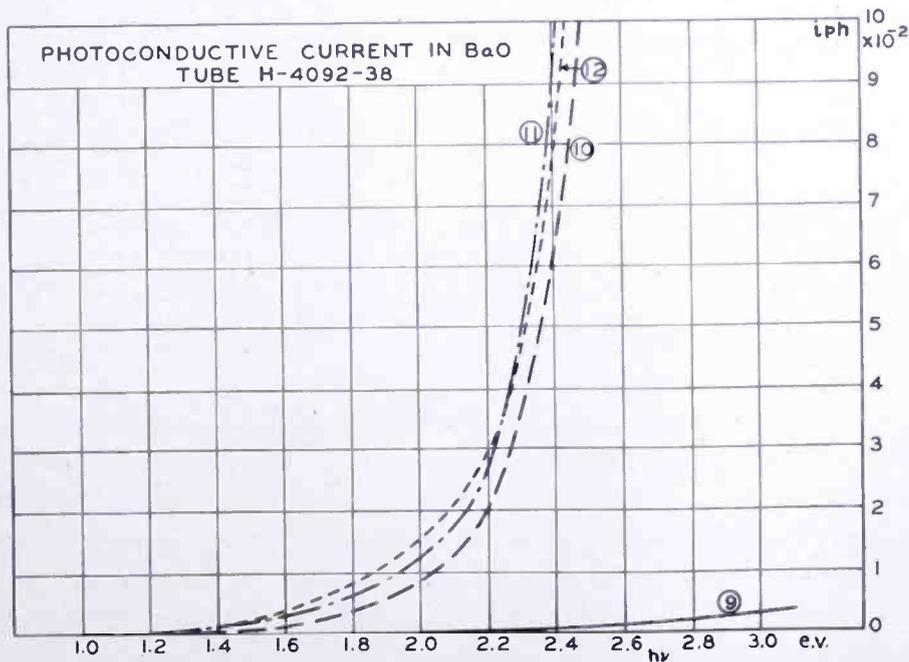
Fig. 6a—Low-energy tails of curves in Figure 6.

While, as is particularly evident in the curves made at high light level, both thresholds can be observed for all states of activation, it is found that photoconduction corresponding to the 2.3 e.v. threshold develops first and is followed by a gradual build-up of the response at the lower energies. Figure 7 shows curves for a tube in which the cathode was well activated by methane treatment and again by evaporation of barium metal onto its heated surface. In these two cases, the build-up of the low-energy portion of the tail has progressed to the point that the 2.3 e.v. threshold is no longer observable.
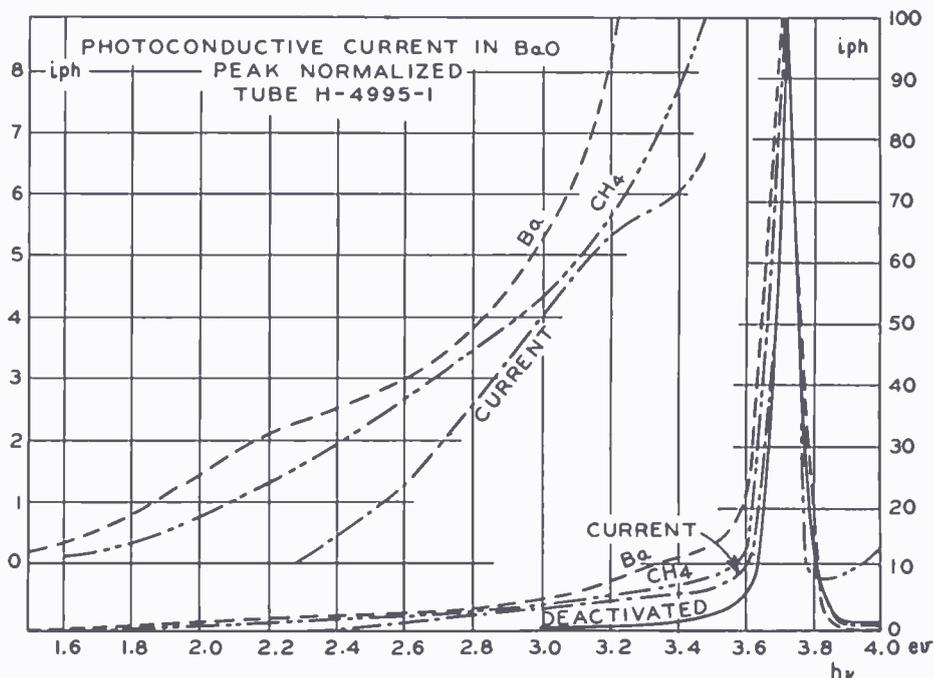
Fig. 7—Photoconductive current in BaO, activated thermally, by methane treatment, and by Ba evaporation.

It has been found generally that exposure of the barium oxide to radiation which it absorbs strongly ($h\nu > 3.6$ e.v.) increases the photoconductive response to light having photon energy less than 2.8 e.v. and decreases the response to higher energy radiation. Subsequent exposure to radiation for which $h\nu < 2.6$ e.v. reverses these changes. These effects are particularly conspicuous in activated samples. The normalized photocurrents observed at high light levels are smaller than those found at low light levels. This results from the fact that the radiation is scanned from low energy to high energy, some 10-15 minutes being required to trace out a curve. During the high-intensity, long-wave-length irradiation, the response of the sample is reduced.

Some studies have been made with barium oxide containing a small

concentration of known impurity. The materials from which these samples were made included (1) barium carbonate + magnesium carbonate, both mixed mechanically and coprecipitated, (2) barium carbonate + aluminum oxide, mixed, (3) barium carbonate + indium oxide, mixed, and (4) barium carbonate + cerium carbonate, coprecipitated. In each case, the concentration of the additive was such as to give one foreign metal atom to 1000 barium atoms. In the first three
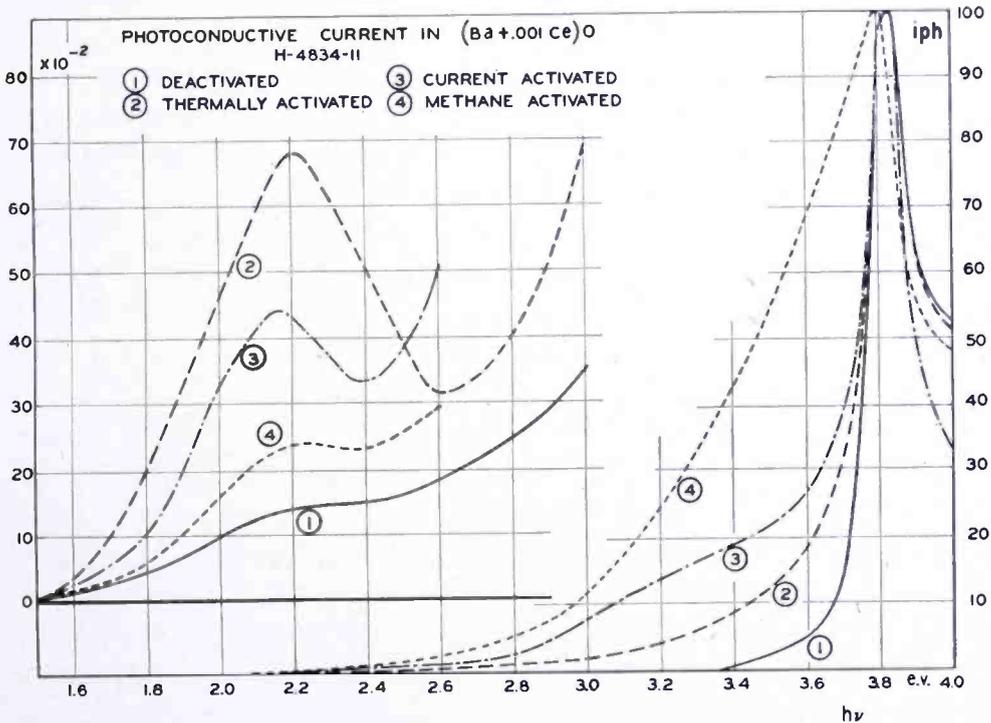
Fig. 8—Photoconductive current in BaO containing cerium.

cases, the photoconductivity curves were essentially indistinguishable from those for pure barium oxide. In the case of cerium, however, there always appeared a small peak, centered at 2.2 e.v. A representative set of curves for a cerium-doped barium oxide is shown in Figure 8.

DISCUSSION

These photoconduction studies indicate that the process of activation for thermionic emission results in the formation of two groups of donor levels, of undetermined width, with their upper edges lying approximately 2.3 e.v. and 1.4 e.v., respectively, below the bottom of the conduction band. Of these, the 2.3 e.v. levels are formed first, the 1.4 e.v. group following, as the activity is increased, and eventually becoming predominant. On deactivation, both groups of donors tend

to be eliminated. It may be argued that only one group of donor levels is present, with its edge 1.4 e.v. below the conduction band, and that the threshold at 2.3 e.v. represents an increase in transition probability when photons having higher energy than this fall on the crystal. This assumption, however, seems incompatible with the different rates of growth of photocurrents corresponding to the two thresholds as the cathode is activated.

Two possible explanations for these results have been proposed. The first assumes that in the deactivated state there is an excess of oxygen, i.e., there are barium defects in the lattice. These would represent the equivalent of the V-centers found in alkali halides and would be electron acceptors. The process of activation, which is chemically a reduction process, consists of the formation of oxygen vacancies containing surplus electrons (F-centers). As these are introduced, the electrons drop from the missing oxygen sites to the missing barium sites, resulting in the filling of these sites with excess electrons which may be transferred to the conduction band by photon absorption. The 2.3 e.v. band represents transitions of the electrons trapped in the barium vacancy positions. As the concentration of the oxygen defects increases, a point is reached at which the barium defect sites are substantially filled by the extra electrons. Further creation of the oxygen F-centers now forms a new group of donors at the level established by the oxygen vacancy sites. This gives rise to the 1.4 e.v. band.

One outstanding drawback to this picture lies in the initial assumption of barium defects in the lattice. As acceptors, they should permit removal of electrons from the filled band and consequent hole conduction in the deactivated state. However, experiments made to test this, in which the barium oxide was heated and cooled in comparatively high pressure (several millimeters) of oxygen, have failed to yield any evidence of such behavior.

The second explanation assumes that the barium oxide has substantially stoichiometric proportions in the deactivated state. Activation, as before, proceeds by the formation of oxygen defect F-centers, and the energy levels of these are located 2.3 e.v. below the conduction band. This is supported by calculations of the energy of an oxygen defect containing two electrons,[8] which indicate that the removal to the conduction band of the first and second electrons requires 2.4 e.v. and 3.4 e.v., respectively. The 1.4 e.v. band may be attributed to the agglomeration of excess barium atoms, following upon the removal of the oxygen, forming colloidal barium particles distributed through

---

[8] N. Schwartz, Cornell University—Private communication.

the lattice. This assumption gains some support from the observation that the sum of this energy and the electron affinity for barium oxide is rather close to the work function for metallic barium (2.5 e.v.).

The observations on the change in photoconductive response with exposure to radiation may be explained on the assumption of the presence of electron traps and/or unoccupied donor levels. Then exposure to radiation in the absorption region frees electrons from the filled band and some of these electrons may drop into the traps or the donor levels. In these positions, the electrons may be released by photons of lower energy than 2.8 e.v., giving an augmented photocurrent. The reduced response for $h\nu > 2.8$ e.v. may be caused by the excess holes in the valence band, left by the trapped electrons, which can effect an increase in the rate of recombination of conduction electrons. Exposure to radiation having quantum energy less than 2.6 e.v. serves to liberate the trapped electrons and restore the original condition of the crystal.

ACKNOWLEDGMENT

STUDIES OF THE OXIDE CATHODE*

BY

L. S. NERGAARD

Research Department, RCA Laboratories Division,
Princeton, N. J.

Summary—A series of studies of the oxide cathode is described. The series includes studies of the decay and recovery of pulsed emission, the internal resistances of the cathode, the dependence of the apparent work function on cathode current, and the activation of cathodes by operation in barium vapor and by barium deposition in a mass spectrometer. A barium–strontium oxide amplifier is described.

The results of these diverse studies lead to a model of the oxide cathode in which the donors which make the cathode active are mobile, i.e., can electrolyze and diffuse. This model provides a simple and coherent explanation of the major anomalies exhibited by the oxide cathode.

Evidence that the donors in barium oxide are F-centers formed from oxygen vacancies is adduced. These F-centers, oxygen–barium vacancy pairs, and traps lying near the valence band are shown to account for observed conductivity and emission phenomena.

INTRODUCTION

FOR the past few years, work on the oxide cathode has been carried on in this laboratory in the hope of reaching an understanding of the physical phenomena which govern the behavior of the cathode. Certain aspects of this work have been reported from time to time, but much of the work remains unreported.[1-4] Out of this work has emerged a physical model of the cathode which accounts for the more regular behaviors of the cathode and for many of the anomalous behaviors, as well. The model is probably incomplete; details must be worked out and refinements added before it can be considered satisfactory. However, it has proved so fruitful in planning experiments that it seems worth while to report the model and the experimental

---

[1] R. M. Matheson and L. S. Nergaard, "The Decay and Recovery of the Pulsed Emission of Oxide-Coated Cathodes," *Jour. Appl. Phys.*, Vol. 23, pp. 869-875, August, 1952.

[2] R. M. Matheson and L. S. Nergaard, "High-Speed Ten-Volt Effect," *RCA Review*, Vol. 12, pp. 258-268, June, 1951.

[3] L. S. Nergaard, "Cathode Impedance and Tube Failure," Reported at the Tenth Annual Conference on Physical Electronics, Massachusetts Institute of Technology, 1950.

[4] L. S. Nergaard, R. H. Plumlee, and R. M. Matheson, "Study of the Activity of an Oxide Cathode by Means of a Mass Spectrometer," Reported at the Twelfth Annual Conference on Physical Electronics, Massachusetts Institute of Technology, 1952.

work from which it derives at this time with the thought that it may be helpful or at least stimulating to others.

In scanning the experimental work reported in this paper, it may appear that the work has covered a very wide field none too thoroughly. This appearance stems from the general philosophy behind the work. During the past 50 years, almost every aspect of the oxide cathode has been studied, some aspects intensively. Still, no complete and coherent picture of the cathode has emerged. It has been our feeling that a broad general picture of the cathode was necessary, if merely to serve as a reference frame for cataloguing the diverse behaviors of the cathode. This general picture must include all of the idiosyncrasies of the cathode. This point of view implies an obligation to study the irregular and anomalous behaviors of the cathode in order to extend the catalogue of behaviors and to determine the nature of the framework which will embrace them. Accordingly, many quirks of behavior have been studied. This may have led the work off on tangents on a few occasions and it has certainly made it impossible to study any particular aspect exhaustively. However, it is fondly hoped that this approach to the problem has kept the trees from obscuring the forest.

In brief, the work has proceeded as follows: A major anomaly is the pulse behavior of the oxide cathode. Accordingly, the first work was an extended examination of the pulse behavior. This work led to a conviction that pulse decay is not a simple surface effect, nor is it solely an anode effect, as held by some, but is caused in part by some internal mechanism of the oxide. The early work of Becker on electrolysis in cathodes and the work of Sproull on decay effects suggested a mechanism involving the electrolysis of the donors which make the cathode active. This hypothesis led to a series of experiments on the conductivity of the cathode including attempts to separate out interface, bulk, and "front surface" impedances; and a series of experiments to determine the effect of electrolysis on work function. The most prominent interface effects are those due to insulating compounds formed at the metal–oxide interface by the reaction of the oxides with reducing agents diffusing out of the base metal. Because these layers are not a necessary part of the cathode and can be avoided by choice of base metal, the work on such layers will not be included in this report. The conductivity and work function measurements bear out the model of mobile donor centers. It then appeared appropriate to try to determine the nature of the donors, and one of the approaches to this problem is to study how they may be formed. Accordingly, activation studies were undertaken. Progress has been made, but the studies are incomplete.

RÉSUMÉ OF PAST WORK

The present paper is not a general survey paper, but is intended as a report on the work at a particular laboratory. Nevertheless, it seems proper to make brief reference to the history of the oxide cathode and to acknowledge the past work on which the present work is based.

The oxide cathode was discovered just 50 years ago and the first publication appeared two years later.[5] In 1908, Deininger reported that the emission of an oxide cathode is not critically dependent on the base metal.[6] The literature of the next fifteen years appears to hold little of current interest. In 1920, Arnold reported on his work with oxide-coated platinum-iridium filaments.[7] The unipotential cathode was introduced in 1925, and with its introduction the use of nickel as a base metal became common. In this same year, Koller proposed the hypothesis that free barium was responsible for the activity of the oxide cathode.[8] This hypothesis has held sway ever since, and the role of barium, free or otherwise, was amply demonstrated by Becker, and Becker and Sears, in their papers of 1929, and 1931.[9,10] In 1930, B. J. Thompson reported emission under pulse conditions substantially higher (4 amperes per square centimeter) than that obtained under direct-current (d-c) conditions at that time.[11] At about the same time, the conductivity of the oxide cathode was studied extensively by Becker and Sears[12] and by Reimann and Murgoci.[13] The latter reported nonlinear current–voltage characteristics for the oxide and a linear relation between conductivity and emission current. In 1943, Schade reported pulse emissions as high as 25 amperes per square centimeter

[5] A. Wehnelt, "Uber den Austritt negativer Ionen aus glühenden Metallen," *Ann. der Phys.*, Series 4, Vol. 14, No. 8, pp. 425-468, 1904.

[6] F. Deininger, "Uber den Austritt negativer Ionen aus einiger glühenden Metallen und glühendem Calcium-Oxyd," *Ann. der Phys.*, Series 4, Vol. 25, No. 2, pp. 285-308, 1908.

[7] H. D. Arnold, "Phenomena in Oxide-Coated Filament Electron Tubes," *Phys. Rev.*, Vol. 16, pp. 70-82, July, 1920.

[8] L. R. Koller, "Electron-Emission from Oxide-Coated Filaments," *Phys. Rev.*, Vol. 25, pp. 671-676, May, 1925.

[9] J. A. Becker, "Phenomena in Oxide-Coated Filaments," *Phys. Rev.*, Vol. 34, pp. 1323-1351, November, 1929.

[10] J. A. Becker and R. W. Sears, "Phenomena in Oxide-Coated Filaments II," *Phys. Rev.*, Vol. 38, pp. 2193-2213, December 15, 1931.

[11] B. J. Thompson, "High Efficiencies of Emission from Oxide-Coated Filaments," *Phys. Rev.*, Vol. 36, pp. 1415-1417, October 15, 1930.

[12] J. A. Becker and R. W. Sears, *loc. cit.*

[13] A. L. Reimann and R. Murgoci, "Thermionic Emission and Electrical Conductivity of Oxide Cathodes," *Phil. Mag.*, Vol. 9, pp. 440-464, March, 1930.

and gave a phenomenological explanation of pulse decay.[14] In 1945, Sproull published the results of his work on the pulse decay of emission from oxide-coated cathodes.[15] He used square pulses as long as 300 microseconds—pulses substantially longer than those which had been used in the war-time pulse-radar work. He found long-time decays of the type observed by Schade, and advanced a decay theory based on the electrolytic depletion of the dipole layer at the emitting surface. In 1946, the group working on oxide cathodes at the Massachusetts Institute of Technology (M.I.T.) Radiation Laboratory published the results of their war-time work, comprising work on d-c and pulsed emission, oxide and interface structure, coating and interface resistance, and sparking.[16-18]

This brings the present brief review up to what can be regarded as current literature, to which reference will be made subsequently. However, no listing is adequate without mention of the review articles of Dushman,[19] Becker,[20] Blewett, [21,22] and Eisenstein,[23] and the books of Hermann and Wagener.[24]

THE PRESENT PHYSICAL MODEL OF THE OXIDE CATHODE

In discussing the electrical characteristics of the oxide cathode, it is customary to divide the cathode into four more or less distinct

---

[14] O. H. Schade, "Analysis of Rectifier Operation," *Proc. I.R.E.*, Vol. 31, pp. 341-361, July, 1943.

[15] R. L. Sproull, "An Investigation of Short-Time Thermionic Emission from Oxide-Coated Cathodes," *Phys. Rev.*, Vol. 67, pp. 166-178, March 1 and 15, 1945.

[16] A. Eisenstein, "A Study of Oxide Cathodes by X-Ray Diffraction Methods," Part I, *Jour. Appl. Phys.*, Vol. 17, pp. 434-443, June, 1946; Part II, *Jour. Appl. Phys.*, Vol. 17, pp. 654-663, August, 1946.

[17] E. A. Coomes, "The Pulsed Properties of Oxide Cathodes," *Jour. Appl. Phys.*, Vol. 17, pp. 647-654, August, 1946.

[18] A. Fineman and A. Eisenstein, "Studies of the Interface of Oxide-Coated Cathodes," *Jour. Appl. Phys.*, Vol. 17, pp. 663-668, August, 1946.

[19] S. Dushman, "Thermionic Emission," *Rev. Mod. Phys.*, Vol. 2, pp. 381-476, October, 1930.

[20] J. A. Becker, "Thermionic Electron Emission and Adsorption," *Rev. Mod. Phys.*, Vol. 7, pp. 95-128, April, 1935.

[21] J. P. Blewett, "Properties of Oxide Cathodes," Part I, *Jour. Appl. Phys.*, Vol. 10, pp. 668-679, October, 1939; Part II, *Jour. Appl. Phys.*, Vol. 10, pp. 831-848, December, 1939.

[22] J. P. Blewett, "Oxide-Coated Cathode Literature, 1940-1945," *Jour. Appl. Phys.*, Vol. 17, pp. 643-647, August, 1946.

[23] A. Eisenstein, "Oxide-Coated Cathodes," *Advances in Electronics*, Academic Press, Inc., 1948.

[24] G. Hermann and S. Wagener, *The Oxide Cathode*, Volumes I and II, Chapman and Hall, London, 1951.

regions as shown in Figure 1. The first region at the left is the base metal. This offers no direct electrical problems although it may contribute to the problems in the second region, the interface layer. The interface layer is formed by the reduction of the oxides by reducing agents diffusing out of the base metal. The reducing agents in the base metal may be residues of so-called scavengers used to free the metal from oxides, or they may be agents introduced in controlled amounts to facilitate the initial activation of the cathode and to maintain activity over long periods of time.[25,26] Commonly used reducing agents are silicon, titanium, manganese, magnesium, aluminum, and carbon. All of these react with BaO to form oxides and many of the oxides in turn react with BaO to form higher compounds such as silicates, titanates, etc.[27-29] From the electrical point of view, the worst
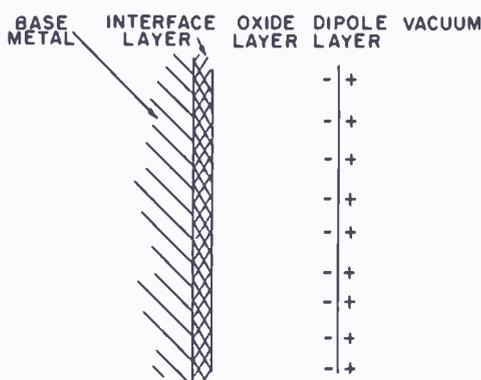
Fig. 1—The four principal regions of the oxide cathode.

of these compounds is $2\,BaO \cdot SiO_2$, which has a very low conductivity.[30] Present evidence indicates that $2\,BaO \cdot SiO_2$ is an impurity semiconductor with a relatively low conductivity at best. When a barium orthosilicate layer is present, it inserts a capacitance in the order of 10^{-9} farad in parallel with a resistance which may range from tenths of an ohm to thousands of ohms per square centimeter of cathode area

[25] A. M. Bounds and T. H. Briggs, "Nickel Alloys for Oxide-Coated Cathodes," *Proc. I.R.E.*, Vol. 39, pp. 788-799, July, 1951.

[26] H. E. Kern and R. T. Lynch, "Initial Emission and Life of a Planar-Type Diode as Related to the Effective Reducing Agent Content of the Cathode Nickel," *Phys. Rev.*, Vol. 82, p. 574, May 15, 1951.

[27] H. P. Rooksby, "Applications of X-Ray Techniques to Industrial Laboratory Problems," *Jour. Roy. Soc. Arts*, Vol. 88, pp. 308-336, February, 1940.

[28] H. P. Rooksby, "Applications of X-Ray Techniques to Industrial Laboratory Problems," *G.E.C. Journal*, Vol. 11, pp. 83-95, August, 1940.

[29] H. P. Rooksby, "Identification by X-Rays of Interface Compounds on 'Oxide' Cathodes," *Nature*, Vol. 159, p. 609-610, May, 1947.

[30] A. Eisenstein, "Some Properties of the Ba₂ SiO₄ Oxide Cathode Interface," *Jour. Appl. Phys.*, Vol. 20, pp. 776-790, August, 1944.

in series with the electrical circuit. This network has a time constant of the order of 1 microsecond.[31] Because this time constant is small compared to other decay time constants, it may be used as an indicator of the presence of a substantial interface layer. The interface resistance can cause substantial voltage drops; tens of volts have been observed, and, if not corrected for in emission measurement, may lead to very pessimistic estimates of the actual emission capabilities of the cathode.[32] Under high current density conditions, the joule losses in the interface layer may become large enough to cause sparking. The interface layer and its concomitant difficulties may be avoided, at least for thousands of hours, if the silicon content of the base metal is held below about 0.01 per cent. Other reducing agents also form interface layers, but their conductivities seem to be high enough so that no substantial voltage drops appear across them. Because the interface layer is not a necessary and inherent part of a cathode, and because it presents a separable problem when present, it will receive little further attention, per se, in the present paper.

The next region of the cathode consists of the bulk oxide. The bulk oxide is considered to be an impurity semiconductor of high conductivity in its "active" state. Its electronic structure is discussed below. Electrically, it gives rise to voltage drops which are small compared to those observed across interface layers.

The fourth region is the emitting surface which probably has a dipole layer.

Some investigators find evidence that the region immediately to the left of the emitting surface in Figure 1 exhibits characteristics quite different from those of the bulk oxide.[33,34] In particular, they find that its conductivity is very much lower than that of the bulk oxide and that it is the source of substantial voltage drops. This is a matter on which new evidence will be presented in a later section of the paper.

Figure 2 shows an energy-level diagram of a barium-oxide cathode in a relatively active state. It is assumed that there is no current flow so that the system can be considered in thermodynamic equilibrium. The filled band has been set at 3.8 electron volts (e.v.) below the edge

---

[31] A. Eisenstein, "The Leaky-Condenser Oxide Cathode Interface," *Jour. Appl. Phys.*, Vol. 22, pp. 138-148, February, 1951.

[32] See Reference (3).

[33] R. Loosjes, H. J. Vink, and C. G. J. Jansen, "The Potential Distribution in Pulsed Oxide-Coated Cathodes and Its Consequences for the Velocity Distribution of the Emitted Electrons," *Jour. Appl. Phys.*, Vol. 21, p. 350, April, 1950 (L).

[34] R. Loosjes, H. J. Vink, C. G. Jansen, "Thermionic Emitters Under Pulsed Operation," *Philips Tech. Rev. 1*, Vol. 13, pp. 337-345, June, 1952.

of the conduction band.[35,36] The electron affinity has been set at 0.7-1.0 e.v. above the bottom of the conduction band.[36-38] Two sets of energy levels in the forbidden gap are shown, one set of levels at 2.3 e.v. below the conduction band,[36] and a second set of levels at 1.4 e.v. below the conduction band.[39] It seems possible that there are acceptors just above the filled band. In activated cathodes these seem to be overridden by the donors. Arizumi and Narita report that BaO shows p-type conductivity at oxygen pressures of 10^{-1} to 100 millimeters of mercury.[40] These results can be construed in either of two ways, 1) that excess oxygen forms acceptor sites, or 2) that "excess" oxygen removes donor sites so that acceptor sites already present predominate. It should be noted that DeVore[39] has found no evidence of donors
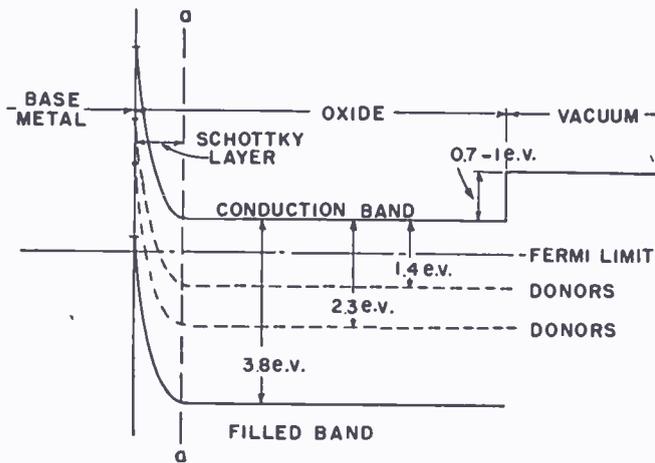
Fig. 2—The energy level structure of BaO.

lying closer to the bottom of the conduction band than 1.4 e.v. The possible implications of this result will be discussed later.

Figure 2 shows a Schottky exhaustion layer adjacent to the base metal. In actual cathodes this layer does not exist or is exceedingly

[35] W. W. Tyler and R. L. Sproull, "Optical Absorptions and Photoconductivity in Barium Oxide," *Phys. Rev.*, Vol. 83, pp. 548-555, August 1, 1951.

[36] H. B. DeVore and J. W. Dewdney, "Photoconductivity and Photoelectric Emission of Barium Oxide," *Phys. Rev.*, Vol. 83, pp. 805-811, August 15, 1951.

[37] L. Apker, E. Taft, and J. Dickey, "On the Photoelectric Emission and Energy Structure of BaO," *Phys. Rev.*, Vol. 84, pp. 508-511, November 1, 1951.

[38] J. A. Krumhansl, "Energy Levels in BaO," *Phys. Rev.*, Vol. 82, p. 573, May 15, 1951.

[39] Private communication from H. B. DeVore.

[40] T. Arizumi and S. Narita, "Application of Nyboer's Theory to the Semiconducting Emitters and its Modification," *Phys. Rev.*, Vol. 85, p. 388, January 15, 1952.

thin. It has long been known that the base metal has little effect on the performance of a cathode. Therefore, a potential barrier amounting to the difference between the work function of the metal and the electron affinity of the semiconductor seems out of the question. The barrier may be removed by the formation of a barium layer with a strong dipole moment at the interface or by a high density of surface states on the oxide.[41] In either event, the experimental evidence indicates that the base metal interface should have been shown as lying on a line such as $a - a$ in Figure 2.

ANOMALIES IN THE BEHAVIOR OF OXIDE CATHODES

While the model discussed in the previous section may be a reasonable representation of the situation under conditions of thermodynamic equilibrium, it appears inadequate under conditions of current flow. The major items, "anomalies," for which it fails to account are:

1) False Boltzmann Temperatures

It is a common experience to find that the cathode temperatures derived from retarding field plots on diodes of good geometry are higher than the pyrometric temperatures. This situation obtains even when cathode resistances are taken into account.[42] Heinze and Hass have reported a set of experiments in which they found excellent agreement between Boltzmann and pyrometric temperatures up to about 1200°K.[43] Fan reports similar agreement.[44] There are other reports of agreement between Boltzmann and pyrometric temperatures, for example that of Hung.[45] However, all of the recent reports that have come to the writer's attention, including Fan's, extend to a maximum temperature of about 950°K. This is the temperature range in which reasonably good agreement is found in this laboratory. Above 1000°K, however, a marked deviation between Boltzmann and pyrometric temperatures is found. This is illustrated in Figure 3, which shows the retarding field and pyrometric temperatures of an oxide cathode versus

[41] J. Bardeen, "Surface States and Rectification at a Metal Semiconductor Contact," *Phys. Rev.*, Vol. 71, pp. 717-727, May 15, 1947.

[42] W. R. Ferris, "Some Characteristics of Diodes with Oxide-Coated Cathodes," *RCA Review*, Vol. 10, pp. 134-149, March, 1949.

[43] W. Heinze and W. Hass, "Determination of Oxide Cathode Temperature from Retarding Field Emission Characteristics," *Zeit. f. Tech. Physik*, Vol. 19, pp. 166-180, 1938.

[44] H. Y. Fan, "Thermionic Emission from Oxide Coated Cathodes," *Jour. Appl. Phys.*, Vol. 14, pp. 557-560, October, 1943.

[45] C. S. Hung, "Thermionic Emission from Oxide Cathodes: Retarding and Accelerating Fields," *Jour. Appl. Phys.*, Vol. 20, pp. 37-43, January, 1950.

heater power. It will be noted that the temperatures diverge with increasing heater power and the disparity amounts to about 300° at a pyrometric temperature of about 1250°K. These measurements were obtained on a cylindrical diode of good geometry. The Schottky formula for cylindrical structures was used, and corrections for the emissivity of the cathode and bulb absorption were computed. None of these corrections accounts for the observed disparity in temperatures above a pyrometric temperature of about 1000°K.
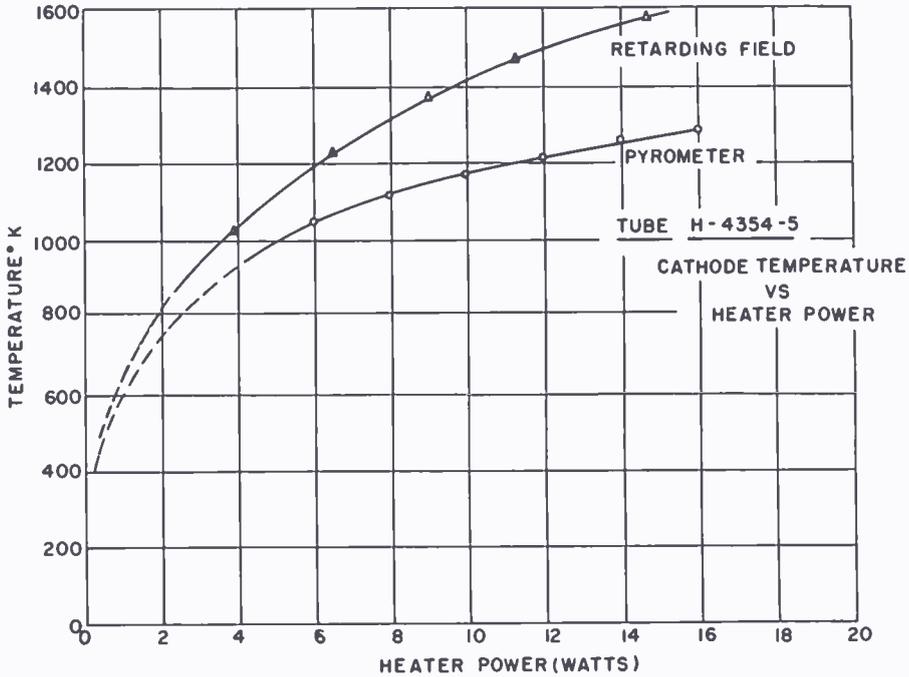
Fig. 3—A comparison of the temperature of an oxide cathode as determined by pyrometric measurements and by retarding-field measurements.

2) False Schottky Temperatures

With oxide cathodes, it is common to find Schottky slopes corresponding to about room temperature or to find that Schottky plots have no region in which the points lie along a straight line. Figure 4 shows the Schottky plot of a tube operating under 5-microsecond pulse conditions. The cathode area is about 13 square centimeters and the cathode temperature is 1100°K. The points have been corrected for the effects of residual space charge.[1] The points fall more or less on two straight lines, neither of which has a slope that bears any apparent relation to the cathode temperature. The steeper slope corresponds to about 150°K and the lower slope to about 450°K.

In the course of pulse-decay and recovery studies,[1] current-voltage characteristics were taken at various times throughout the decay and recovery of the anode current. These characteristics all appear to be

the same in form and to differ by a scale factor only. Accordingly, all of the characteristics were normalized to the same peak current and were found to coincide within the experimental accuracy (see Figure 7). The resulting curve is plotted in Schottky coordinates in Figure 5. The curve defies any attempt to connect three consecutive points by a straight line.
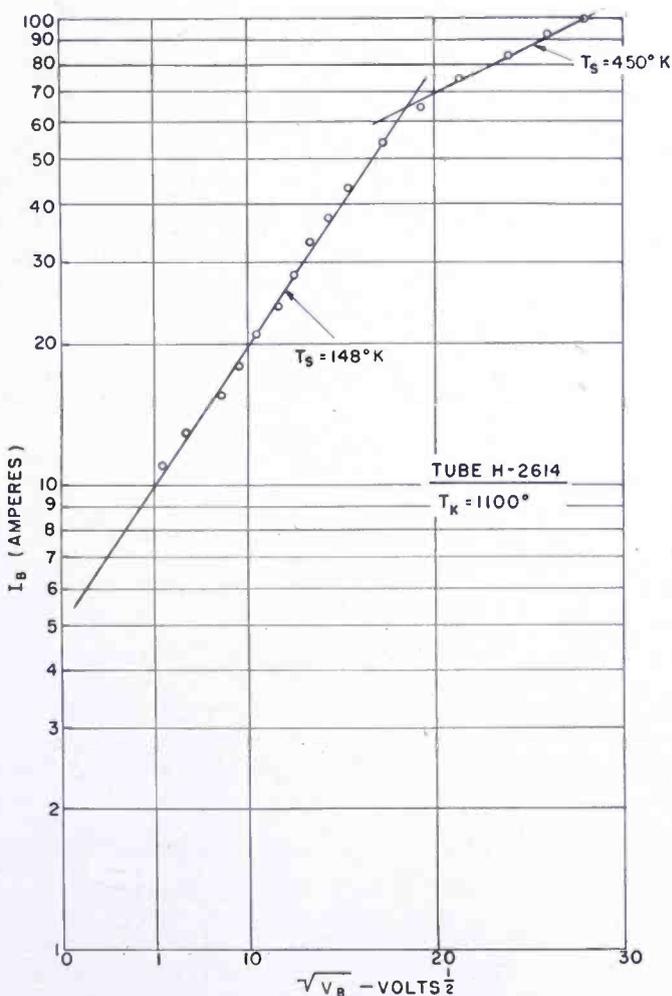
Fig. 4—The anomalous Schottky lines of a diode-connected triode under 5-microsecond-pulse conditions. The cathode was coated with (BaSr)O and has a coated area of about 14 square centimeters.

Many examples of this anomalous behavior are to be found in the literature. Blewett cites a number of examples.[22] A recent example is to be found in the paper of Horak.[46] He finds linear Schottky plots for temperatures up to about 900°K. However, the slopes of his lines are very similar regardless of cathode temperature. A computation of

[46] F. A. Horak, "Correlation of DC and Microsecond Pulsed Emission from Oxide Coated Cathodes," *Jour. Appl. Phys.*, Vol. 23, pp. 346-349, March, 1952.

the apparent Schottky temperature using the plots and the cited cathode–anode spacing yields a value of about 290°K.

The observation of Schottky lines with slopes corresponding to temperatures other than that of the cathode temperature raises questions about the meaning of cathode emission when it is defined as the intercept of a Schottky plot. The use of Schottky plots to determine
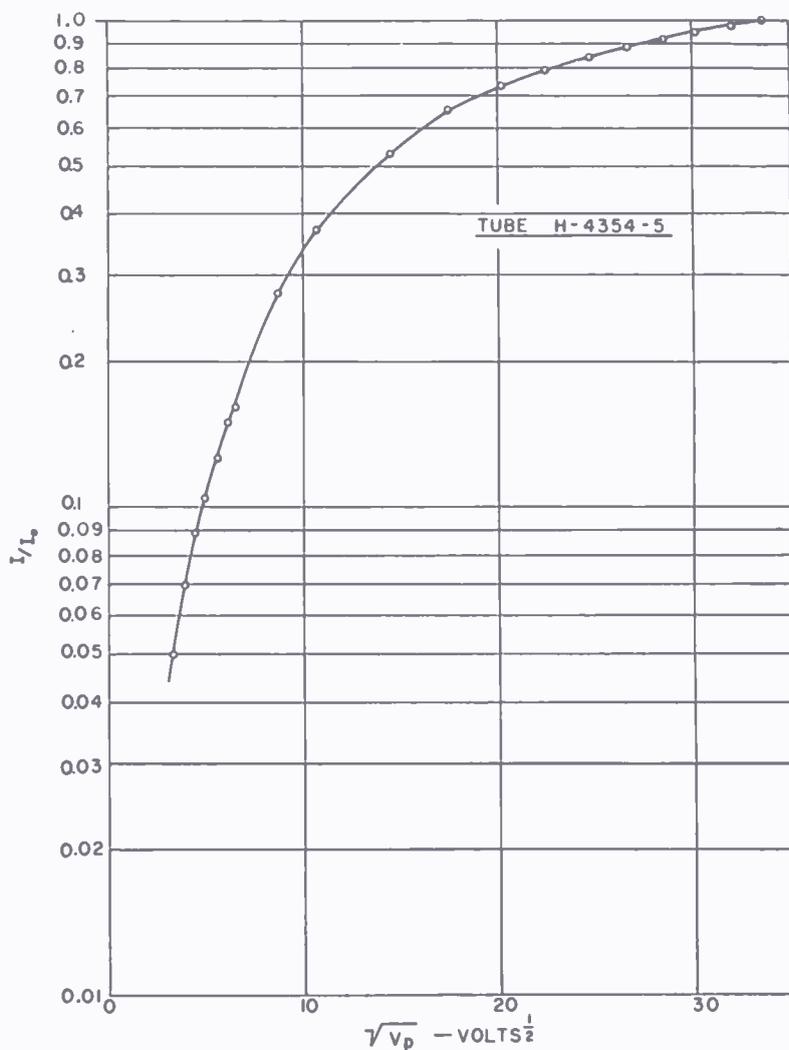
Fig. 5—A Schottky plot of the current–voltage characteristics of a diode.

the field-free emission of a cathode assumes a model for the cathode resembling the Sommerfeld model for a metal, and, in particular it assumes that the surface may be represented by a potential barrier whose height varies with the electric field external to the surface in accordance with simple image-field considerations. This model is borne out experimentally for metals. It is not obvious, a priori, that the same model applies to semiconductors. It seems reasonable that such

a model should apply if the electron density in the conduction band or the density of surface states is high enough so that image theory applies. However, when theory is not matched by experiment, theory is frequently at fault, and the present writer feels reluctant to accept a definition based on a model which apparently does not accord with experiment in major details. When he sees a Richardson plot based on the intercepts of Schottky curves whose slopes correspond to the actual cathode temperature, he will admit that the emission of the cathode, in the usual sense, has been measured. He knows of no such measurements. An acceptable alternative is the construction of a model which does accord with experiment and the definition of emission in terms of this model. Such a model will be discussed after aditional experimental data has been adduced.
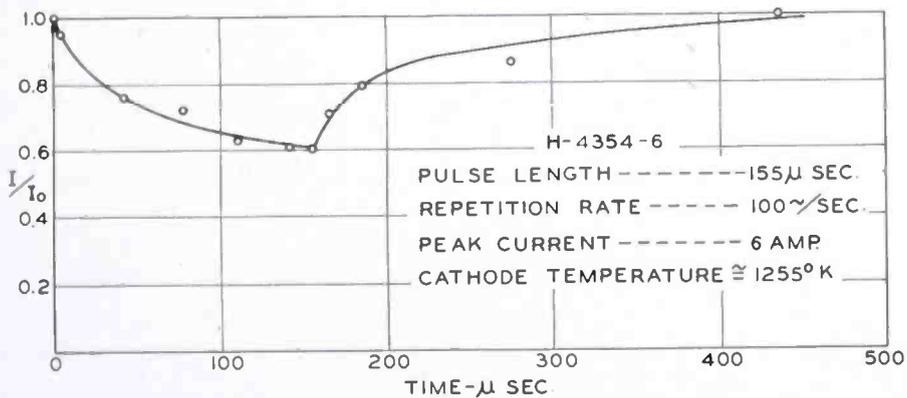
Fig. 6—The decay and recovery of the anode current during and subsequent to a pulse.

3) *"Temperature-Limited" Current Decay*

Sproull and Matheson and Nergaard have studied the decay of the pulsed "emission" of oxide cathodes with pulse lengths ranging from a few microseconds to seconds.[1,15] Sproull attributed the decays to actual emission decay and developed a theory involving the electrolytic depletion of the emitting-surface dipole layer to account for his results. The form of decay predicted by the theory is in good agreement with the experimental results. It should be noted that his particular model is not unique in giving this type of decay. Matheson and Nergaard found similar decays. The form of the decay curves can be fitted quite satisfactorily by Sproull's decay formula. By the use of a short sampling pulse subsequent to the main pulse, the recovery of the cathode after pulse decay was measured. A typical decay and recovery cycle is shown in Figure 6. The pulse shows a decay of about forty per cent in 155 microseconds. The points to the right of 155 micro-

seconds on the time scale show the current available at various times after the main pulse has ceased. The sampling pulse was also used to trace out the current–voltage characteristics of the diode during recovery. Further, the sampling pulse was inverted and used to trace current–voltage characteristics during the decay. All of the current–voltage characteristics appeared to have the same form. When the characteristics are normalized to the same peak current, they coincide within the experimental accuracy, as shown in Figure 7. This behavior
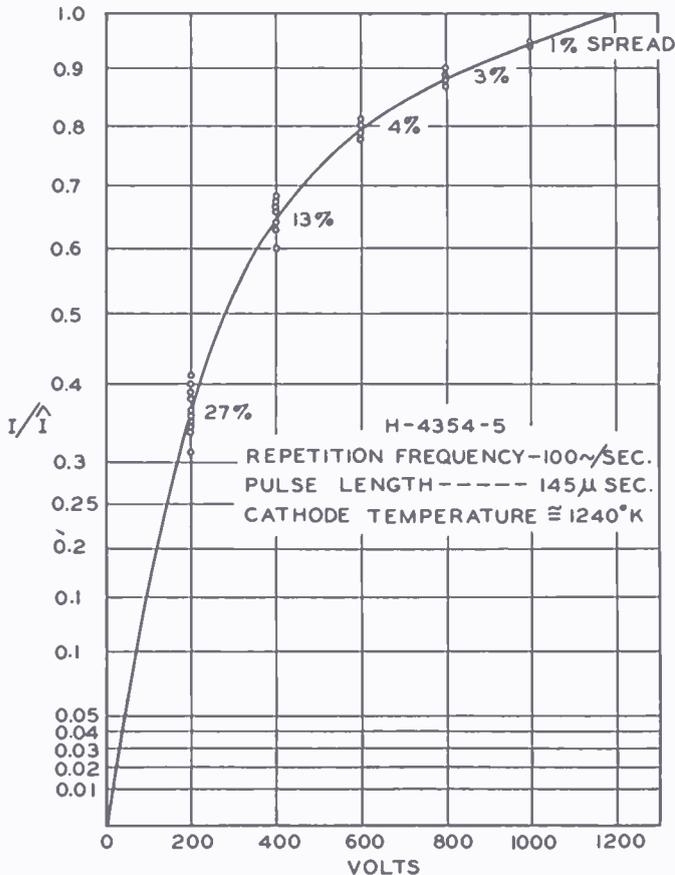
Fig. 7—Decay and recovery voltage-current characteristics of a diode normalized to the initial pulse current.

hardly accords with a simple emission limitation in the accepted sense. If the current decay were a simple emission decay, the behavior would be as shown in Figure 8. In the region of complete space-charge limitations, the characteristics would follow the perveance line; then, as emission limitation sets in, the characteristics should break away from the perveance line and approach Schottky curves. A "normalization" of these characteristics, such as was used in Figure 7, would not bring all of the characteristics into coincidence. These results suggest

strongly that the decay process is not a simple emission decay, but involves substantial voltage drops within the cathode.

In the above experiments, the peak pulse current was limited by sparking at the end of the pulse. The incidence of sparking seems to be governed by the rough rule that the product of peak current and pulse length be a constant. The sparking which occurs when the product
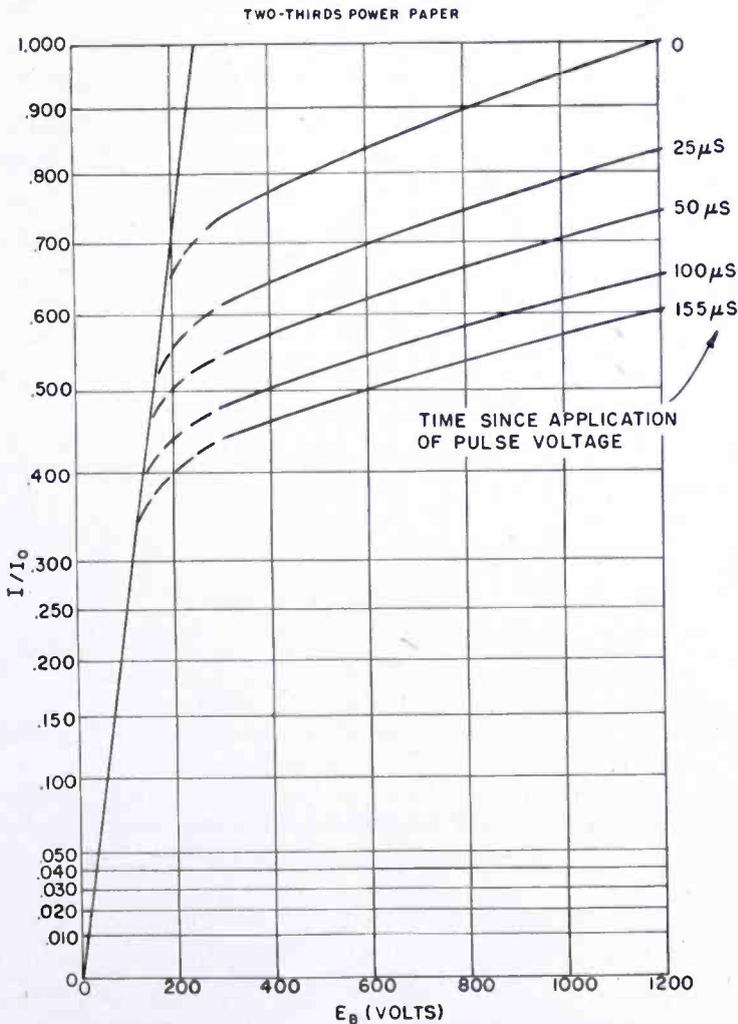
Fig. 8—Computed curves showing the form of the voltage–current characteristics during current decay if the current were emission limited.

exceeds the constant is not disruptive if the vacuum is good so that no gas discharge is possible, the cathode surface shows no pitting as a result of the sparking, and the cathode invariably activates as a result of sparking. The possible implications of this behavior will be discussed later in the paper.

It is found that cathodes which have been operated at high pulse currents for a hundred hours or so may show no decay in the course

of a 300-microsecond pulse. However, the peak current which may be drawn without sparking remains a function of the pulse length. Over a considerable range of operating conditions, the peak current which may be drawn varies in a simple manner with duty, as shown in Figure 9. In these experiments, the peak current was limited by anode dissipation, not by the cathode itself. The cathode is capable of about 40 amperes per square centimeter under 1-microsecond pulse conditions. Figure 9 also shows that the pulsed and direct currents approach one another as the cathode temperature is reduced and, at temperatures below about 800°K, pulsed and direct currents may be much the same. The correlation between direct-current and pulsed emission has been
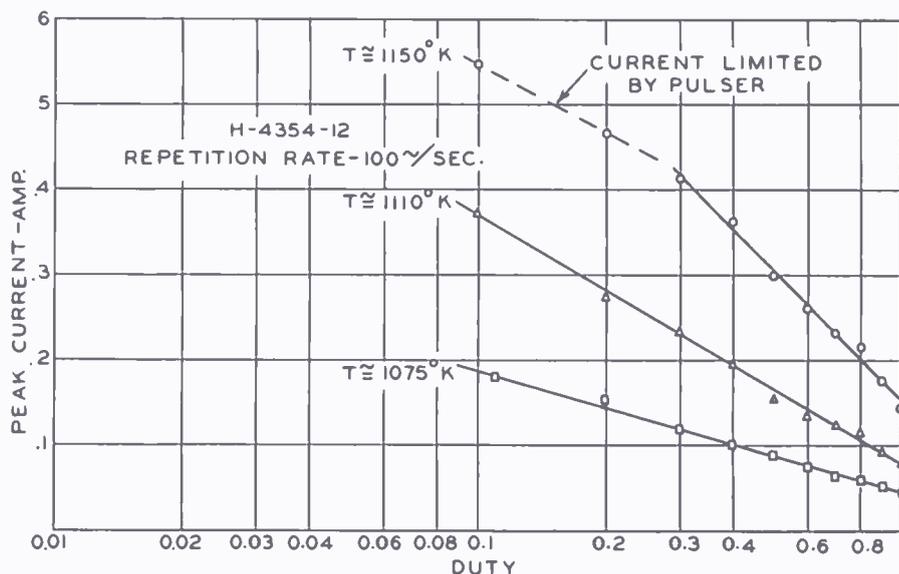
Fig. 9—The peak pulse current of an oxide cathode as a function of duty with cathode temperature as a parameter. Throughout the dotted section of the upper curve, the current was limited by the pulser, not by the cathode.

studied by many, e.g., Horak. The general result of these studies is the conclusion that there is no difference between pulsed and direct-current emission.[46] However, all of these studies, with two notable exceptions to be cited below, have been confined to the low-temperature region. The results in this low-temperature region accord with experience in this laboratory. However, the results shown in Figures 6 and 9 suggest that the one-to-one correspondence between pulse and direct-current emission found at low cathode temperatures should not be extrapolated into the high temperature range.

A further example of pulse decay is shown in Figure 10. The figure shows the decay of current over a period of 1 second on application of a "unit-function" voltage. It should be noted that there is no substantial decay during the first few hundreds of microseconds, an example

of a behavior cited above, and that the current decays to about the direct-current level in a tenth of a second. The peak current in this example is limited by the plate voltage which may be applied without exceeding the anode dissipation capabilities of the tube.

The cause of current decay has been the source of much speculation. Sproull attributed the decay to an internal mechanism of the cathode. However, the literature shows a general inclination to attribute the decay to the release of "poisoning agents" from the anode or other surfaces under electron bombardment. The studies of Fineman and of Dillinger are frequently cited to support this thesis. Fineman obtained a direct-current emission of 14 amperes per square centimeter for several hours at 1175°K and Dillinger obtained direct-current emission of 18 amperes per square centimeter at 1100°K.[47] These re-
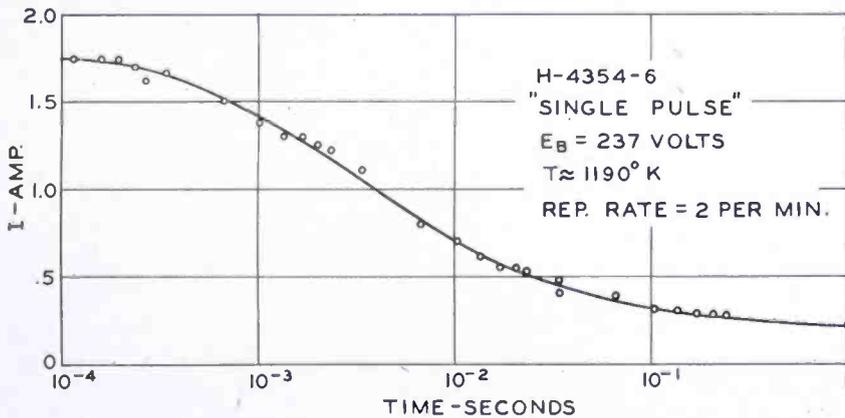
Fig. 10—The decay of the anode current of a diode on application of a unit-function voltage.

markable results are attributed, at least in part, to the elimination of contaminants in their tubes. While these experiments seem to be unique, the writer inclines to the view that the explanation of the results is not. There are circumstances when a cathode may become "self-activating" so that decay effects are offset by the activation. This behavior is usually not stable. However, stability for a matter of hours might be achieved by proper controls. This subject will be elaborated upon later.

Whatever the explanation of the phenomenal results cited above, the observation of decay is general. It occurs in gas rectifiers as well as in vacuum tubes. If the decay were due to gases liberated from electrodes in vacuum tubes, it might be expected that the decay might be much more severe in gas tubes. The fact is that the decays observed in gas tubes and vacuum tubes are much the same. A rather crude

---

[47] Cited by Eisenstein in Reference (23).

experiment on the effect of gas pressure on pulse decay may be worth citing in this connection. The tube on which the experiment was performed had a cylindrical oxide-coated cathode with a platinum probe imbedded in the coating and a nickel anode surrounding the cathode, all sealed into a glass envelope. The tube was provided with a batalum getter to clean up gases evolved in the course of the experiment. The tube was operated with 1000-microsecond pulses, about 100 volts amplitude, and a 60-cycle per second repetition rate. The plate current was observed to decay about 30 per cent in the course of the pulse. It was also observed that the probe voltage rose about 10 volts with respect to the cathode base in the course of the decay. This is direct evidence of a change in internal impedance of the cathode during decay. The gas pressure in the tube was then raised by torching the glass envelope, a process supposed to be very deleterious to cathodes. There
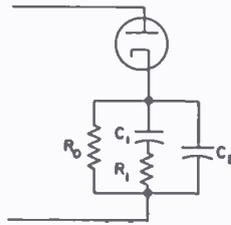
EQUIVALENT CIRCUIT

Fig. 11—The equivalent circuit of a diode with an oxide cathode. The diode shown is presumed to obey the Child–Langmuir Law.

was no significant change in the current decay or the probe behavior until the gas pressure rose so that a blue glow was observed. Then the decay increased quite abruptly. By alternately heating the envelope and partially flashing the getter, the experiment was cycled a number of times. Perhaps this experiment is also unique. However, the general performance of oxide cathodes in gas rectifiers belies this assumption.

4) Space-Charge-Limited Current Decay

The previous section discussed current decay where it was assumed that the current was limited solely or principally by the emission process. The experimental evidence cited renders the assumption dubious, and it may be that in the low-current examples the vacuum voltage drop was determined by space-charge considerations.

There is a relatively simple method of determining whether or not the vacuum drop is determined by space charge: A study of the decay characteristics of diodes under low-current conditions (up to 2 amperes per square centimeter) led to the equivalent circuit for a diode shown in Figure 11. The diode shown in the equivalent circuit is a "good"

diode, i.e., a diode which satisfies the Child-Langmuir Law. The network representing cathode impedance comprises a resistance R_0, which in practical tubes has values ranging from a few ohms to thousands of ohms; a resistance R_1, which is usually 5–10 times R_0; a capacitance C_1 which, together with R_0 and R_1, yields a time constant of the order of a millisecond; and a capacitance C_2 which, in combination with the resistances, yields a time constant of about a microsecond. The capacitance C_2 is associated with interface-layer effects and is of no concern in a discussion of long time decays. Having found a suitable equivalent circuit, it is possible to compare "unknown" diodes with "synthetic" diodes of known characteristics in a circuit such as shown in Figure 12. In this circuit, the "unknown" diode at the right and the synthetic or standard diode on the left are driven from a common alternating-current voltage source. The current of the unknown is displayed along the horizontal axis of an oscilloscope display and the current of the
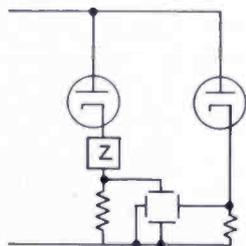
COMPARISON CIRCUIT

Fig. 12—A comparison circuit for determining the cathode resistance of an oxide cathode.

standard along the vertical axis of the display. The network of Figure 11 is adjusted until a straight line is observed on the oscilloscope screen. Then the impedance of the unknown is related to the known impedance of the standard by the simple relation

$$P_x Z_x = P_s Z_s,$$

where Z is the impedance of the network and the symbol P denotes perveance, the subscript x refers to the unknown, and the subscript s refers to the standard. If no adjustment of Z produces a straight line, the diodes may be driven so hard that the cathode impedance of the unknown is not linear and cannot be matched by linear network of the standard, or one or the other of the diodes may be emission limited. In the latter case, the identity of the emission-limited diode may be determined from the curvature of the displayed characteristic. The same measurement of cathode impedance may be made with more precision with the bridge circuit of Figure 13. The details of the bridge will be described elsewhere. It suffices to note here that the standard

comparison diode is a pulse-heated tungsten-filament tube and is free of the complications being studied.

The mere existence of an equivalent circuit such as shown in Figure 11 implies the existence of decays under conditions of space-charge limitation of the current across the vacuum. It merely remains to verify that the equivalent circuit measured under one set of operating conditions, namely, "half-sine-wave" operation, is valid under other operating conditions. This has been done in two ways. First, the equivalent-circuit parameters of a number of diodes have been determined from bridge measurements and from pulse measurements, and have been found to agree. Second, the equivalent-circuit parameters of a number of diode-connected triodes, i.e., triodes with the grid and anode connected together, have been measured with the bridge. In a triode, the cathode impedance is degenerative and pro-
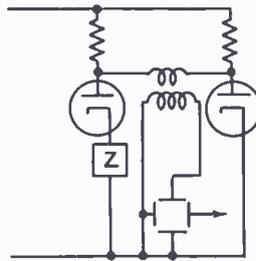
BRIDGE CIRCUIT

Fig. 13—A bridge circuit for determining the cathode resistance of an oxide cathode.

duces an apparent decrease of the transconductance. Because the cathode impedance is frequency sensitive, the apparent transconductance is also frequency sensitive. From measurements of the apparent transconductance of the triodes at three appropriate frequencies, the three pertinent circuit parameters of the equivalent circuit $(R_o, R_1 C_1)$ may be computed. The parameters determined in this way agree with those found by the bridge method. It should be noted that if the impedance were due to semiconducting material on the anode of a triode, it would not degenerate the transconductance.

It seems quite clear that there are current decays due to the cathode in which the emitting surface of the cathode plays no role.

5) *Extraneous Effects*

It may be inferred from the foregoing discussion that the writer is inclined to ignore anode effects. This is not the case. His contention is that anode effects are not the only possible source of decay phenomena.

A number of anode effects are known and recognized. The simplest anode effect, simple in that it is stable under a wide variety of operating conditions, is the so-called high-speed ten-volt effect.[2] This effect manifests itself in a departure from the Child-Langmuir Law at about 10 volts anode voltage. Examples of the effect are shown in Figures 14 and 15. Figure 14 shows a diode characteristic in the low-voltage range and illustrates the abrupt break when the effect sets in. Figure 15 shows the departure from the three-halves law up to 100 volts. The effect is caused by secondary emission from the BaO inevitably evaporated from the cathode onto the anode. It is
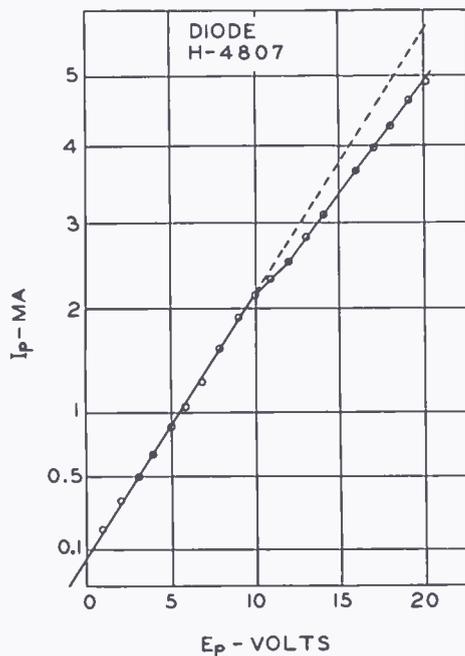
Fig. 14—A diode characteristic showing the onset of the high-speed ten-volt effect.

pertinent to inquire whether or not this deposit produces other effects. In view of stability of the effect under widely varying temperature conditions, it seems unlikely that re-evaporation of the BaO or dissociation of the oxide under electron bombardment with a release of oxygen play roles. There is an effect of this sort which may be confused with the present effect. This second effect will be discussed below. The most likely secondary effect of the deposit under discussion is to display a resistance. The deposited material is probably semiconducting, in which case the resistance should have a marked temperature dependence. Such a temperature dependence was sought. Two diodes in which the copper anodes formed part of the envelopes were checked in the temperature range from —196°C to +250°C.

The first showed no change in 10-volt effect over this temperature range. The second showed a resistance which increased as the anode temperature was reduced. On opening the second tube, the anode was found to have a very heavy black deposit on the anode, a deposit very much heavier than one usually finds in such tubes. Nickel and tantalum anode diodes were checked from ambient temperature to 1600°K
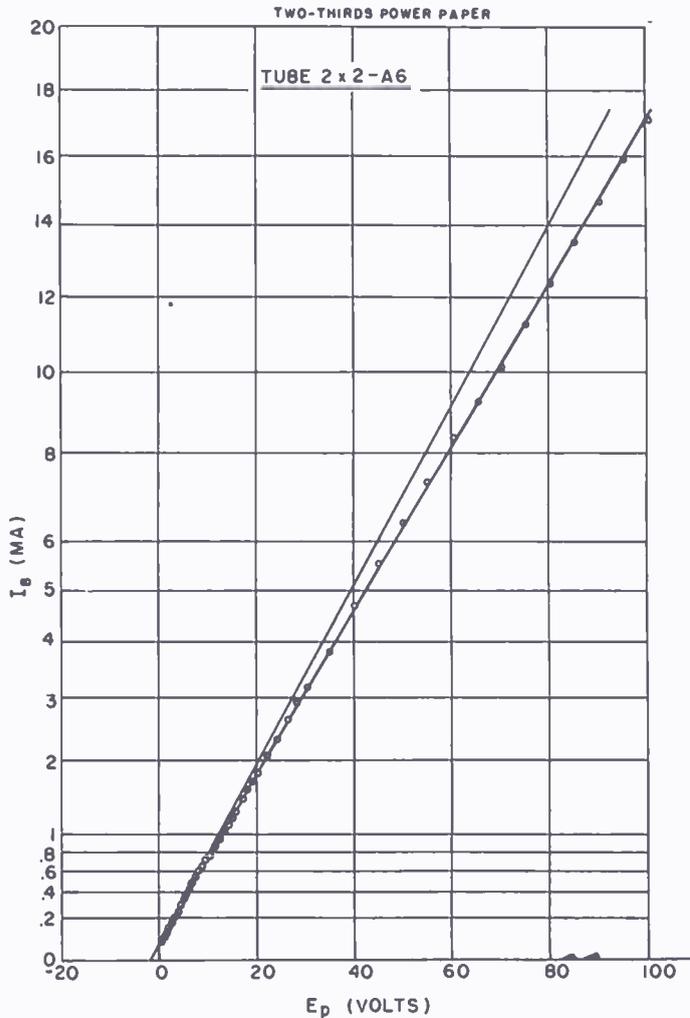
Fig. 15—A diode characteristic showing the magnitude of the high-speed ten-volt effect in the high-voltage region.

with no observed change in the effect. It seems that, if the anode is reasonably clean, the deposit does not contribute a significant resistance at the normal operating temperatures of the anodes.

The second recognizable effect, mentioned above, is the so-called ten-volt slump. This effect usually occurs during the initial activation of the cathode. As the anode voltage is raised during the activation, a severe emission slump may set in abruptly at a rather critical anode

voltage. For mixed oxides at 1050°K, the slump sets in at about 10 volts anode voltage, and seems to be much more severe in close-spaced diodes. Because the effect sets in at an electron energy corresponding to the heat of dissociation of BaO, it has, on occasion, been ascribed to the dissociation of BaO by electrons and poisoning of the cathode by the freed oxygen.
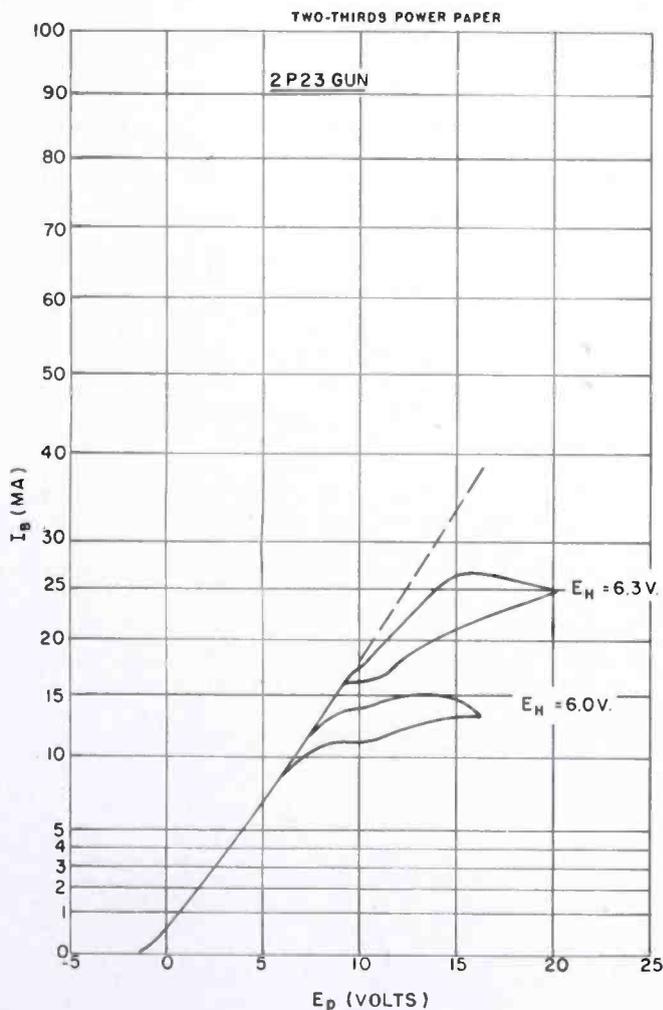
Fig. 16—A diode characteristic showing the ten-volt slump at two cathode temperatures.

To explore the effect in a little more detail, the poisoning effect was studied in a very close-spaced diode, a cathode-ray gun with the first grid used as the anode. It was found possible to keep the effect from completely deactivating the cathode by using a 60-cycle per second anode voltage. The current–voltage characteristic of the diode then appeared as shown by the curve marked $E_H = 6.3$ volts, in Figure 16. It was soon found that the incidence of the effect was temperature sensitive. A diode characteristic at a reduced cathode

temperature is marked $E_{II} = 6.0$ volts in Figure 16. Figure 17 shows the anode current and the anode voltage at which the effect was incident against reciprocal temperature. This result casts doubt on the BaO dissociation hypothesis. The effect is remarkably critical to cathode temperature, *not anode temperature*. It was found that the cathode–heater voltage could be set within a tenth of a volt by the
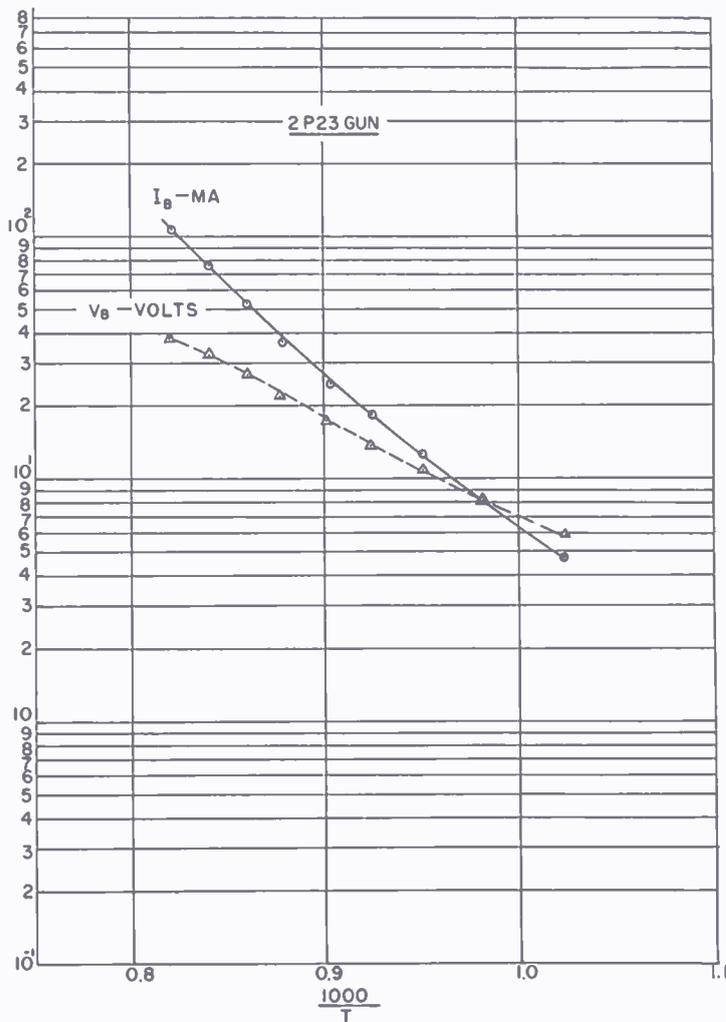
Fig. 17—A plot showing the anode current and the anode voltage at which the ten-volt slump is incident, as a function of cathode temperature.

process of adjusting the cathode temperature so that the slump was incident at an anode voltage corresponding to the desired heater voltage. It should be pointed out that the incidence of the high-speed ten-volt effect in the same voltage range as the incidence of the 10-volt slump must be recognized to avoid confusion in separating the two effects.

The slump effect deserves more study. While the effect is not

understood, at least by the writer, the cure is simple. It consists in running all the electrodes at a dull red heat, the cathode preferably hotter, throughout cathode activation. All of the electrodes must be run hot at the same time. If the electrodes are heated in succession, the contaminants merely move from a hotter electrode to a cooler electrode, an effect known as the "fruit-fly" effect. When all of the electrodes have been run hot during activation, the slump has never appeared in any tube studied here. Needless to say, this method of activation is used whenever it is feasible.

To summarize the contents of the entire section, its burden has been:

1) At sufficiently low cathode temperatures, the behavior of the oxide cathode is much like that of metals, except for Schottky temperature difficulties.

2) At cathode temperatures about $900°K$, irregularities appear. These are:

  a) False Boltzmann temperatures,
  b) False Schottky temperatures,
  c) Current decay under what seems to be emission-limited conditions,
  d) Current decay under space-charge-limited conditions.

3) The anode may play some role in these effects. However, the present state of knowledge of anode effects suggests that they play a minor role if proper precautions are taken during exhaust of the tube and activation of the cathode.

4) No existing hypothesis accounts for the effects in a coherent manner.

DONOR DEPLETION HYPOTHESIS

Because no existing hypothesis accounts for all of the anomalies discussed above, a new hypothesis to explain and relate them was sought. The hypothesis of Sproull[10] together with the work of Becker and Sears[15] on the diffusion and electrolysis of barium provided the foundation for the hypothesis to be advanced here, that of an electrolytic depletion of donors near the emitting surface when current is drawn.[4] Logically, it might be better to introduce this hypothesis after more experimental information has been adduced. However, chronologically, this is the point at which the hypothesis was formulated. Furthermore, the hypothesis guided subsequent thinking, and most of the experiments to be described were designed and carried out with this hypothesis in mind. In order that the reader may be aware of this background, the hypothesis is outlined here, without prejudicing him unduly, it is hoped.

In brief, the hypothesis is:

1) That the cathode is an impurity semiconductor. There is little question about this.

2) That the donors are mobile; can electrolyze and diffuse. This behavior is suggested by the work of Becker and Sears.

3) That when no current is drawn, the donors are uniformly distributed through the cathode, and the situation is much as illustrated in Figure 2.

4) That when current is drawn, donors electrolyze towards the base metal, leaving a donor depletion layer near the emitting surface, said depletion layer having electronic properties approaching those of the intrinsic material.

5) That the donors do not plate out at the cathode base metal. If they did, cathode life would be much shorter than that observed.

6) That under equilibrium conditions, i.e., when the current through the cathode is stable, the electrolysis of donors is everywhere balanced by back diffusion.

The consequences of this hypothesis that bear on the anomalies discussed in the previous section are:

1) The position of the Fermi level is a function of the current drawn. Hence, false Boltzmann and Schottky temperatures are to be expected.

2) Under pulse conditions, the donor distribution changes during the time of a pulse. If the pulse length is sufficiently large, a current decay will appear. If the pulse current is small, the major decay will result from the increase in cathode resistance as the donor depletion layer forms. If the pulse current is large, i.e., near the emission limit of the cathode in its equilibrium state, the major decay will result from an increase in work function as the electron density in the depletion layer falls. The recovery after a pulse is the result of the diffusion of donors back into the depletion layer. If the pulse repetition rate is high, the back diffusion may not be complete before the next pulse starts and the peak current attainable becomes a function of duty cycle.

3) The voltage gradients in the depletion layer may be substantial. This behavior has been noted in the literature.[34] At high current densities, the gradients may become large enough to cause a breakdown which manifests itself as sparking. The breakdown may conceivably form donors, thus leading to the observed activation under what may be called "surface-sparking" conditions.

4) The donor mobility is temperature dependent. This is certainly reasonable. Then the major anomalies should appear at the higher

cathode temperatures, and the cathode behavior should become regular at low temperatures where the donors are "frozen" into the lattice.

5) The donor depletion layer is thin. Hence, the behavior of the cathode is independent of the cathode coating thickness for thicknesses exceeding approximately 10^{-3} centimeter.

While the proposed model encompasses the major behaviors of the oxide cathode, it must also satisfy other requirements, the first and foremost being the fact that it must be physically reasonable.

The remainder of the paper will be concerned with experiments intended to test this point. These experiments include:

1) Direct-current and pulse studies of insulators at elevated temperatures with a view to ascertaining possible voltage distributions in the insulators and the nature of their current-decay characteristics under pulse conditions.

2) Studies of the conductance of cathodes as a function of temperature and current and the separation of bulk conductivity effects from possible depletion-layer conductivity effects.

3) Work-function studies to ascertain the effects of depletion on the work function.

4) Cathode-activation studies to shed light on the nature of the donors.

5) Deposition studies in which donors or activating agents are deposited on the emitting surface during current flow in an attempt to inhibit depletion layer formation.

6) Deposition experiments in which donors or activating agents are deposited on the cathode in an attempt to establish permanent activation.

Experiments on Electrolysis in Solids

The experiments described in this section were intended to show that electrolysis in solids can result in decays of the kind found in oxide-coated-cathode tubes, and to examine the voltage distribution arising from decays. The first material studied was "Pyrex" glass. The choice of "Pyrex" glass as a material to study may be little startling. The explanation is that the first measurements on "Pyrex" glass comprised a "Friday afternoon" experiment. Friday is frequently devoted to a consideration of the week's activities. It often happens that there is a small amount of information needed to complete a story. The problem, then, is to devise an experiment which may provide the required information — an experiment that can be performed in an hour or two. At the time, we were thinking about electrolysis in $2\,BaO \cdot SiO_2$ which we suspected might behave similarly under pulse conditions. Now

$2\,BaO \cdot SiO_2$ is a silicate and so is "Pyrex" glass. The latter was immediately available, so it was used in the Friday afternoon experiment.

The results of this experiment are exhibited in Figure 18 which shows the decay characteristic of a "Pyrex" glass disc of 1.5 millimeters thickness, 15 square centimeters area, operated in an oven at 1075°K. The electrodes were of silver paste, the voltage across the sample was 45 volts. The decay characteristic of a diode (that of Figure 10) has also been plotted for comparison. It will be noted that the peak currents are much the same and that the decays have much the same form.
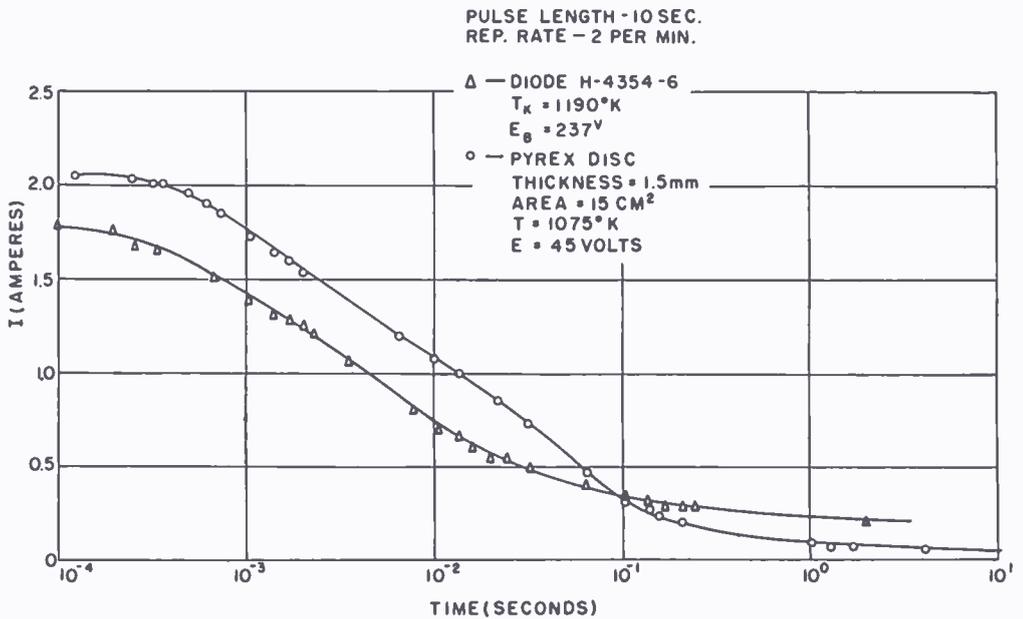
Fig. 18—The current decay on application of a unit-function voltage in a "Pyrex" glass disc at 1075°K, and in a diode for comparison.

The similarity between the decay characteristics of a BaO cathode and a "Pyrex" glass disc at comparable temperatures may be pure coincidence. In any event, it is of interest to ascertain the voltage distribution on a "Pyrex" glass sample where measurements are easily made because no vacuum is required. The physical arrangement for and the results of such an experiment are shown in Figure 19. The sample is a cylinder of "Pyrex" glass, provided with platinum end electrodes and with two intermediate platinum bands, all painted and fired onto the glass. The sample was operated in an oven at a temperature of 600°K. with a constant current of 5 microamperes flowing from end to end. The low temperature was chosen so that decay effects would proceed slowly and would permit manual adjustment of the voltage source to maintain constant current, and ample time to make voltage measurements across the sample and at the probe rings. Some

time after the initial application of voltage, the voltage distribution
was as shown in curve (a) of Figure 19. At this time the current
was reversed, and the voltage measurements showed a distribution of
voltage as depicted by the chronologically consecutive curves (b), (c),
(d), and (e). In every case, substantially all of the voltage drop
occurred between the positive end of the sample and the adjacent probe
ring. All attempts to delimit the region in which the drop occurred by
moving probes toward the positive end failed. Recourse was had to
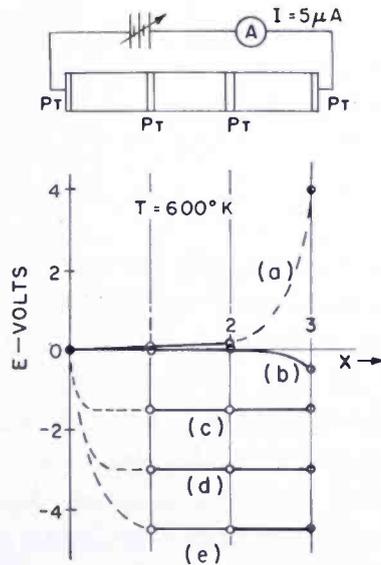
Fig. 19—The upper figure shows the physical arrangement of a "Pyrex"
glass cylinder for the measurement of the voltage distribution along its
length. In the lower figure, (a) shows the voltage distribution when the
applied voltage was reversed; (b), (c), (d) and (e) show successive voltage
distributions after reversal of the applied voltage.

electrical means. The sample was polarized with direct-current and
the capacitance of the depletion layer was measured. The interpreta-
tion of the result involves two assumptions: (1) that the alternating-
current voltage distribution is similar to the direct-current distribution,
(2) that the dielectric constant of the depleted layer is the same as
that of the "Pyrex" glass. If these assumptions are accepted, the
thickness of the depletion layer is of the order of 10^{-6} centimeter.
Table I shows two successive measurements of depletion layer
capacitance together with other quantities of interest. The sample
was operated at 885°K, at a constant current of one microampere.
In the table, V is the applied direct-current voltage; V_o is the voltage
across the depletion layer computed by subtracting the product of the
voltage gradient and the length of the sample from the applied voltage;

C is the measured capacitance; S is the depletion layer thickness computed under the assumptions mentioned above; E_o is the field strength in the depletion layer, assuming a uniform voltage distribution in the layer; R_o is the resistance of the layer; and R_o/S is proportional to the resistivity of the depletion layer. Several items are worthy of note:

Table I — Properties of an Electrolytic Depletion Layer in "Pyrex" Glass

V Volts direct current	V_o Volts direct current	C Farads	S Centimeters	E_o Volts per centimeter	R_o Ohms	R_o/S Ohms per centimeter
2.90	2.70	6.9×10^{-9}	2.2×10^{-6}	1.2×10^{6}	2.7×10^{6}	1.2×10^{12}
7.88	7.64	2.3	6.6	1.2	7.6	1.2

    1. The voltage across the sample increased linearly with time at a rate of ¾ volt per minute over the period of the measurement.

    2. The electric field strength E_o in the depletion layer remained substantially constant as the voltage rose. This implies that the current through the depletion layer is not displacement current. Hence, the current must be ionic or electronic.

    3. The computed field strength is exceedingly high.

    4. The apparent resistivity of the depletion layer remains constant and the increase in resistance is due solely to an increase in the thickness of the layer. This result also implies that the current is not space-charge limited in the depletion layer.

    The resistance of a "Pyrex" glass disc of 1.5 millimeters thickness, 15 square centimeters area, with platinum electrodes on opposite faces was measured under pulse and direct-current conditions. The direct-current readings were taken after the current had become stable at each temperature, the pulse readings at the beginning of the pulse, i.e., before decay set in. The results may be represented by

$$R_o = 8.7 \times 10^{-2}\, e^{\frac{10520}{T}} = \text{pulse resistance,}$$

$$R_x = R_o + 3.37 \times 10^3\, e^{\frac{5260}{T}} = \text{direct-current resistance.}$$

The measurements extended through the temperature range from 450°K to 1080°K. At sufficiently low temperatures, the pulse and direct-current resistances coincide. This accords with observations that voltage is uniformly distributed along "insulators" at low temperatures, so

that bulk properties determine the behavior. At higher temperatures, above 500°K, the depletion layer takes over and the direct-current resistance is determined almost entirely by the properties of the depletion layer. This behavior accords with one of the enumerated consequences of the donor depletion hypothesis. The low-temperature activation energy is about 0.9 volt, in accord with other low temperature data. The high-temperature activation energy is about 0.45 volt.

At low temperature, glass is known to be an ionic conductor. A question raised by the present experiments is as to the nature of the conduction at high temperatures, particularly in the depletion layer. A simple computation shows that, if the conduction were entirely ionic, the sample should have been etched about 10 per cent of the way through its thickness in the course of the above experiments. An examination of the sample showed that the platinum electrodes were still strongly adherent, in fact, an attempt to remove them mechanically proved too laborious. Hence, they were removed with aqua regia. One proved too laborious. Hence, they were removed with aqua regia. The interior of the glass was clear, but two surface effects were observed: a slight etching, and patches of a light red hue. Unfortunately, the sample was destroyed without noting whether these effects occurred on the same or opposite surfaces. Also, no record was kept of the polarity of the two surfaces. However, the lack of mechanical change in the sample makes it seem likely that the conduction is in part electronic at elevated temperatures.

It may be of interest to note that, whereas platinum does not electrolyze into the glass perceptibly, silver does. It appears to replace sodium during electrolysis and the resulting brown boundary is easily followed. Apparently silver does not fit into the crystallites too well because the glass is markedly disrupted throughout the discolored section.

At about this time, a sample of barium orthosilicate became available. The sample was prepared by H. W. Leverenz by firing barium oxide and silica in ortho proportion at 1360°C, until the reaction was complete. $2\,BaO \cdot SiO_2$ is known to be an electronic conductor at elevated temperatures. Hence, it seemed that a brief study of this material might be a little closer to the point than the measurements on "Pyrex" glass. Because $2\,BaO \cdot SiO_2$ is found at the oxide–metal interface in cathodes having silicon in the metal base, measurements on this material are also of interest in connection with interface problems.

The sample was a cylinder, $\frac{3}{8}$ inch in diameter and $\frac{1}{2}$ inch long. It was provided with platinum electrodes on its ends and a platinum probe ring about 1/16 inch from one end of the sample. These were

painted and fired on. Because the behavior of this sample followed the pattern of the "Pyrex" glass sample, the measurements made were less extensive than those on "Pyrex" glass. The pulse behavior at 1210°K, with a pulse voltage of 100 volts, is shown in Figure 20. The peak current was about 200 microamperes. It appeared that the conductivity of $2\,BaO \cdot SiO_2$ is very much lower than that of BaO or "Pyrex" glass at comparable temperatures. It does not follow that the conductivity of $2\,BaO \cdot SiO_2$ is equally low when it appears at the oxide—metal interface in a cathode. In the cathode, one of the electrodes on the silicate is BaO. Furthermore, the normal direction of current
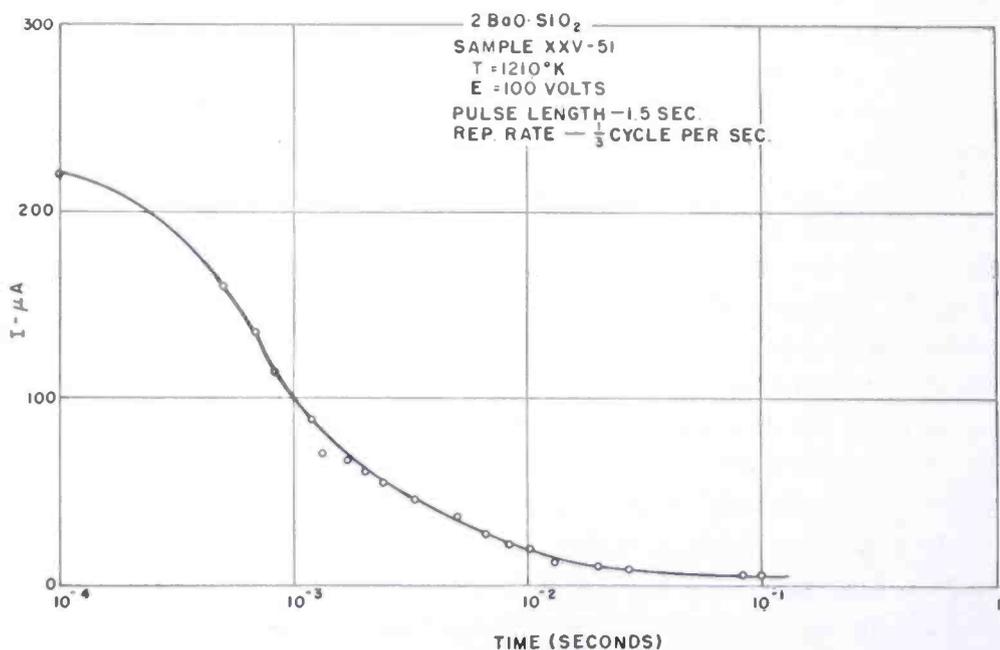
Fig. 20—The decay of the current in a sample of $2BaO \cdot SiO_2$ on application of a unit-function voltage.

flow is such as to carry barium from the oxide into the silicate where it may serve as a donor. This mechanism has been advanced to explain the lowering of interface resistance under conditions of current flow.

The resistance of the bulk material and the depletion layer were determined by measuring the voltage drops from the probe to the remote end and from the probe to the adjacent end with current flowing from end to end (the probe is 1/6 inch from one end and 7/16 inch from the other). The end 1/16 inch from the probe was positive. The results are expressed by

$$R_1 = 29.4\,e^{\frac{9050}{T}} = \text{bulk resistance,}$$

$$R_2 = 0.11 \, e^{\frac{13,800}{T}} = \text{depletion layer resistance.}$$

These are based on measurements in the temperature range from 700°K to 1100°K. At lower temperatures, decay effects are so slow that measurements become excessively time consuming. The bulk conductivity has an activation energy of about 0.78 electron volt, the depletion layer an activation energy of about 1.2 electron volts. The range of activation energies for interface layers found in the literature encompasses both of the above values which suggests that depletion layers may occur in interface layers. The equilibrium conditions at the silicate oxide interface would then be complex, too complex to speculate on here.

In the course of the 2 BaO · SiO_2 experiments, the dielectric constant of the sample was measured by the immersion method using an acetone-benzene dielectric. This is noted here for the benefit of those who may have need of this constant. The dielectric constant was found to be 12.4.

Having explored the general behavior of several insulators at elevated temperatures and having acquired some definite notions about depletion layers, attention was again focused on the oxide cathode. The sample in this case was a diode having a cylindrical cathode of relatively pure nickel (RCA N-81) coated with Malinckrodt "Ultra Pure" BaO, with a spiral platinum probe imbedded in the coating, the cathode enclosed by a cylindrical nickel anode. The tube was operated in the bridge of Figure 13 with the bridge driven at 60 cycles per second. From readings obtained from the bridge, the total cathode resistance was computed. While the readings were being taken, the probe potential was also measured with a high-input-resistance oscilloscope. The probe potential divided by the cathode current is a measure of the resistance of that part of the cathode which lies between the base-metal and the surface in which the probe spiral lies. The measurements were made over the temperature range from 1050°K to 1280°K. The results are shown in Figure 21. An obvious observation is that the total cathode resistance is at least an order of magnitude greater than the resistance between the probe and the base metal. This implies that the major voltage drop occurs between the probe and the emitting surface. In view of the insulator measurements described above, it is not difficult to imagine that the major drop occurs near the emitting surface. It may also be noted that the two resistance lines have different slopes. It is not believed that the experimental accuracy of these measurements justifies any conclusions from the slopes other than that

the activation energies are of the order of 2 electron volts. In the course of these experiments, it was found that the apparent contact potential which had to be inserted in series with the standard diode to obtain a bridge balance varied with the cathode temperature. The variation is shown in Figure 22. The slope of the line is 3.1×10^{-3}
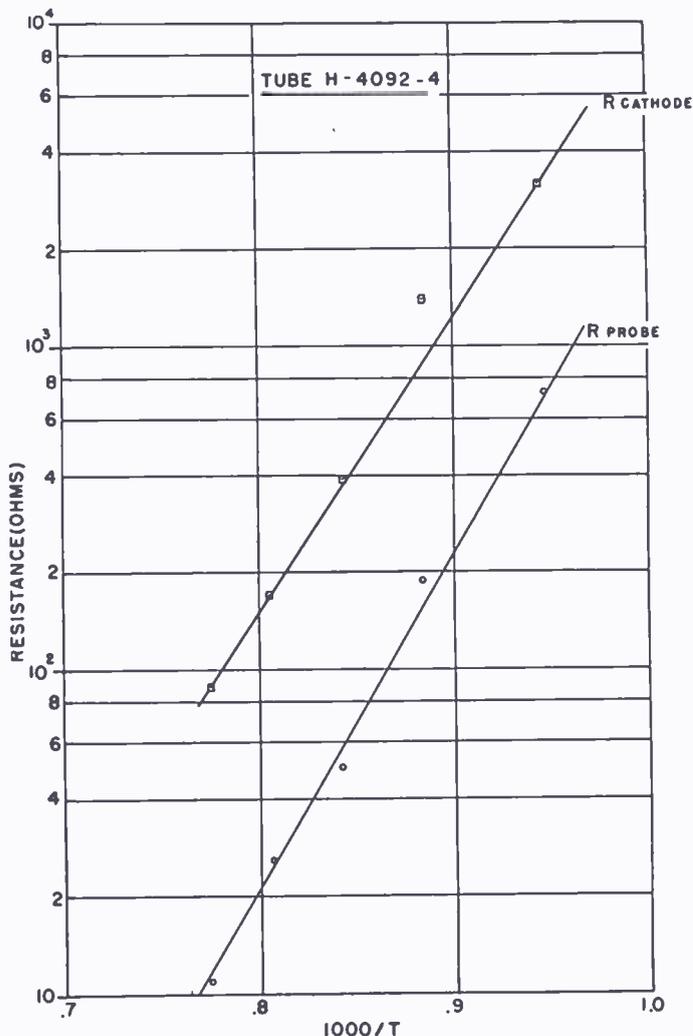
Fig. 21—The internal resistances of an oxide cathode as a function of cathode temperature. The upper curve is the total cathode resistance. The lower curve is the potential of a probe imbedded in the coating divided by the cathode current. It is a measure of the cathode resistance lying between the base metal and the plane of the probe.

volt per degree, a value in fair agreement with the thermoelectric power of BaO found by Blewett.[21]

In pursuing these measurements, a variation of the conductance between base metal and probe with average current was observed. Again the tube was being operated in the bridge, with the bridge driven at 60 cycles per second, so that current–voltage characteristics could be
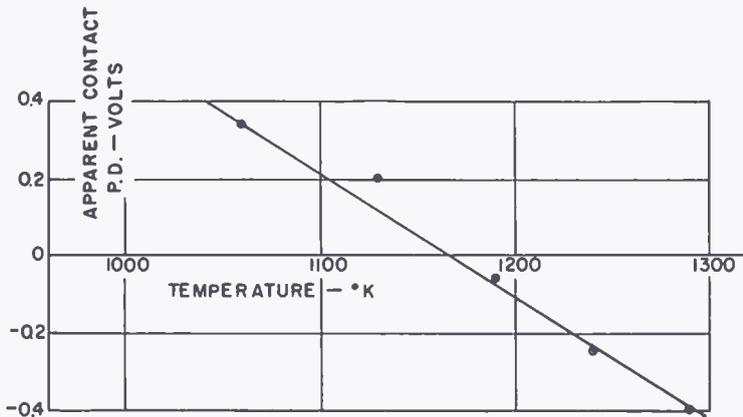
Fig. 22—The apparent contact potential between anode and cathode of a
diode plotted against the cathode temperature.

displayed on an oscilloscope. A series of cathode-current versus probe-
voltage curves were run. The driving voltage was applied to the anode
of the diode and the probe potential was determined with a high-
input-resistance oscilloscope, so that the probe current was of the order
of a fraction of a microampere, i.e., of the order of a thousandth of
the cathode current. The curves are shown in Figure 23. It will be
noted that the initial slopes of the curves increase with increasing peak
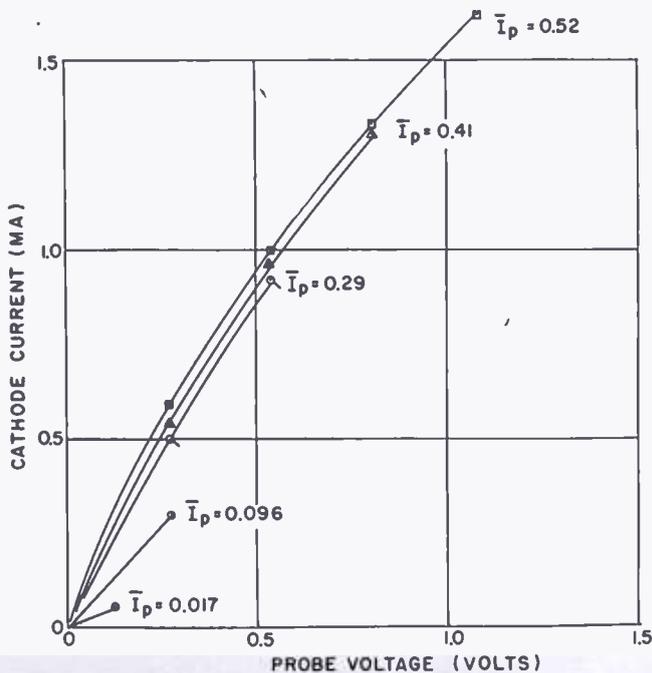
Fig. 23—A series of cathode-current versus probe-voltage characteristics
in a diode with a probe imbedded in the oxide coating. The anode of the
diode was driven with a 60-cycle-per-second voltage. The probe voltage
was read with a high-impedance oscillograph. The parameter, the average
current, was adjusted by adjusting the alternating-current anode voltage.

current (hence with increasing average current in "half-sine-wave" operation). When the initial slopes are plotted against average current, the curve of Figure 24 results. This result is easily interpreted in terms of the donor depletion hypothesis. As the average current increases, the donor depletion layer becomes thicker and "deeper." The donors removed from the depletion layer move towards the base metal and increase the conductivity in the "bulk" material. When the current is increased sufficiently, at a given cathode temperature and duty cycle (50 per cent in this case), back diffusion of donors begins to overtake the electrolysis and an asymptotic value of conductivity is approached.
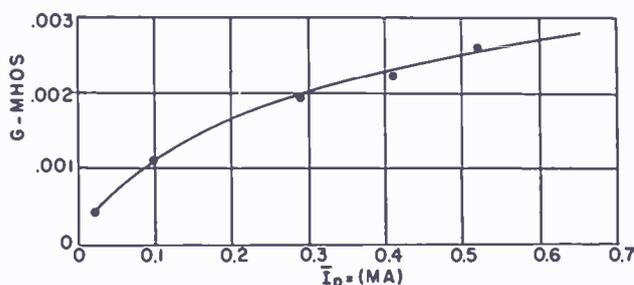
Fig. 24—The zero-current slopes, G, of the characteristics of
Figure 23 versus the average current.

With this evidence that a depletion layer at the cathode surface could be made thick enough to react on a probe imbedded in the coating, a new avenue of investigation opened up. This led to the achievement of an amplifier using $BaO + SrO$.[48] The aspects of this device which relate to oxide cathodes will be described in the next section.

A BaO – SrO Amplifier

In pursuing studies of the reaction of the surface depletion layer on a probe imbedded in an oxide cathode, it was found that when an alternating-current voltage was applied to the anode of the diode, the alternating-current voltage observed on the probe increased with increasing direct-current bias on the probe. By successive approximations, the optimum cathode temperature and optimum direct-current biases on both the probe and anode were found. With these operating conditions, a voltage gain of 10 and a power gain of 2.5 were achieved.

The diode under study had a mixed-oxide $(BaO + SrO)$ cathode. The diode geometry was planar. The probe was a single 0.001-inch platinum wire laid across the cathode within the coating. The cathode was centered in an aperture in a thimble, the skirt of which extended

---

[48] The following paper describes what may be a similar device. The description given is ambiguous with regard to geometrical arrangement and performance: T. R. Scott, "Crystal Triodes," *Proc. I.E.E.*, Vol. 98, Part 3, pp. 169-183, May, 1951.

back over the probe and cathode leads to reduce electron collection by either set of leads as far as possible. The diode was operated in the circuit shown in Figure 25. The operating conditions were

$$T = 780°\text{K.} = \text{cathode temperature,}$$

$$E_A = 4.5 \text{ volts} = \text{direct-current anode voltage,}$$

$$E_P = 135 \text{ volts} = \text{direct-current probe voltage,}$$

$$I_A = 76 \text{ microamperes} = \text{direct anode current,}$$

$$I_P = 34 \text{ microamperes} = \text{probe direct-current.}$$

It should be noted that the anode of the diode was used as an input electrode, and the probe as an output electrode. These operating conditions yielded the voltage gain of 10 and power gain of 2.5 cited above. The output voltage was 9 volts. It should also be noted that the input and output voltages were in phase, not 180° out of phase, at low frequencies.
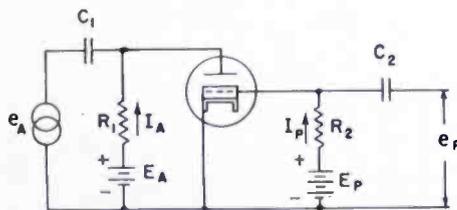
Fig. 25—A circuit diagram showing the electrode connections for operation of an oxide cathode as an amplifier.

A complete family of electrode characteristics is shown in Figure 26. An examination of the input (anode) characteristics suggested that substantial voltage drops were appearing across the vacuum. To estimate the magnitude of the drop, the input characteristics were plotted on three-halves paper as shown in Figure 27. The parameter E_P is the probe potential. It was found that each of the curves could be represented by the equation

$$I_A = P (E_A - R_P I_A)^{3/2},$$

where P is the perveance of the diode and R_P is a resistance which depends on the probe potential. This relation implies that the current across the diode is space-charge limited and that the drop through the coating may be represented by a linear resistance. The current-voltage characteristics of the coating, computed by subtracting the vacuum voltage-drop from the applied anode voltage, are shown in Figure 28 in which ΔE_A is the voltage drop across the coating and the parameter E_P is the probe voltage. It will be seen that all of the

characteristics, except that for $E_p = 0$, are nearly linear. The amplifier characteristics of Figure 26 may now be replotted, replacing E_A by ΔE_A as in Figure 29. This family of curves shows the characteristics of the device if the anode were moved sufficiently close to the cathode surface to make the vacuum voltage drop negligible. The characteristics are represented approximately by the following empirical relations:

$$I_p = 2 \times 10^{-5} e^{+0.0612 \, (E_p - 8.75\Delta E_A)},$$

$$I_A = \frac{1.2 \times 10^{-4} \, \Delta E_A}{1 + 2.53 \, e^{-0.105 E_p}}.$$
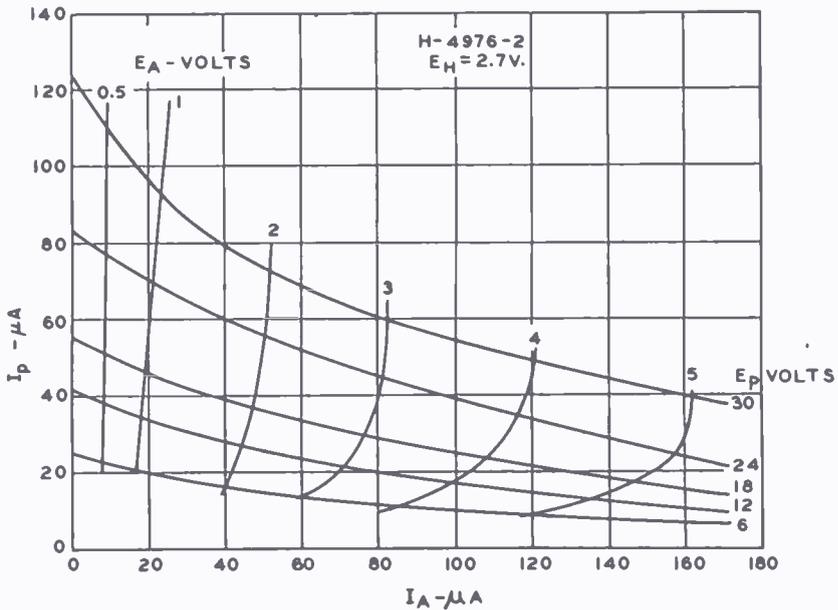
Fig. 26—The constant–voltage characteristics of a diode with a probe imbedded in the oxide coating. The subscript A refers to the anode of the diode and the subscript p to the probe.

An examination of the characteristics shows that very substantial power gains may be achieved in a device of this kind.

The frequency response of the device has been explored. The gain begins to drop and a phase shift between input and output voltages becomes apparent at about 2 kilocycles. The gain becomes unity and the phase shift about 90 degrees at 30 kilocycles. This behavior is to be expected in a device in which ion mobility is believed to play a major role. In fact, the phase characteristic accords with that to be expected from pulse-decay time-constant considerations.

It remains to discuss the bearing of this device, and the experiments which led to it, on the donor depletion hypothesis.

1) When the probe takes no current, the voltage drop between the

base metal of the cathode and the probe is small, even though the cathode current may be substantial. However, when current is taken by the probe in the proper sense (the probe positive with respect to the base), the voltage drop becomes substantially greater. When no current is taken by the probe, the apparent probe resistance may be of the order of ohms; with current it may be, and frequently is, of the order of megohms. These observations indicate that current flow decreases the conductivity of the oxide at positive boundaries.

TWO-THIRDS POWER PAPER

TUBE H — 4976 - 2

$E_H = 2.7$ V

PERVEANCE LINE

E_p (VOLTS)

30 24 18 12 6 0

$I_A - \mu A$

E_A (VOLTS)
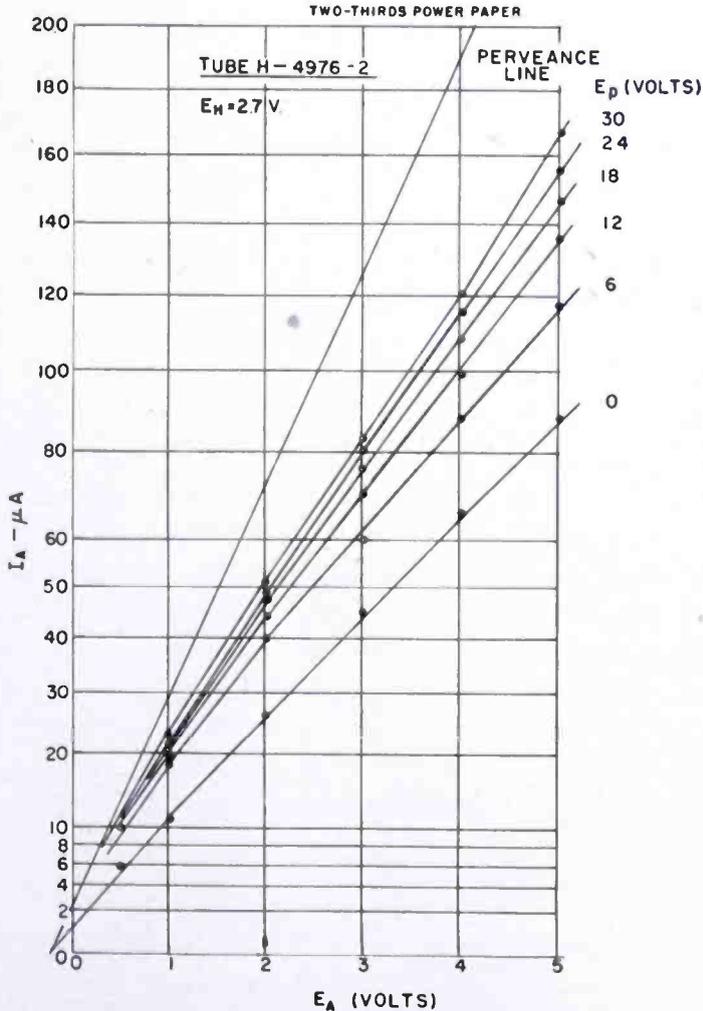
Fig. 27—The anode current–voltage characteristics of the diode of Figure 26 with probe voltage as a parameter.

2) The combination bridge and probe measurements which separate "bulk" and "surface" resistance also demonstrate a decrease of conductivity at a positive boundary, the emitting surface in this case.

3) The increase in conductivity between base metal and probe with increasing current shows that whatever decreases the con-
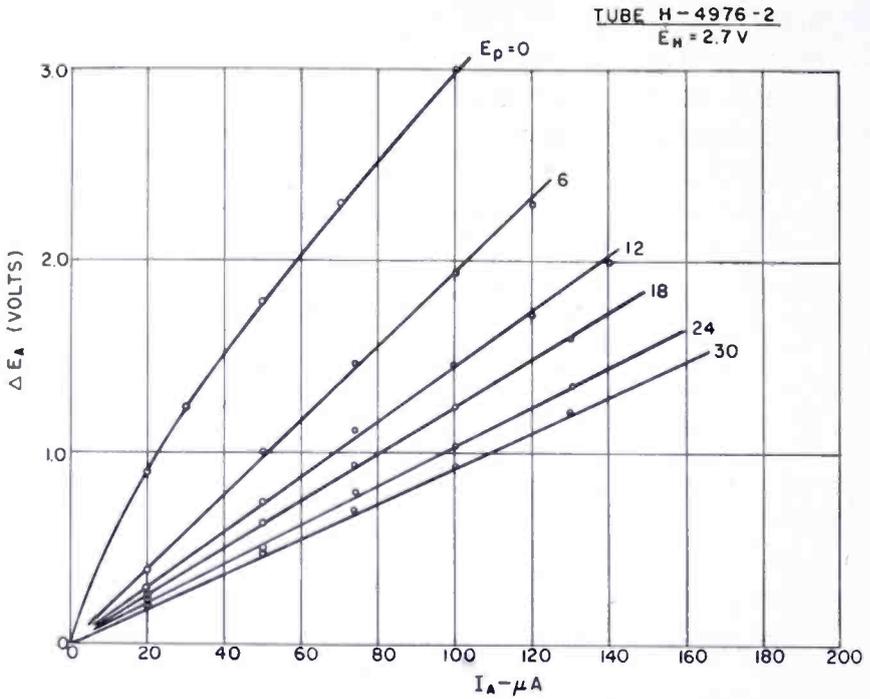
Fig. 28—The current–voltage characteristics of the cathode of the
diode of Figure 26, with the probe voltage as a parameter.
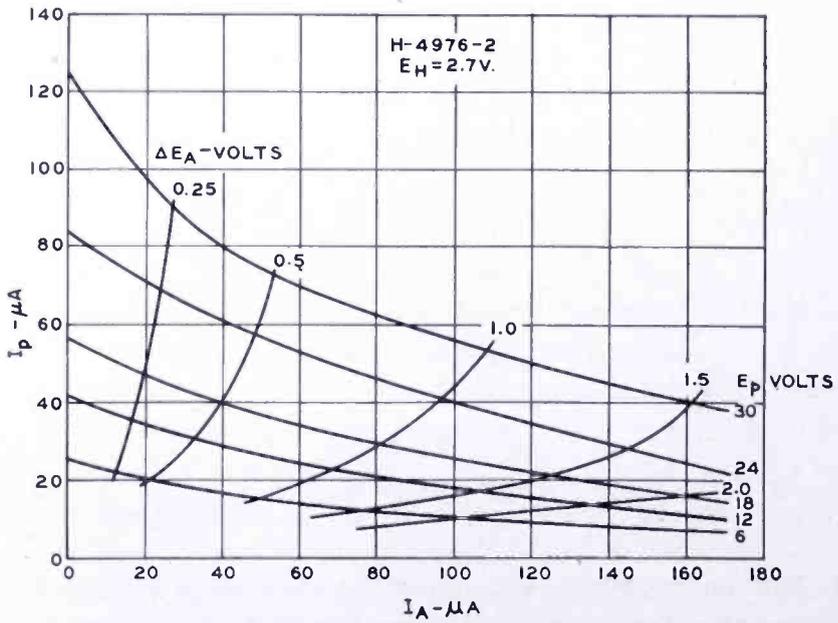
Fig. 29—The constant–voltage characteristics of the cathode of the diode
of Figure 26. I_A is the anode current, ΔE_A is the corresponding voltage drop
across the cathode, and I_p and E_p are the probe current and probe voltage,
respectively.

ductivity at a positive boundary increases the conductivity at a negative boundary. A reasonable inference is that donors are transported electrolytically from positive boundaries toward negative boundaries.

4) The observation that an increase in conductivity in the neighborhood of a negative boundary approaches an asymptotic value as the current increases indicates the presence of a competing mechanism which limits the change in conductivity and restores the system to its initial condition when current flow is interrupted.

5) The times required for changes of conductivity are too long to correspond to electronic relaxation times. Instead, they seem appropriate to ionic phenomena, an observation in accord with the electrolytic transport of donors inferred in 3) above.

These observations accord with and find their simplest explanation in the donor depletion hypothesis advanced in an earlier section of this paper. It has been said that a theory is a system for remembering the results of experiment. This definition is probably too narrow; sometimes theory predicts the results of experiments yet to be performed. In the restricted sense the donor depletion hypothesis can be regarded as a theory; in the broader sense, it has had its successes.

In the language of the donor depletion hypothesis, a language which will be used freely hereafter, the amplifier described above operates by virtue of overlapping depletion layers. The probe has a donor depletion layer which makes it a high-resistance electrode. The emitting surface of the cathode also has a depletion layer. When the cathode depletion layer is made to overlap the probe depletion layer, the probe resistance rises. Thus, the resistance of the output circuit is controlled by the current in the input circuit.

FURTHER RESISTANCE MEASUREMENTS

In view of the experiments described in the preceding section, it seemed worth while to study cathode resistances somewhat further with a view to separating the bulk and depletion-layer resistances and to determining their dependence on current.

The measurements to be described were made on a diode having a cylindrical cathode of nickel (RCA-N81) coated with Mallinckrodt "Ultra Pure" BaO, with a bifilar probe imbedded in the coating. The probe was of 0.001-inch platinum. The ends of the probe were shielded by a disc normal to the axis of the cathode to prevent electron collection from the interelectrode space. The cathode was provided with an alumel-chromel thermocouple to monitor its temperature. The anode was an N-81 nickel cylinder, coaxial with the cathode and pierced

by a 0.020-inch aperture opposite the cathode to permit calibration of the cathode thermocouple against a pyrometer.

The diode was operated in the bridge of Figure 13 and the probe potential was measured with a high-impedance oscilloscope as in the previous measurements. The bridge was driven at 60 cycles per second, so that the tube was in class B (half-sine-wave) operation. The cathode temperature was determined by means of the thermocouple after its calibration had been determined by comparison with a Leeds and Northrup pyrometer. At each value of temperature and plate current, the bridge was balanced and the probe oscilloscope read. The total resistance of the cathode was determined from conditions of balance of the bridge. The apparent resistance between probe and base metal was computed by dividing the probe potential by the cathode current. It should be noted that this is not the resistance between probe and base metal which would be obtained if the probe were taking an appreciable fraction of the total cathode current. The purpose of the probe in this experiment was to determine the potential distribution in the cathode.

A set of results obtained as described above is shown in Figures 30 and 31. It should be noted that two other sets of data obtained in the same way are in substantial agreement with the results of Figures 30 and 31. There was a gradual activation of the cathode as the experiments progressed, so that later data show resistances about half as large as the initial data. It should also be noted that the cathode was relatively inactive at all times. No apology is made; as much can be learned from a poor cathode as from a good cathode.

Figure 30 shows the variation of the apparent resistance between probe and base metal (the probe potential divided by the cathode current) as a function of average current with cathode temperature as a parameter. For temperatures below about $1200°K$, the "probe resistance" rises slightly with average current. The studies of the oxide amplifier suggest that the donor depletion layer increases in thickness with current at lower temperatures. Hence, the increase of resistance with current at temperatures below $1200°K$. may be due to an overlap of the probe by the surface depletion layer. Above $1200°K$, the apparent probe resistance decreases with current, a behavior which accords with that of Figure 24. At higher temperature, the depletion layer becomes thinner and the apparent probe resistance is diminished by the electrolysis of donors into the region between the base metal and probe. This behavior has been noted at lower temperatures with mixed oxides $(BaO + SrO)$. This observation accords with pulse decay studies on BaO and on mixed oxides. The same phenomena

are observed; however, current decays found at 1200°K with BaO are comparable with those observed at about 1000°K in mixed oxides.

Figure 31 shows the total cathode resistance as a function of the average current, with temperature as a parameter. These resistances are about an order of magnitude higher than the apparent probe resistances. At temperatures below about 1070°K, the cathode resistance increases with current, a behavior to be expected from the donor depletion hypothesis. Above 1070°K, the cathode resistance diminishes with cathode current. At currents below 0.1 milliampere, the resist-
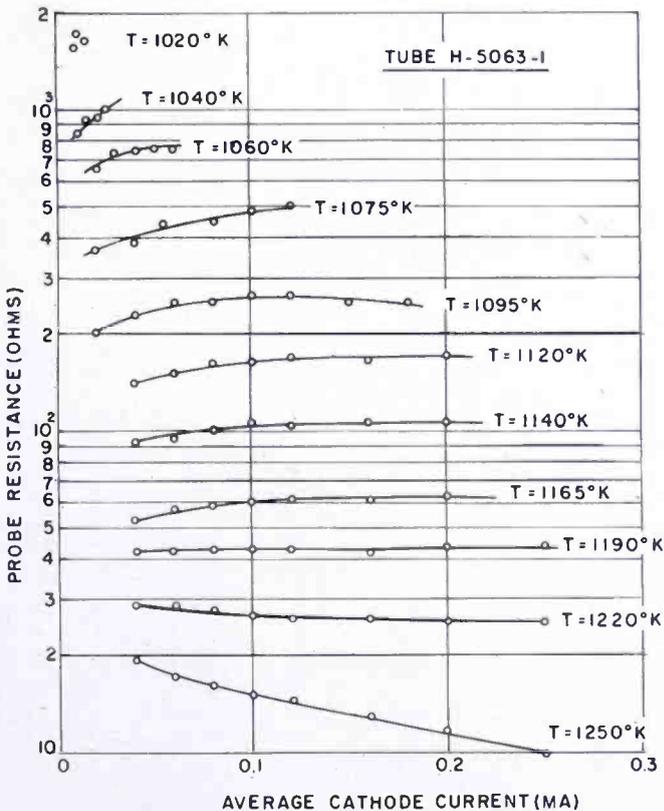
Fig. 30—The resistance between the base metal of an oxide cathode in a diode and a probe embedded in the coating plotted against average cathode current with cathode temperature as a parameter. The anode was driven at 60 cycles per second and the probe voltage was read with a high-impedance oscilloscope.

ance, R_k, is proportional to i^n, where n lies between $-\frac{1}{2}$ and $-\frac{2}{3}$. In a later section it will be shown that this is the behavior to be expected if the current is space-charge limited in the depletion region. At higher currents, the resistance varies more rapidly with current than indicated above and a slow activation of the cathode is observed.

The latter observation suggested that the mechanism called "electrolytic activation" was involved. With this in mind, the curves of

Figure 31 were replotted in terms of cathode resistance versus average cathode drop (the product of cathode resistance and average cathode current) as shown in Figure 32. It will be noted that at the higher temperatures, the curves tend towards constant voltage characteristics. This is a behavior one associates with breakdown phenomena. The form of these characteristics, the observed activation, and the previous measurements on the fields that may exist in depletion layers
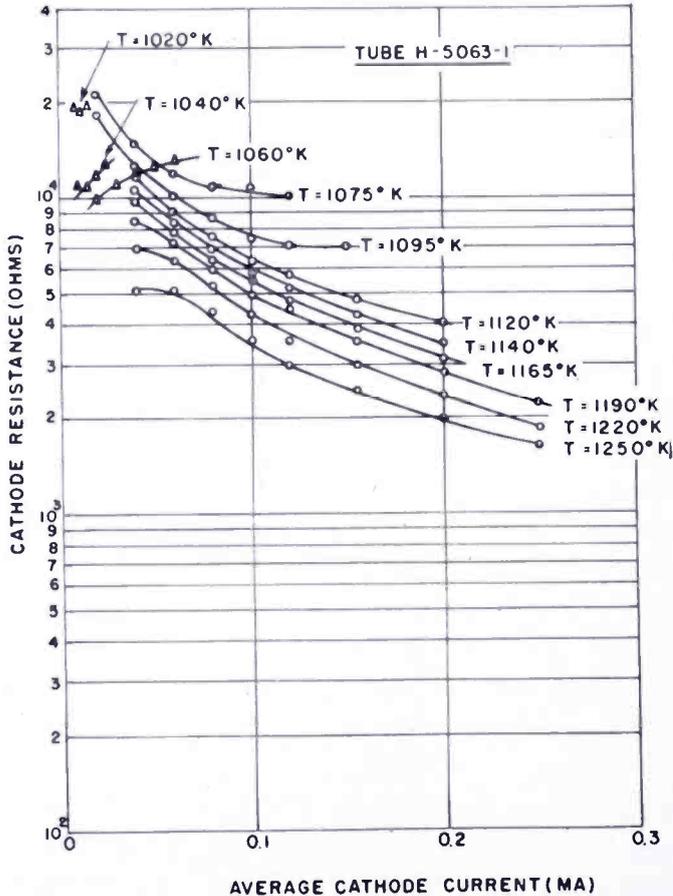
Fig. 31—The total cathode resistance of the cathode of Figure 30 versus average cathode current with cathode temperature as a parameter. These measurements were read simultaneously with those of Figure 30.

suggest that donors may be formed by deformation of the ion lattice field by high applied fields, a Schottky effect on the Madelung field, to a point where oxygen can escape with the formation of donors. If this were the case, the phenomenal direct-current emissions obtained by Fineman and Dillinger could be accounted for in a manner consistent with the notions set forth in preceding sections of this paper. It would also account for the familiar activation procedure which consists in applying a relatively high voltage to the anode of the diode

with the cathode several hundred degrees above normal operating temperature, the so-called "electrolytic activation" process. In this connection, it is of interest to recall that Becker[49] and Plumlee and Smith[50] find an oxygen evolution from oxide cathodes which is proportional to the applied field, not to the cathode current. This behavior suggests the production of excess barium by field-enhanced evaporation of oxygen.
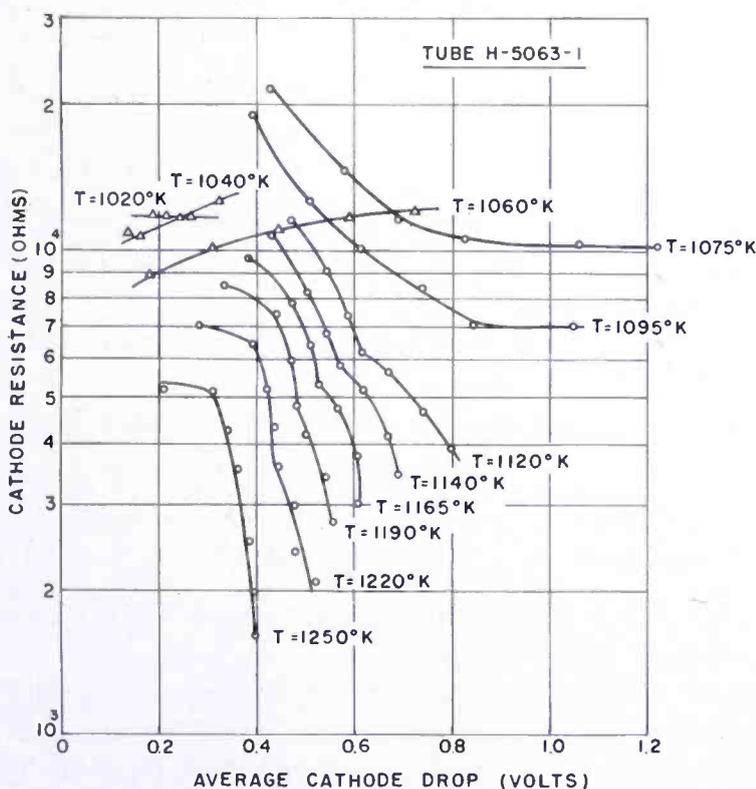
Fig. 32—The data of Figure 31 plotted with average cathode voltage drop as abscissas to show the constant-voltage tendencies of the resistances at higher temperatures.

It is also possible that the Zener effect may increase the conductivity at high fields. This should produce no permanent effect, i.e., no permanent activation. Hence, it seems unlikely that it is the only breakdown effect playing a role.

Because it is clear that there are differences between the bulk oxide and the region adjacent to the surface of the cathode under conditions of current flow, it is interesting to inquire if differences also exist

[49] J. A. Becker, "Phenomena in Oxide Coated Filaments," *Phys. Rev.* Vol. 34, pp. 1323-1351, November 15, 1929.
[50] R. H. Plumlee and L. P. Smith, "Mass Spectrometric Study of Solids. I. Preliminary Study of Sublimation Characteristics of Oxide Cathode Materials," *Jour. Appl. Phys.*, Vol. 21, pp. 811-819, August, 1950.

under conditions of no current flow. Relevant data can be obtained by measuring the zero current intercepts of the resistance versus current characteristics. These measurements are difficult because the bridge sensitivity decreases with applied voltage, contact potentials must be balanced out with precision at low currents to obtain satisfactory bridge balances, and the velocities of the emitted electrons affect the apparent perveances of the diodes. Hence data obtained in this way is of dubious reliability. The activation energies obtained from reciprocal temperature plots of the zero-current intercepts are as follows:

	$T < 1100°K$	$T > 1100°K$
Surface layer	1.0 e.v.	0.5 e.v.
Bulk oxide	3.4 e.v.	1.7 e.v.

It appears that there is a significant difference between the oxide lying between the base metal and the probe, and that lying between the probe and emitting surface.

It is interesting to compare these results with values obtained by Hannay, McNair, and White.[51]

Their activation energies may be summarized as follows:

	$T < 1170°K$	$T > 1170°K$
Active cathode	1.0 e.v.	0.3-0.4 e.v.
Inactive cathode	3.9 e.v.	1.8 e.v.

They cite the active values; the inactive values were obtained from Figure 3 of their paper.

It appears that the surface layer of the present inactive cathode has activation energies comparable with the Hannay, McNair, and White values for an active cathode, and that the bulk oxide has activation energies comparable with their values for an inactive cathode.

These results, considered independently or in juxtaposition, pose a number of interesting questions:

1) In view of the known energy gap and the known positions of the impurity levels of BaO, how can any activation energy exceed three volts? A possible mechanism involves traps. Suppose that there are no donors but that there are traps of density N_T lying at an energy ϵ_1 below the conduction band. Then the Fermi level can be determined by setting the sum of the density of electrons in the conduction band and the density of electrons in the traps equal to the number of holes in the oxygen band:[52]

---

[51] N. B. Hannay, D. McNair, and A. H. White, "Semi-conducting Properties in Oxide Cathodes," *Jour. Appl. Phys.*, Vol. 20, pp. 669-681, July, 1949.
[52] W. Shockley, *Electrons and Holes in Semi-Conductors*, D. Van Nostrand, New York, N. Y., 1950.

$$N_C e^{\frac{-\epsilon}{KT}} + \cfrac{N_T}{e^{\frac{\epsilon - \epsilon_1}{KT}} + 1} = N_C e^{\frac{-(\epsilon_2 - \epsilon)}{KT}} \quad .$$

All energies are measured from the bottom of the conduction band. N_C is the effective density of states in the conduction band and in the oxygen band, i.e.,

$$N_C = 2 \left(\frac{2 \pi m k T}{h^2} \right)^{3/2},$$

ϵ is the Fermi limit and ϵ_2 the width of the forbidden band. The Fermi limit may be eliminated in terms of the density of electrons, n, in the conduction band. Then

$$n + \cfrac{n N_T}{n + N_C e^{\frac{-\epsilon_1}{KT}}} = \frac{N_C^2}{n} e^{-\frac{\epsilon_2}{KT}} \quad .$$

If

$$n \gg N_C e^{\frac{-\epsilon_1}{kT}},$$

the equation is

$$n^2 + n N_T - N_C^2 e^{\frac{-\epsilon_2}{kT}} = 0.$$

The solution exhibits two forms:

$$n \approx \frac{N_C^2}{N_T} e^{-\frac{\epsilon_2}{kT}} \quad \text{for} \quad N_C e^{-\frac{\epsilon_2}{2kT}} < \frac{N_T}{2},$$

$$n \approx N_C e^{-\frac{\epsilon_2}{2kT}} \quad \text{for} \quad N_C e^{-\frac{\epsilon_2}{kT}} > \frac{N_T}{2}.$$

At low temperatures, the activation energy is ϵ_2, at high temperatures the activation energy is $\epsilon_2/2$, the required behavior.

To match the experimentally observed behavior, ϵ_2 must be about 3.5 volts and the temperature break must occur at about 1200°K. Therefore, the density of traps must be

$$N_T = 2\,N_0\, e^{\frac{-\epsilon_2}{2kT}} \approx 10^{12}.$$

At the temperature break, the density of electrons in the conduction band is

$$n = \frac{\sqrt{2}-1}{2}\,N_T \approx 2 \times 10^{11}.$$

Hence the conductivity is

$$\sigma = ne\mu \approx 10^7 \text{ mhos per centimeter.}$$

In making this computation μ was assumed to be three.[53] The value of conductivity is within reason for an inactive cathode.

The above results are subject to the assumption that

$$n \gg N_0\, e^{-\frac{\epsilon_1}{kT}}.$$

The temperature range of measurement is such that for the computation to be valid

$$10^7 > N_0\, e^{-\frac{\epsilon_1}{kT}}.$$

Therefore, ϵ_1 must exceed 2.4 volts. This result suggests that the traps lie between the 2.4-volt donor levels found by DeVore, and the top of the oxygen band.

In the above attempt to fit a mechanism to experimentally observed results, two assumptions were implicit. First, it was assumed that hole mobility is so small that the conductivity is predominantly n-type. This assumption can only be justified on pragmatic grounds. Secondly, it was assumed that the density of traps is independent of temperature. A discussion of this matter will be deferred until the active case has also been considered.

It is, of course, possible that some other mechanism is responsible for the observed behavior. For example, the conductivity break may

---

[53] E. M. Pell, "The Hall Effect in Single Crystals of Barium Oxide," *Phys. Rev.*, Vol. 87, pp. 457-462, August 1, 1952.

be due to parallel mechanisms such as electronic and ionic conduction. However, in parallel mechanisms, the mechanism with the higher activation energy predominates above any temperature break. a behavior not consistent with the observations under discussion.

2) In view of the known positions of the impurity levels in BaO, how can the activation energy for conductivity in an active cathode be as large as one volt? A mechanism well-known in the alkali-halides may be responsible. This mechanism envisages donors and vacancies lying at the same energy below the conduction band.[54] If N_V be the density of vacancies, N_D the density of donors, and ϵ_1 their position in energy measured from the bottom of the conduction band, the density of electrons in the conduction band is

$$n = \sqrt{N_C N_D}\, e^{-\frac{\epsilon_1}{2kT}} \quad \text{for} \quad N_V < \sqrt{N_C N_D}\, e^{-\frac{\epsilon_1}{2kT}},$$

$$n = \frac{N_C N_D}{N_V}\, e^{-\frac{\epsilon_1}{kT}} \quad \text{for} \quad N_V > \sqrt{N_C N_D}\, e^{-\frac{\epsilon_1}{kT}},$$

subject to the assumption that

$$n \ll N_D.$$

If this mechanism is to display the observed temperature break with a ratio of conductivities of about 2:1, N_D and N_V must be independent of temperature and the donor density must be high enough so that the "intrinsic" behavior of 1) above is completely masked. The two observed activation energies correspond approximately to the 1.4 e.v. levels found by DeVore and to a Fermi level lying halfway between these levels and the conduction band. Hence, it seems reasonable to assume that the observed behavior is due to vacancies and donors lying 1.4 e.v. below the conduction band. A discussion of how the donors and vacancies may be formed will be deferred until later.

It is of interest to compute the donor and vacancy densities required to match the experimental behavior. At the temperature break, the conductivity in an active cathode may be

$$\sigma = 10^{-3} \text{ mho per centimeter,}$$

i.e., about four orders of magnitude greater than intrinsic. Then the electron density in the conduction band is

---

[54] Mott and Gurney, *Electronic Processes in Ionic Crystals*, Second Edition, Oxford University Press, 1948.

$$n \approx 10^{15} \text{ cm}^{-3}.$$

The temperature break occurs at about 1200°K. Inserting these values and $\epsilon_1 = 1.4$ e.v. in the equation for the electron density gives

$$N_D \approx 10^{17} \text{ cm}^{-3}.$$

The vacancy density required to place the break at 1200°K is then

$$N_V \approx 10^{15} \text{ cm}^{-3}.$$

Another mechanism which might account for the observations discussed is the thermal generation of vacancy-pairs and F-centers. The former are formed by the removal of positive and negative ions to the surface in pairs, the latter by the removal of neutral oxygen to the surface. In this mechanism, the densities of vacancy-pairs and F-centers are determined by thermodynamic considerations, and are temperature dependent. Because this mechanism is called for by very general considerations, it should be present. However, this mechanism alone has failed to account for the experimental observations, particularly as to magnitudes. It is suspected that the disorder activation energies are so large that any disorders are frozen in at normal operating temperatures.

A third possible mechanism is a quasi-stationary mechanism in which the activity of the cathode is determined by donor generation by reduction of the oxide at the metal interface, donor diffusion through the oxide, donor generation by oxygen evaporation at the emitting surface, donor depletion by barium evaporation at the emitting surface, and deactivation by the adsorption of stray gases at the surface. This mechanism is too involved to consider without more extensive data. Because a mechanism of this kind must determine the life of a cathode, it deserves future attention.

3) Why does the "surface resistance" of the cathode display activation energies comparable with those of Hannay, McNair, and White for an active cathode, yet show resistance orders of magnitude greater than those expected in active oxide? No explanation is offered. The comparable activation energies may be more than fortuitous. On the other hand, there is other evidence that the oxide very near the emitting surface differs from the bulk oxide. This evidence will appear in a later section.

Work Function

According to Fowler,[55] the thermionic emission of a semiconductor

---

[55] R. H. Fowler, *Statistical Mechanics*, Second Edition, Cambridge Press.

is given by the Richardson equation

$$ j_\epsilon = D\,n\,e\,\sqrt{\frac{kT}{2\pi m}}\,e^{-\frac{e\chi}{kT}}\,, $$

where n is the electron density at the emitting surface, χ is the electron affinity, and D is the transmission coefficient of the surface. If the semiconductor is an impurity semiconductor having N donors per unit volume at an energy ϵ below the conduction band, and if

$$ N >> N_C\,e^{-\frac{\epsilon}{kT}} = 2\left(\frac{2\pi mkT}{h^2}\right)^{3/2} e^{\frac{-\epsilon}{kT}}\,, $$

then the emission formula may be written

$$ j_e = A'\,DT^{5/4}\,e^{-\frac{e\chi}{kT} - \frac{e\epsilon}{2kT}}\,, $$

an equation sometimes called the Fowler emission equation. Hence, the work function is

$$ \phi = \chi + \frac{\epsilon}{2}\,. $$

According to the donor depletion hypothesis, the density of donors at the emitting surface is a function of the current through the cathode and diminishes as the current increases. Therefore, the electron concentration at the surface decreases with current, and the conventional interpretation of the emission equation is not valid.

The donor depletion hypothesis implies that the work function is dependent on current under steady state conditions and dependent on both current and time under transient conditions. The latter behavior was demonstrated using one of the diodes built for the study of the decay and recovery of pulsed emission.[1] The anode was driven by a constant-current source and the anode voltage was measured as a function of time. The measurements were made with a cathode temperature of about 950°K so that the change of anode voltage with time was slow enough to be measured easily. Readings were taken at four constant-current values. These currents are plotted against the initial values of voltage in Figure 33. The perveance line of the diode is shown for reference. The variation of anode voltage with time for the four values of constant current is shown in Figure 34.

It is quite apparent that voltage required to maintain the current constant increases with time and that the greater the current, the more rapidly the required voltage increases. According to the donor depletion hypothesis, these results are interpreted to mean that the work function increases with current flow and that this increase in
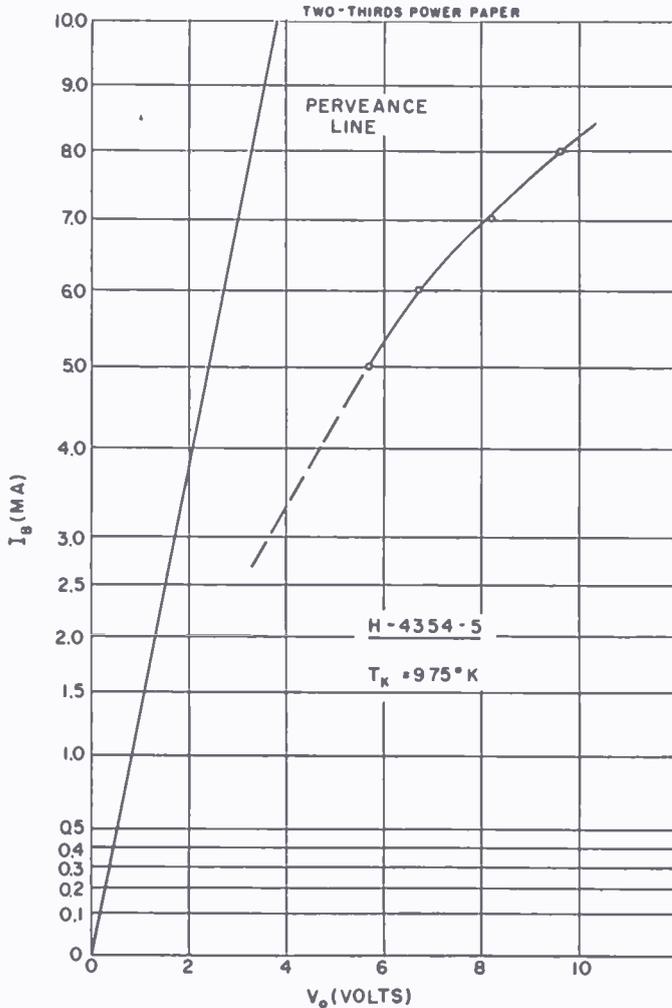
Fig. 33—The anode current versus the initial anode voltage in a diode operated at constant current. The perveance line is shown for reference.

work function must be offset by an increase in Schottky effect if the current is to be held constant.

Estimates of the magnitude of the change in work function with average current were obtained in a second set of experiments performed on the same tube. In these experiments, the cathode was operated at a fixed temperature and anode voltage until the current became stable. A voltage pulse was then superposed on the direct-current anode voltage to delineate the Schottky curve. The results of
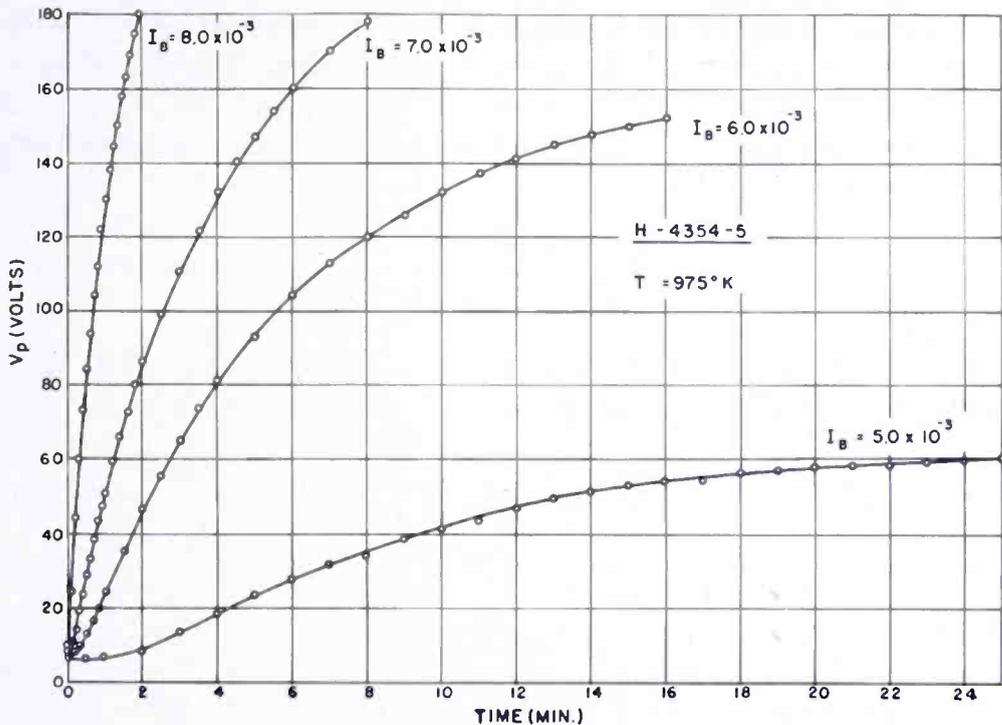
Fig. 34—The anode voltage required to maintain the anode current of a diode constant versus time for various currents.

measurements with a cathode temperature of about 1010°K and a series of direct currents are shown in the Schottky plots of Figure 35. The zero intercepts of the curves and the apparent Schottky temperatures are shown in Table II. The apparent Schottky temperatures are consistently about 370°K, about forty per cent of the actual cathode temperature. The intercept current, which is usually

Table II — The Field-Free Emission and Apparent Schottky Temperature of an Oxide Cathode as a Function of Average Current

$$H - 4354\text{-}5 \quad T_k = 1010°K$$

I_{DC} Amperes	I_o Amperes	T_o Degrees Kelvin
3.5×10^{-6}	24.3×10^{-3}	367
3.0×10^{-3}	11.3	367
6.0	17.2	367
8.95	10.1	371
10.6	8.61	367
11.2	8.09	369
11.9	7.60	371
13.2	7.29	369

interpreted as the field-free emission current, decreases rapidly with current at first, then approaches a limiting value. This behavior is shown in Figure 36.

If the change in intercept is ascribed to a change in work function, the change is given by

$$\Delta\phi = \frac{kT}{e} \ln \frac{I_{00}}{I_0},$$

where I_0 is the intercept current and I_{00} is the value of I_0 with no average current. In the present case, I_{00} was taken to be 24.3
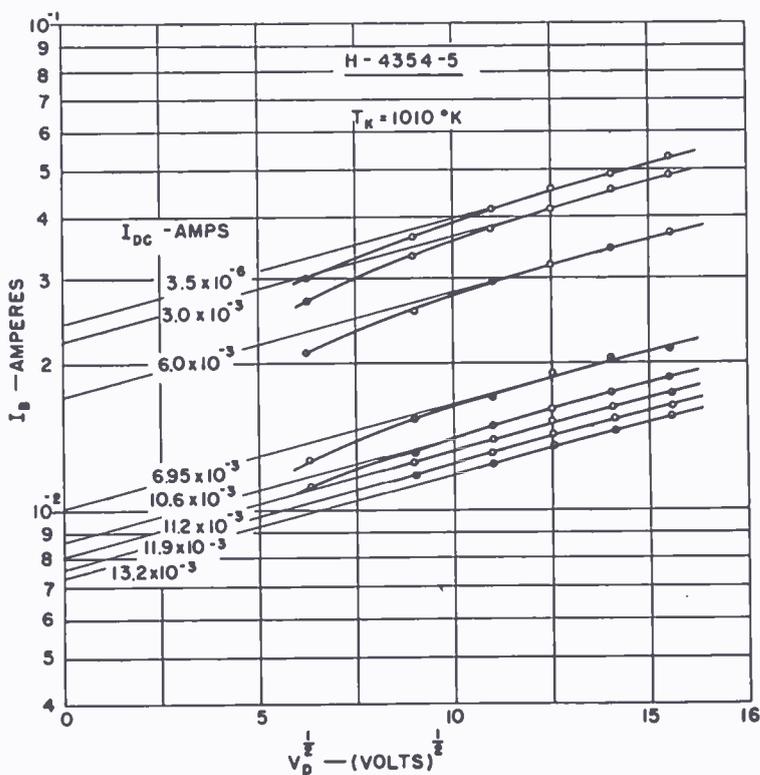
Fig. 35—The pulse Schottky lines of a diode operated at various average anode currents.

milliamperes, corresponding to an average current of 3.5×10^{-6} ampere. The variation in work function computed in this way versus the average current divided by the zero-average-current intercept is shown in Figure 37, which also shows the results of similar measurements at two other cathode temperatures. It will be noted that the changes in work function are small, much smaller than those corresponding to change of the semiconductor from an active to an inactive state near the emitting surface. An obvious implication is that the volume near the emitting surface of the cathode is well depleted of

donors by fields high enough to reach the anomalous Schottky region, so that variations in work function due to changes in current result from variations in electron density controlled by some mechanism other than thermal excitation to the conduction band, or result from changes in the electron affinity, in consequence of a depletion of the dipole layer as suggested by Sproull, perhaps.
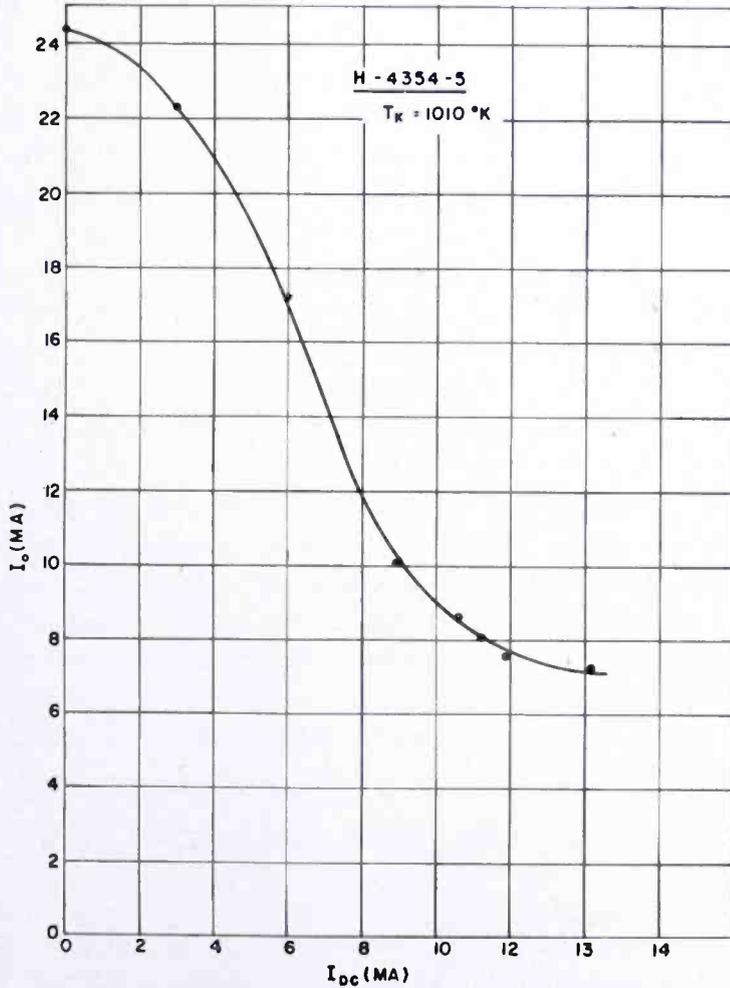
Fig. 36—The zero-field intercepts of the Schottky lines of Figure 35 versus average anode current.

The literature on oxide cathodes abounds in values of work function ranging from 0.8 volt to 2 volts. Many of these values are obtained from Richardson plots of Schottky intercepts. In view of the known positions of the energy levels of BaO and in view of the complex behavior described above, how is it possible to obtain apparent work functions as low as those cited? It will be shown in a later more speculative section, that the "work functions" observed and the false

Schottky temperatures displayed in the measurements from which they are derived can be accounted for if the current in the donor depletion layer is space-charge limited.

In the manufacture of tubes with oxide cathodes, it is customary to assay the emission of a cathode in terms of a departure of the current–voltage characteristics of the tube from the three-halves law. In view of the cathode resistance measurements described in earlier sections, and in view of variations of work function described in this section, it appears dubious that such "emission checks" give significant information on the actual emission capabilities of a cathode. Such a measurement undoubtedly gives a significant indication of the quality of the cathode; however, the result cannot be construed as a direct measure of the emission. It is easy to see that the actual emission
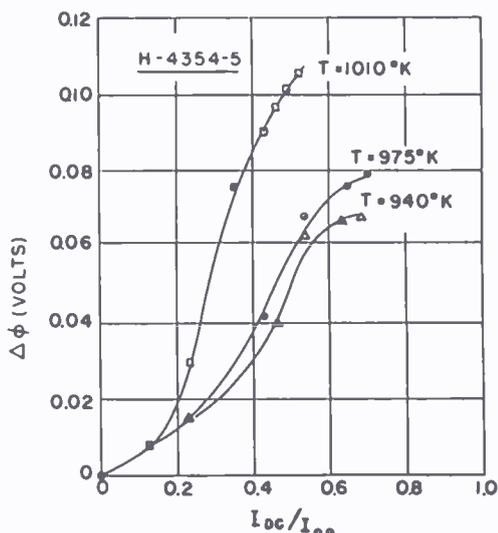
Fig. 37—The apparent change in work function versus average current at three cathode temperatures.

capabilities of the cathode are somehow involved. Assume that the departure from the three-halves law is due solely to cathode resistance. Then the plate current in a diode should be given by

$$i = P \, (V - iR)^{3/2},$$

where P is the perveance of the diode, V is the plate voltage and R is the cathode resistance. If the emission current i_e is defined in terms of a departure from the three-halves law by a factor B,

$$i_e = P \, (V - i_e R)^{3/2} = B \, P \, V^{3/2}.$$

When the voltage V is eliminated, the following relation results

$$\frac{1}{R} = i_\epsilon^{1/3} \frac{P^{2/3}}{B^{-2/3} - 1},$$

i.e., the conductance must vary as the cube root of the "emission current" if the departure is to be accounted for by a resistance in the cathode. The relation usually observed is a linear variation of conductance with emission current.[51] Hence, the behavior is not accounted for by the presence of a constant cathode resistance or by a resistance which varies as i^n where $-2/3 < n < -1/2$, as found in the measurements of the preceding section, and there is some limiting of the current by the emitting surface.

Recently, E. O. Johnson and W. M. Webster of this laboratory observed a further anomaly in the behavior of the emission of an oxide cathode. They were making measurements on a gas tube which had sufficient cathode resistance to increase the tube voltage drop significantly. That the additional drop was occurring in the cathode was verified by probes situated immediately in front of cathode. The resistance measured by the probes was reasonable for a well-activated cathode. It has frequently been observed that a cathode with appreciable cathode resistance will heat when the cathode current is increased. They, however, observed a cooling of the cathode as the current was increased. By measuring the additional heater power required to restore the cathode to its initial temperature, and by computing the I^2R power due to the cathode resistance they arrived at the conclusion that the latent heat of vaporization of electrons must be about 2.5 volts in the cathode under observation.

When this observation was brought to our attention, some further exploratory experiments were undertaken. These experiments are mentioned with diffidence because they have not progressed to a point where the experimental techniques are well in hand. However, the results are sufficiently provocative to bear mention and they raise questions about the proper interpretation of certain experiments designed to measure cathode resistance. In these cathode resistance measurements, the cathode temperature is monitored as the anode current is increased. As the current increases from zero, the cathode temperature drops due to evaporation cooling, reaches a minimum as the joule heating due to cathode resistance becomes appreciable, and then rises with a further increase in current. At some current I, the joule heating just balances the evaporation cooling and the cathode is again at the zero-current temperature. At this current, the cathode resistance is

$$R_k = \frac{\phi}{I},$$

where ϕ is the work function. In many such measurements, a value of ϕ has been assumed or derived from other measurements and R_k has been computed from the relation above. This computation assumes that ϕ has a value which is independent of the current and is properly determined by the emission measurement. In the present experiments, the same measurement was made and, in addition, R_k was measured in the cathode-resistance bridge at the current at which the temperature was restored to the zero-current temperature. With this information, the work function can be computed. In the present experiments, the cathode temperature was monitored by measuring the heater resistance. The heater formed one branch of a bridge whose balance was read with an amplifier driving an oscilloscope. The sensitivity was such that an inch deflection on the oscilloscope corresponded to a change of temperature of 0.07 degree at 1000°K. Unless the emissivity of the oxide coating changes with current, a restoration of cathode temperature to the zero-current temperature should eliminate errors due to changes in lead losses, changes in spectral distribution and changes in emissivity with temperature. Measurements were made on a series of tubes known to have substantial interface resistances. The work functions computed from the above relation ranged from about 1 volt to 3 volts for the various tubes. While the results must be considered tentative and perhaps dubious, they certainly raise questions which must be answered by further, more careful measurements.

It is of interest to inquire how a latent heat of evaporation of electrons as high as 2 volts might arise. According to the Fowler emission equation, the work function is the sum of the electron affinity and the energy gap between Fermi limit and the bottom of the conduction band. At sufficiently high current densities, the oxide adjacent to the emitting surface might become completely depleted of donors with the result that the oxide becomes intrinsic. In this event, the work function would be the sum of the affinity (about 1 volt) and one half of the width of the forbidden energy band (about 1.9 volts), i.e., about 2.9 volts. Hence, if the donor depletion hypothesis is accepted, the explanation of a latent heat as high as 2.0 volts is straightforward.

SIMPLE ACTIVATION EXPERIMENTS

With the growing conviction that the major anomalies of the oxide cathode are accounted for by the donor-depletion hypothesis, it ap-

peared desirable to study the nature of the postulated mobile donors. The groundwork for such a study had been laid in the beautiful experiments of Becker and Sears on the activation of oxide cathodes by barium deposition and by electrolysis.[9,10] Their measurements are pertinent to the present problem and might almost suffice. However, it appeared worth while to undertake a new set of experiments, planned in the light of present knowledge and, in particular, in the light of the donor-depletion hypothesis.

In considering the results of Becker and Sears, it seemed that two effects of barium deposition might be apparent, (1) a permanent activation, and (2) an inhibition of donor-depletion-layer formation if barium were deposited during current flow. In order to get some rough notions of the deposition rate required to observe these effects, a "Friday afternoon" experiment was tried. A commercial diode with an open structure and a large getter splash facing the cathode (a 2X2) was operated with alternating current voltage on the anode. The tube was selected from a box of tubes which had been discarded after a long life. The current–voltage characteristic of the diode was displayed on an oscilloscope. The activation process consisted in turning a blowtorch on the getter splash. The result was immediate and spectacular; the "emission" increased about 50-fold at the first touch of the torch. It was apparent that a more carefully controlled experiment was in order.

To this end, the tube was stripped of its base and mounted in an oven so that the bulb temperature, i.e., the getter-splash temperature, could be controlled. The results of this experiment are shown in Figure 38. The initial current–voltage characteristic was as shown by the curve for a bulb temperature of 320°K. As the bulb temperature was increased, the characteristic took on the succession of forms shown, culminating in a linear characteristic on three-halves paper at a bulb temperature of 520°K. As the bulb temperature was reduced, the characteristics collapsed as shown by the dashed curves until, at ambient temperature, the characteristic was as shown by the upper curve for a bulb temperature of 290°K. It appears that the bulb temperature cycle increased the activity of the cathode about 10-fold, and that the 26-fold increase with a bulb temperature of 520°K was in part due to the inhibiting of donor-depletion-layer formation by the formation of donors at the emitting surface.

In order that such measurements be meaningful, they must admit of complete cycles. After a little groping, it was found that cathodes which had been activated by deposition could be deactivated by operating them at about 1200°K for a matter of minutes *without plate*

current. If they were operated at elevated temperatures with plate current, the cathodes activated. The lower curve for a bulb temperature of 290°K, in Figure 38, shows the result of such a deactivation, the third for this cathode, i.e., the data shown being taken on the third complete cycle of the cathode.
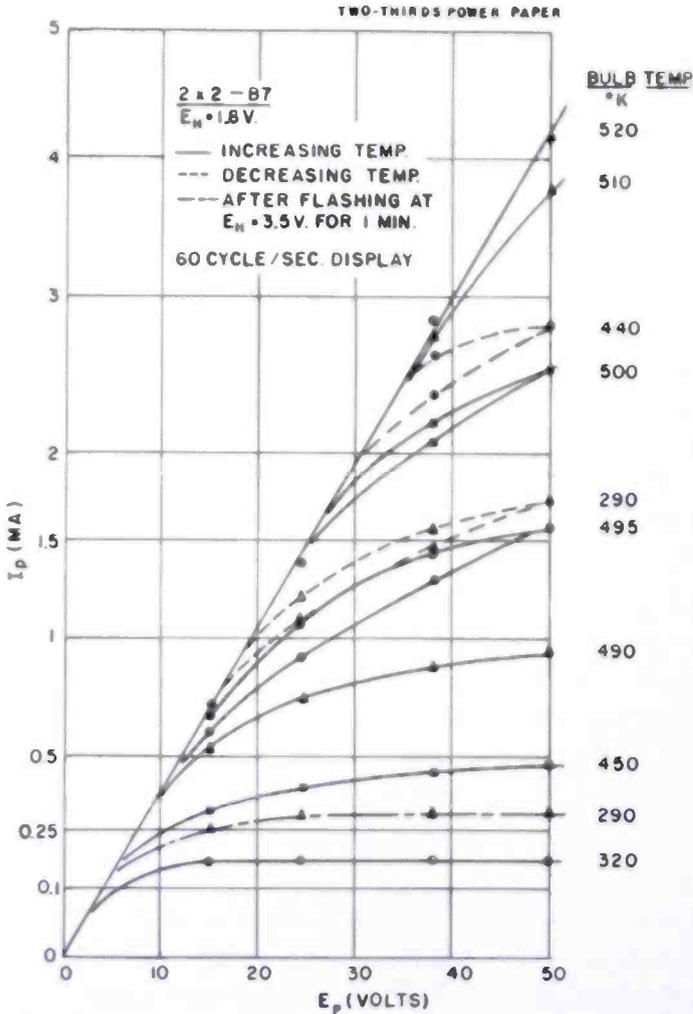
Fig. 38—The activation of a cathode by operation barium vapor. The solid lines show the voltage–current characteristics of the diode as the barium vapor pressure is increased. The dotted lines show the voltage–current characteristics as the vapor pressure is reduced. The dot-dash line shows the voltage–current characteristic after cathode deactivation by overheating without plate current.

Similar experiments were performed on tubes having probes imbedded in the oxide coating. These experiments showed that an activation of the cathode resulted in a marked increase of the cathode conductivity, a result in conformity with past results, for example, those of Hannay, McNair, and White.[51]

These simple experiments showed that:

1) Substantial activation of an oxide cathode is possible by operation of the cathode for minutes in barium vapor at a pressure of 10^{-10} millimeter of mercury.[56] The deposition rate is then of the order of 10^{-4} monolayer per second.

2) The formation of a donor depletion layer is inhibited by barium deposition rates of the order of 10^{-4} monolayer per second.

3) A cathode may be deactivated by operating it at a temperature a few hundred degrees above the normal operating temperature if no current is drawn from the cathode.

4) A cathode activates further if barium is deposited on its emitting surface and then current is drawn from the surface.

With these results in hand, it appeared quite feasible to undertake the experiment proposed at an earlier date by R. H. Plumlee of this laboratory, namely, the activation of a cathode using a mass spectrometer as a barium source. The mass spectrometer method has the notable advantage that it leaves no doubt as to what is responsible for any observed activation. Such is not the case when a blowtorch is applied to the envelope of a tube.

ACTIVATION EXPERIMENTS IN THE MASS SPECTROMETER

In order to perform the deposition experiment, the 60-degree mass spectrometer built by R. H. Plumlee was appropriately modified. A series of batalum getters was installed ahead of the ionization chamber in the source to serve as a barium source. The receiver assembly was modified as shown in Figure 39. Figure 39 also shows the mass-defining aperture and an oxide cathode separated by a series of guard plates with a probe, which subtends half of the defining aperture, inserted between the second and third guard plates. The probe is used to monitor the ion beam and the guard plates to isolate the probe from the diode consisting of the final guard plate and the cathode. The cathode is rectangular in section and is coated with $BaO + SrO$ on the side facing the spectrometer and the side opposite. The area of each coated section is 0.053 square centimeter. The spray weight is 10 milligrams per cubic centimeter, and was of a consistency to give a coating density of about one half relative to crystalline BaO. The coated surfaces contain about 6×10^{19} molecules per square centimeter of emitting surface. The coatings have platinum probes imbedded in them so that the conductivity of the coating can be estimated. The cathode surface remote from the defining slit is faced by an anode to form a diode which is used as a comparison standard so that any

---

[56] W. Espe and M. Knoll, *Werkstoffkunde der hochvakuumtechnik*, Julius Springer, Berlin, 1936.

changes in cathode activity due to background gases can be distinguished from changes due to deposition. The computed geometrical perveance of the receiver diode is 1.20×10^{-5} ampere per volt$^{3/2}$. The measured perveance is 1.40×10^{-5} ampere per volt $^{3/2}$, a reasonable agreement considering the difficult geometry.

After extensive bake-out of the entire system, the cathodes were activated by applying a 60-cycle per second voltage, 60 volts peak, to both anodes and gradually increasing the cathode temperature. When active, the cathodes gave about 300 milliamperes per square centimeter at 1050°K. The batalum getters comprising the barium source were then outgassed and partially flashed, in the course of which the system
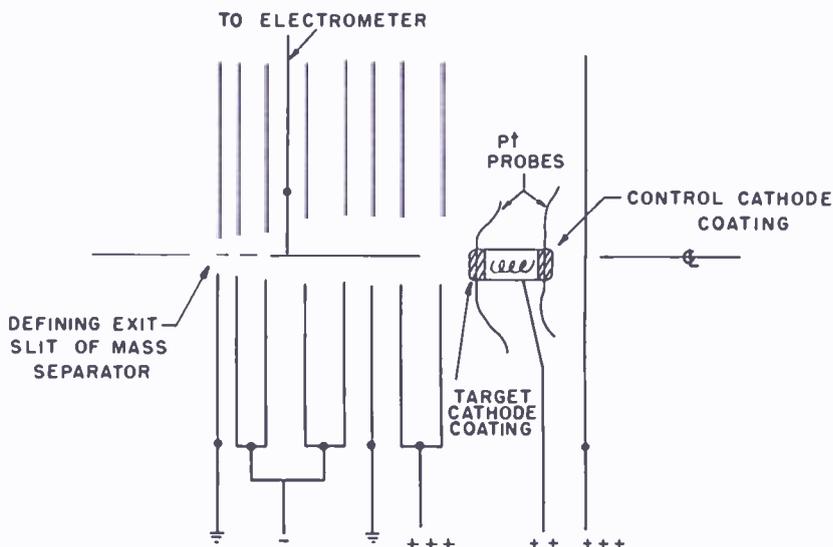
Fig. 39—A schematic drawing of the receiver assembly for the deposition of barium on an oxide cathode in the mass spectrometer.

pressure dropped below 10^{-7} millimeter of mercury and remained there throughout subsequent experiments. At the same time, the mass spectrum cleaned up and only the Ba peaks (single and multiple charged), a small CO peak, and trivial CH_4 peaks remained. The average Ba partial pressure in the ionizing chamber during operations was estimated to be about 10^{-6} millimeter and the CO and CH_4 partial pressures about 10^{-9} millimeter.

The deposition experiments were performed with the cathodes operating at about 900°K. This temperature was chosen for two reasons, (1) the cathode is very sensitive to Ba deposition in this temperature range, and (2) saturation current could be drawn with an anode voltage less than 20 volts, so that possible disturbing effects due to ionization of residual gases were minimized. The anodes were operated on alternating voltages to permit continuous displays of

the current–voltage characteristics on an oscilloscope. A typical current–voltage characteristic is shown in Figure 40. It should be noted that no part of the characteristic coincides with the perveance line. From this it is inferred that the diode is not emission-limited until the knee is approached and that most of the applied voltage appears across the cathode.
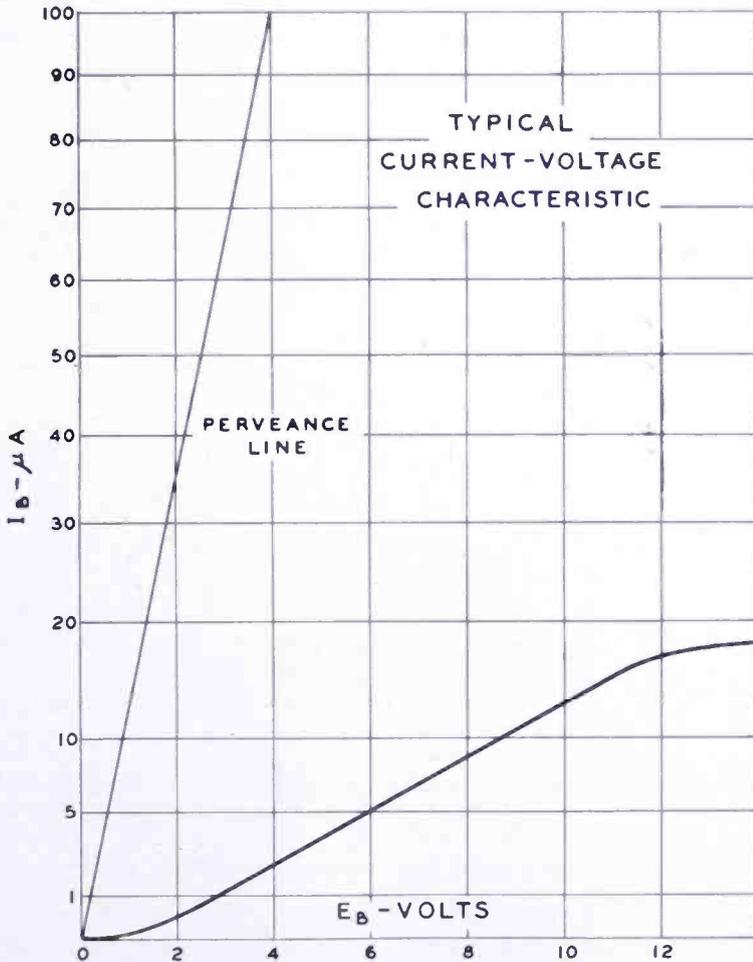
Fig. 40—A typical current–voltage characteristic of the diode in the mass-spectrometer experiment. The measured perveance line is shown for reference.

Measurements at a particular state of the cathode showed that an anode voltage of 19.3 volts was required to obtain a cathode current of 15.6 microamperes. A simple computation shows that 18.2 volts of the required voltage appears across the cathode. Hence, the cathode resistance was about 1.2×10^6 ohms. In order to determine whether or not this resistance was reasonable, the probe was biased 22.5 volts positive with respect to the cathode base. The probe current stabilized

at a value of 35 microamperes. Hence, the probe resistance, after polarization, was about 0.7×10^6 ohms, a value in reasonable accord with the value computed for the total cathode resistance. It may also be remarked that the cathode with its probe displayed the amplifying effects described earlier.

Figure 41 shows activation as the result of barium deposition on the cathode. The cathode temperature is about 900°K and the peak alternating-current anode voltage is 19 volts. The ordinate is the
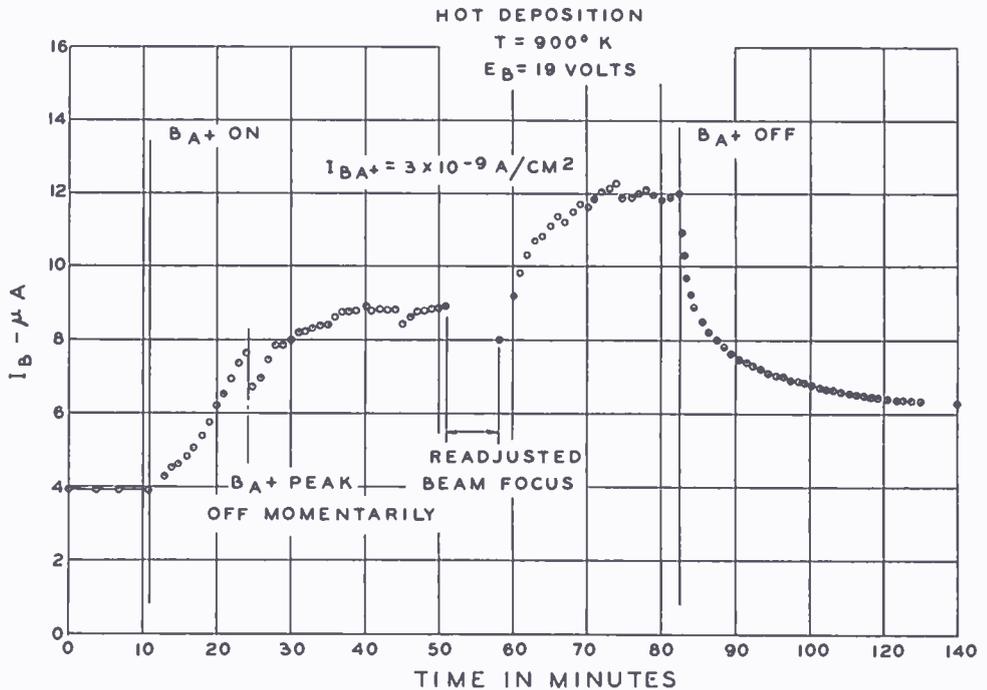
Fig. 41—The effect on cathode activity of barium deposition. I_B is the plate current of the diode at the knee of the voltage–current characteristic.

plate current at the knee of the current–voltage characteristic. It will be noted that the activation curve is quite irregular. This results from the extreme sensitivity of the cathode to Ba deposition. Minor fluctuations in the various voltage and field supplies of the spectrometer are quite conspicuous and, as a matter of experience, it was found that the best way of keeping the beam on the receiver was to monitor the cathode activity. The barium beam current is cited as 3×10^{-9} ampere per square centimeter of cathode area. This value, and the same is true of other cited values, is the beam current measured with the cathode as a receiver, with the cathode cold, and with direct current on the anode. It represents an upper limit to the ion current reaching the cathode when the diode is in operation. The activation curve shows a 3:1 activation with the Ba beam on. The activation reaches what appears to be a stable value. When the beam is cut off, the activity

decays to a value about 50 per cent greater than the initial value. It appears that the immediate effect of deposition was to inhibit donor-depletion-layer formation. However, the major effect of the deposition had not taken place, a matter to be discussed after further examples of the direct effect of Ba deposition have been exhibited.

Figure 42 shows the effect of deposition on a cold cathode. After each deposition period, the Ba beam was turned off and the cathode heater and anode voltages were turned on. The anode shows a characteristic decay from a relatively high initial value to a low stable value. In one case, the heater and Ba beam were left off for what
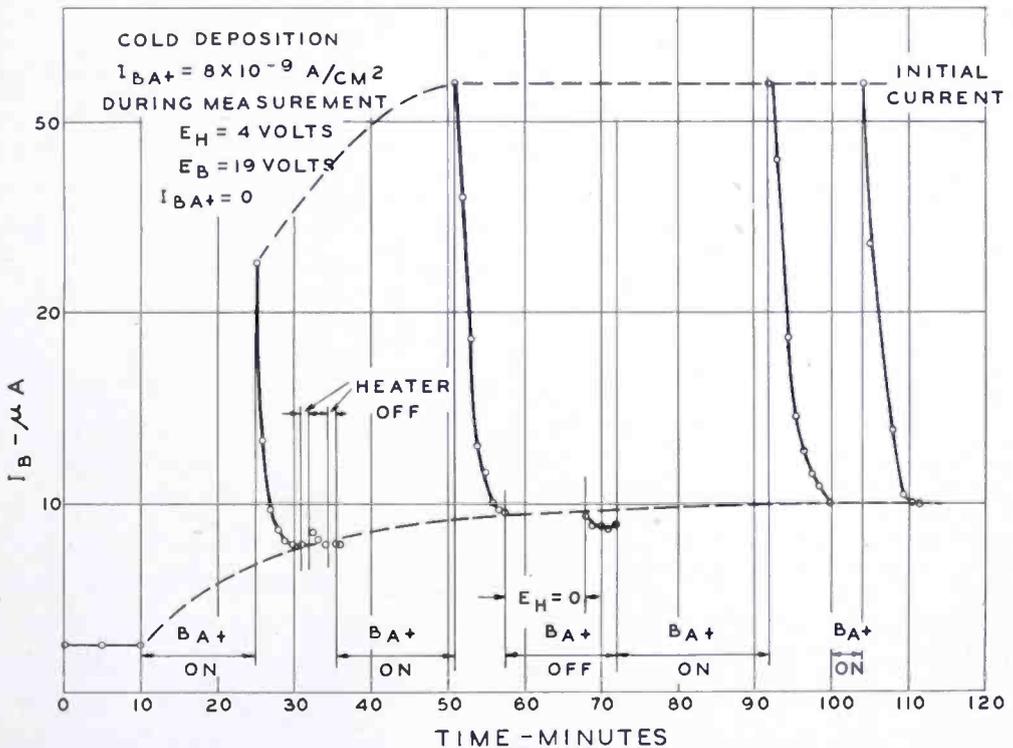
Fig. 42—The effect of barium deposition with the receiver cathode cold. At about 60 minutes on the time scale, the cathode was left cold for a reasonable deposition period to verify that the observed increases on barium deposition were due to deposition.

would have been a reasonable deposition period, just to be sure that deposition was responsible for the high peak currents. Both peak and ultimate currents increase with Ba deposition and reach equilibrium values. Unfortunately, sufficient time for complete current decay was not provided. This came about because the data were obtained with a recorder. Current decays which appear incomplete on the compact time scale of Figure 42 seemed complete on the recorder tape. In this experiment, a donor depletion layer forms when current is drawn. The depletion layer is then "frozen in" by turning off the heater. That it

remains frozen in during deposition periods is evident from the lack of recovery in the instance when the heater was turned off and no barium was deposited. In other cases, the depletion layer was removed, at least in part, by the deposition of barium during the off period of the heater.

Figure 43 shows the effects of deposition when the current is sampled with 0.4-second pulses. The pulse length was determined by the response time of the recorder. The current is independent of the sampling rate for rates less than 12 per minute. Accordingly, a sampling rate of 12 per minute was used for most of this experiment. It
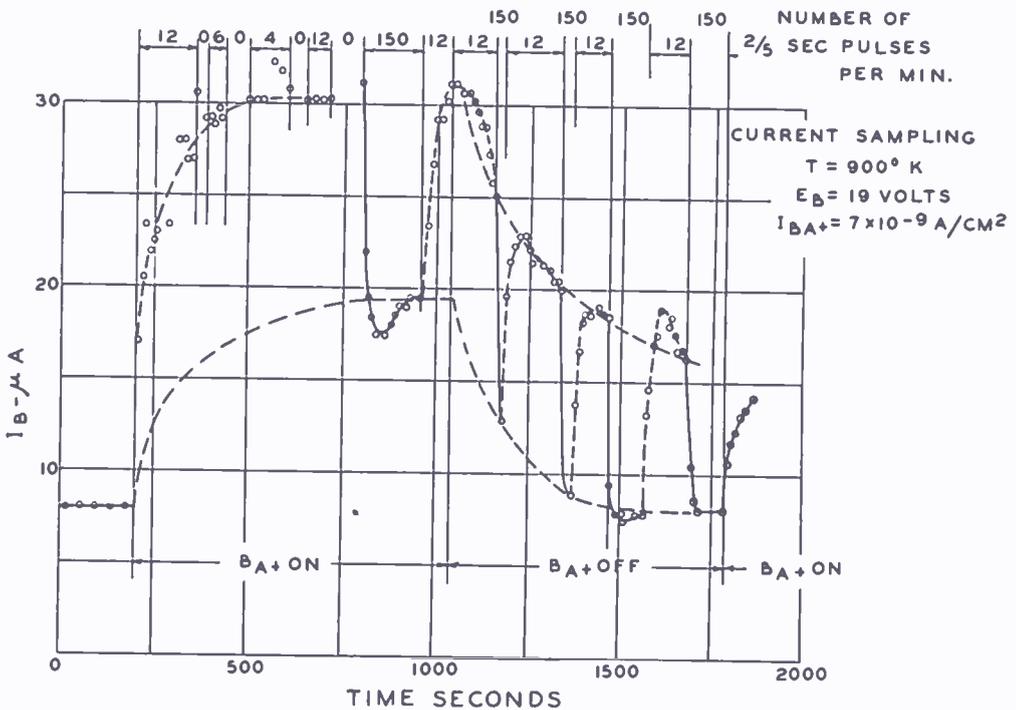
Fig. 43—The effect of barium deposition under pulse conditions. The anode voltage is a 60-cycle-per-second voltage applied in 0.4-second pulses. The effect of the continuous application of the anode voltage is also shown.

will be noted that the current rises to a stable value when the Ba beam is turned on. When the anode voltage is applied continuously rather than in pulses, the current decays to a stable value. When pulsing is resumed, the current recovers its former pulse value in about a minute. When the Ba beam is turned off, the pulse current decays. When the anode voltage is applied continuously, the current decays relatively rapidly to a much lower value. When pulsing is resumed, the current recovers to a value which lies on the pulse decay line. Here again the final activity of the cathode was about what it was initially. Hence the immediate effect of the barium deposition was to

limit the donor depletion. The major difference between this experiment and the previous one was that here the cathode temperature was maintained between pulses so that back diffusion of donors into the depletion layer could occur. This is apparent in that part of the curve where no barium was deposited. When pulsing was resumed after operation on a continuous voltage, back diffusion restored the conductivity of the cathode to a value determined by the average pulse current and the surface density of donors. The slow decay of the peak pulse current after deposition indicates that donors are stored near the surface of the cathode and that these donors are bound more firmly in the lattice than those somewhat more remote from the surface where the donor depletion layer forms. That the binding near the emitting surface should differ from that in the bulk oxide seems quite reasonable; an ion on the surface has, on the average, about half as many nearest neighbors as does an ion well within the oxide. The situation at a metallic contact may be quite different because here the "surface" sees an image field in the metal and the surface may have properties which resemble those in the bulk material. The present experiments suggests that, under conditions of current flow, the oxide of a cathode may be described in terms of three more or less distinct regions: a region very near the emitting surface where the ion binding differs from that within the oxide so that no substantial donor depletion occurs under short pulse conditions, a second region underlying the surface layer in which electrolytic donor depletion does occur, and a region where the bulk properties are modified only to a relatively minor degree by passage of current.

Figure 44 shows the immediate effect of barium deposition on the conductivity of the oxide between the base metal and the platinum probe. In this experiment the anode was biased slightly negative so that there was no significant anode current. When there is no anode current, there is no surface depletion layer which can react on the probe (the reaction is quite apparent when the anode is biased positively), and there is no field to electrolyze donors into the probe region, so that any observed effect is due to donor diffusion. Because the experiment shows no net increase in conductivity, it seems likely that the increase in probe current with barium deposition was due to a limiting of the depletion layer about the probe.

As remarked earlier, the direct effect of barium deposition is an increase in cathode activity which decays to approximately the initial value when Ba deposition is stopped. However, the major and "permanent" effect of Ba deposition depends on the subsequent treatment of the cathode. To illustrate this, Table III shows an excerpt from

PROBE RESISTANCE
T = 900° K
E_B = -1.5
PROBE VOLTAGE = +4.5 VOLTS
$I_{BA+} = 7 \times 10^{-9} = A/CM^2$
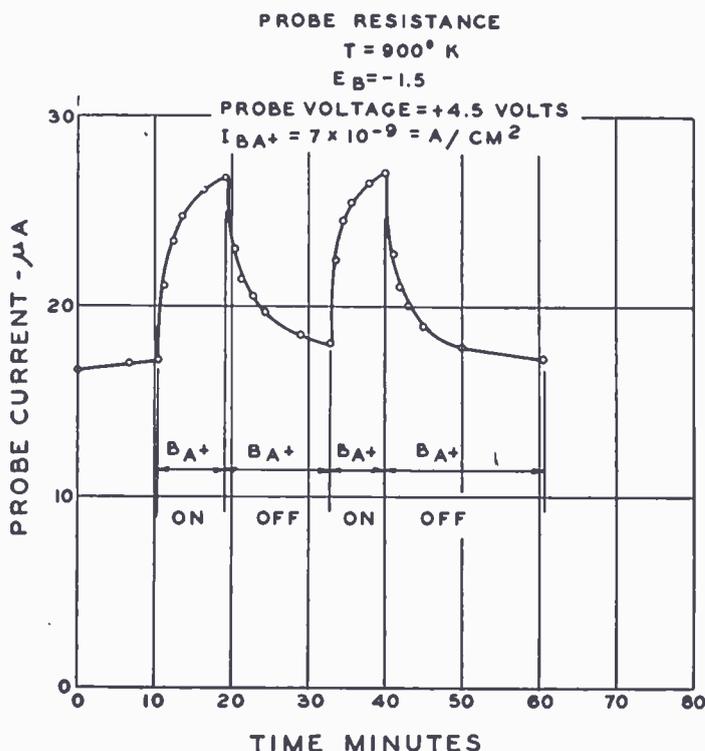
Fig. 44—The effect of barium deposition on current to a probe embedded in the cathode coating.

the complete record of the status of the cathode from initial activation to the completion of the experiments. The information is consecutive and without omissions. The first column numbers the row for easy reference. The next four columns show the conditions of operation

Table III — The Effect of Aging, Subsequent to Barium Deposition, on the Resistance of an Oxide Cathode

No.	E_H Volts	E_B Volts	t Minutes	I_{BA+} Amperes per square centimeter	I_B* μA
1	4.0	19	15	2×10^{-9}	103
2	8.7	19	3	0	228
3	8.7	19	3	0	152
4	7.0	0	4300	0	15
5	4.0	19	116	2×10^{-9}	29.3
6	0	0	8400	0	66.0
7	4.0	19	10	0	91.6
8	3.5	19	0	0	42.9
9	8.0	0	3	0	116
10	4.0	19	180	10^{-9}	195
11	7.0	0	1260	0	12.1

* Read with $E_H = 4.0$ volts; $E_B = 19$ volts except Nos. 8 and 9. Nos. 7 and 8 corresponding readings—No. 7 at $E_H = 4.0$; No. 8 at $E_H = 3.5$. No. 9 read with $E_H = 3.5$ volts.

immediately prior to reading the current shown in the last column. Row 1 shows the cathode quite active following a succession of deposition experiments. Row 2 shows the effect of flashing the cathode at about 1170°K for 3 minutes. The flashing has resulted in a 2.2-fold increase in activity. Row 3 shows the deactivation which results from flashing for another 3 minutes, and row 4 shows the further decrease due to operating the cathode at about 1100°K over a weekend. These experiments accord with previous experience in the activation of cathodes by the direct evaporation of barium onto cathodes and by operation in barium vapor. In all of these experiments, flashing for short periods subsequent to Ba deposition, 30 seconds to a minute at about 1200°K, leads to activation. More extended flashing at 1200°K or long flashing at more modest temperatures *without anode voltage* leads to deactivation. With anode voltage, activation results. Row 5 shows the state of the cathode after a deposition run. Row 6 shows the activation which resulted from leaving the cathode at room temperature for 140 hours. By coincidence, the increase in activity is 2.2-fold, which is the same increase found for rows 1 and 2 in the table. If both activations are due to temperature dependent diffusion, this indicates an activation energy for diffusion of the order of a quarter volt. Row 7 shows the further increase in activity due to drawing current for 10 minutes, row 8 shows the corresponding current at a lower cathode temperature, and row 9 shows the further increase of activity after flashing at about 1140°K for 3 minutes.

Rows 10 and 11 show another deactivation by extended overheating without anode voltage.

As a final bit of experimental data, it is noted that the monitoring diode remained completely inactive after the deactivation immediately subsequent to the initial activation of both cathodes.

While these deposition experiments have been interpreted in terms of the donor depletion hypothesis as the experiments were described, it is interesting to note that the depletion hypothesis can be inferred directly from the deposition experiments, without reference to the earlier work. The argument proceeds as follows:

1) The deposition of 0.01 monolayer of barium may lead to a large increase in activity of the cathode if the cathode is initially inactive.

2) The deposition of 0.01 monolayer probably does not change the dipole layer appreciably. Exploratory attempts to measure changes in work function have shown no changes within the experimental accuracy.

3) A 0.01 monolayer of barium, uniformly distributed throughout the present cathode, would increase the Ba concentration by about 1 part in 10^7. If barium or a barium deposition by-product forms

donors, such an increase in donor concentration is adequate to increase the conductivity manyfold if the cathode is initially inactive. Estimates of the bulk conductivity by means of the probe show the expected increase in conductivity.

4) The inference that the effect of barium deposition is to raise the Fermi level is re-enforced by the observation that no permanent effect of barium deposition is observed until the donors have been permitted to diffuse into the body of the cathode by the passage of time, of the order of 100 hours at room temperature, of the order of a minute at 1200°K, or until the donors have been electrolyzed into the body of the coating by the passage of current.

5) The observation that the deposition of many monolayers of barium on a cathode surface does not change the work function significantly until the cathode is subjected to further treatment suggests that the excess barium is stored as BaO with the formation of oxygen vacancies. The oxygen vacancies serve as F-center donors.

6) Probe potential measurements indicate that most of the voltage drop across the cathode appears between the probe and the emitting surface, a voltage distribution in accord with that found by Loosjes, Vink, and Jansen.

7) The observations of 4) above regarding diffusion and electrolysis, the observations of 6) above regarding the potential distribution, and the experimental observation of pulse decay and recovery of Figure 43, taken together, suggest that the current decay is due to an electrolytic depletion of donors near the emitting surface when current is drawn. The extent of the depletion depends on the cathode temperature, the current drawn, the duty cycle, and the barium concentration at the emitting surface. The pulse recovery is due to back diffusion into the depletion layer. The postulated electrolysis of donors from the emitting surface has its counterpart in the experiments of Becker and Sears in which they activated cathodes by electrolyzing cations to the cathode surface.

The barium deposition experiments using the mass spectrometer as a barium source have served three major purposes:

1) They were free from the objection that unknown materials may have contributed to observed activations.

2) The donor depletion hypothesis can be inferred independently of earlier experiments.

3) They suggest that the donors in BaO are F-centers, at least in part.

DONORS IN BaO

Throughout this paper it has been assumed that BaO has two sets of donor levels, one set at about 1.4 e.v. below the bottom of the conduction band, another set at about 2.4 e.v. below the bottom of the conduction band, i.e., the donor levels found by DeVore in his photoconductivity measurements. So far, no other donor levels have been required to account for the observed conductivity and emission phenomena. In order to account for the inactive conductivity, it was necessary to postulate a set of traps lying close to the valence band. Because of the low density of traps required to account for the conductivity behavior, their presence might well be unobservable in the background near the onset of the 3.8 e.v. transition in a photoconductivity measurement. It is now pertinent to try to account for the observed energy levels.

As a result of the mass spectrometer measurements, it was conjectured that the donors might be F-centers formed from oxygen vacancies. Pertinent data bearing on this conjecture have been obtained at Cornell University in work on single crystals of BaO.[57] Crystals grown under conditions where liquid barium can form on the crystal surface show a red coloration. Crystals grown in an excess of barium under conditions where liquid barium does not form on the crystal show a blue coloration. A possible inference is that a vast excess of barium leads to crystals having interstitial barium or barium agglomerates which act as donors which absorb in the blue, and that a more modest excess of barium leads to crystals having oxygen vacancies which form F-centers which absorb in the red. Whatever their nature, it is obvious that the latter donors lie closer to the conduction band than do the former.

R. W. Reddington has studied the barium diffusion rates in BaO using Ba^{140} as a tracer.[58] He finds diffusion constants for charged and uncharged barium diffusion with apparent activation energies of the order of 11 e.v. in the high temperature range. The reciprocal temperature plot for uncharged diffusion shows a temperature break and a low-temperature slope which corresponds to an activation energy of 0.44 ± 0.03 electron volt. He interprets the low-temperature activation energy as the activation energy for simple diffusion and the high-temperature activation energy as the sum of the activation energy for diffusion and one half the energy required to move a barium atom

from a lattice site to an interstitial position. The energy required to produce an interstitial barium atom in this manner is computed to be 23 ± 5 e.v. He makes a similar interpretation of the high-temperature slope for barium ion diffusion and finds an activation energy for diffusion of 0.30 ± 0.05 e.v. He attributes the ion diffusion to a vacancy mechanism. Reddington finds that the low-temperature diffusion is structure sensitive, i.e., the diffusion rate depends on the past heat treatment of the oxide. In a crystal quenched from $1475°$K, he finds a diffusion constant as high as 10^{-8} cm^{-2} sec^{-1} at about $1200°$K.

Mrs. R. S. Bever of Cornell University has measured the diffusion rate of the blue color centers.[59] Between $1100°$K and $1500°$K, the apparent rate of diffusion for the color centers is several orders of magnitude greater than the apparent rate for barium. Mrs. Bever finds an activation energy for diffusion of the color centers of about 2.4 e.v. If the blue color centers are in fact due to oxygen vacancies, their diffusion rate should be comparable with that of barium vacancies because the ionic radii of barium and oxygen are much the same, and, as will be shown later, so are the "ionic radii" of their vacancies. In the mass-spectrometer studies of thermal activation subsequent to barium deposition, it was found that the same activation could be obtained in 140 hours at room temperature as in 3 minutes at about $1200°$K. From this an activation energy for the diffusion of donors of 0.27 e.v. was computed. This value is about the same as that measured for barium vacancies. It is suggested that the activation energy for the simple diffusion of oxygen vacancies is about 0.3 e.v., and that the 2.4 e.v. observed by Mrs. Bever arises in part from some other mechanism as in Reddington's experiments in the same temperature range.

R. M. Matheson and the writer have computed the energy required to remove a barium ion and an oxygen ion, independently, from BaO. The computation followed the method of Mott and Littleton for alkali-halides.[60] In the alkali-halides, the halogen ion has by far the larger polarizability and by far the larger ionic radius. Because of the latter circumstance, the halogen ions overlap and the effect of the polarization which arises from the internal polarization of an ion and that which arises from its displacement from its equilibrium position must be computed separately. In BaO, the polarizabilities of the two ions are about the same, as are their ionic radii. Accordingly, it was as-

---

[59] Private communication.

[60] N. F. Mott and M. J. Littleton, "Conduction in Polar Crystals," *Trans. Faraday Soc.*, Vol. 34, Part 34, pp. 485-499, March, 1938.

sumed that the overlap in BaO is trivial. This assumption was checked by computing the high-frequency dielectric constant, using Bever and Sproull's low-frequency dielectric constant,[61] Fajans' and Joos' polarizabilities,[54] and the classical formula relating these constants. A value of about 3.5 was obtained, a value in fair agreement with a measured refractive index of 1.98. Because the classical formula assumes no overlap of ions, this result is construed as a confirmation of the assumption of no overlap. With this modification in the computation of the polarization energy, the energies to remove oxygen and barium ions from lattice sites to infinity were computed. The results indicate that 17.7 e.v. are required to remove a Ba^{++} ion, and 17.6 e.v. to remove an O^{--} ion. Because of the uncertainties in the computation of the polarization energies, these values are not considered accurate within several volts.*

If the computed energies are assumed to be correct, the energy to form a vacancy pair, i.e., the energy to remove a pair of ions minus the lattice energy (31.58 e.v.),[62] is about 4 e.v.

Because the radii of the two ions in BaO are about the same, and because the polarizabilities of the ions are not greatly different, the relaxation of the crystal is about the same where Ba^{++} or O^{--} is removed. Hence, it is to be expected that if an oxygen vacancy is made electrically neutral by the insertion of two electrons, the energy gained will be about the same as if a barium vacancy is made electrically neutral by the insertion of two holes. In other words, the energy levels for holes in a barium vacancy should lie at about the positions of the energy levels for electrons in F-centers. This conclusion is independent of the actual locations of the energy levels in either barium or oxygen vacancies. The implications of this inference will be considered later.

With the ion-removal energies computed above, the energy of formation of F-centers by various reactions can be computed from Born-Mayer cycles. If it is assumed that the 1.4 and 2.4 donor levels are F-center levels, and if it is assumed that the electron affinity is 0.5 volt, the energy required to form an F-center is

By O evaporation	7.1 e.v.
By O_2 evaporation	7.2 e.v. (per pair)
By Ba deposition	—3.6 e.v.

[61] R. S. Bever and R. L. Sproull, "The Dielectric Constant of Barium Oxide," *Phys. Rev.*, Vol. 83, pp. 801-805, August 15, 1951.

[62] F. Seitz, *Modern Theory of Solids*, McGraw-Hill Book Company, Inc., New York, N. Y., 1940.

* Note added in proof. R. L. Sproull has informed the writer that: (1) R. W. Reddington has made a similar computation; and (2) there is evidence that the ionicity of BaO is about 1.6, hence, the above computation must be regarded with further reserve.

It remains to discuss the possible energy level structure of BaO in terms of the considerations above. In the discussion of the conductivity of an inactive cathode, it was shown that the behavior could be accounted for by a forbidden band having a width of about 3.8 e.v. in accord with DeVore's result, and a set of traps with a density of about $N_t = 10^{12}$ lying just above the valence band. Now suppose the cathode is taken to a temperature high enough so that vacancy pairs form and the cathode is then quenched to absolute zero so no electrons are in the conduction band. If the donor levels are due to F-centers, the F-center levels lie 1.4 and 2.4 e.v. below the conduction band. From the arguments adduced above, the barium-vacancy levels lie about 1.4 and 2.4 e.v. above the valence band, i.e., they coincide with the F-center levels approximately. Hence, the barium vacancies will lose electrons to the traps until the traps are filled. If the number of pairs is sufficient to more than fill the traps, the 2.4 levels will start to fill. Any further increase in pairs will increase the occupancy of the 2.4 levels. The density of electrons in the 2.4 e.v. levels will then be $2N_p - N_t$, where N_p is the density of pairs. If F-centers are now added, the electrons in the 1.4 e.v. levels will start to fill the 2.4 e.v. vacancies and the density of electrons in the 2.4 e.v. levels will be $2N_p - Nt + N_f$ where N_f is the density of F-centers. When the density of F-centers becomes great enough to fill the 2.4 e.v. levels, the 1.4 e.v. levels will begin to fill. The electron density in the 1.4 e.v. levels will be $N_f - N_t$, i.e., there will be $N_f - N_t$ donors and $2N_p + N_t$ vacancies at the 1.4 e.v. level. This account of the gradual activation of a cathode accords with the photoconductivity experiments of DeVore.

In a preceding section, it was estimated that the density of traps in an inactive cathode is 10^{12} per cubic centimeter, and that the density of vacancies in an active cathode is 10^{15} per cubic centimeter. Hence, the density of traps is small compared to the density of vacancies if the density of traps is not increased in the activation process. It is of interest to compute the temperature from which the cathode must be quenched to freeze in 10^{15} vacancies per cubic centimeter formed by a thermal pair production. The disorder constant is

$$\gamma \stackrel{.}{=} \frac{N_v}{N} = e^{\frac{-U}{2kT}},$$

where N is the number of lattice sites and U is the energy to form a pair.[54] With $N_v = 10^{15}$ and $U = 4$ e.v., as estimated above, the required temperature is about 1400°K, a value which seems reasonable.

In summary, a model of the BaO cathode has been deduced which comprises

1) A forbiden band of 3.8 e.v. width.

2) A set of traps located close to the oxygen band.

3) A set of donor levels at 2.4 e.v. below the conduction band and an equal number of vacancies at 1.4 e.v. below the conduction band, both formed by thermal pair generation.

4) A set of donor levels at 1.4 e.v. below the conduction band and an equal number of donor levels at 2.4 e.v. below the conduction band, both formed by an activation process which removes oxygen atoms from the lattice.

This model may not be unique in describing the observed behavior of cathodes. However, it is the simplest model yet adduced which accords with the experimental data at hand.[63]

SPECULATION

The donor depletion hypothesis has been described in phenomenological terms in the preceding sections of the paper. Before the hypothesis achieves the rank of a theory, it must be formulated in more precise terms so that it can be compared with experiment on a quantitative basis. During the course of the experiments, some humble beginnings were made. These computations were made in an attempt to understand certain aspects of the experimental data. They do not form a consistent whole, yet they shed enough light on the behavior of the postulated donor depletion layer so that the inclusion of some of the computations seems justified.

a) *The Limiting Current Through a Semiconductor with Mobile Donors.*

Consider a semiconductor having a donor density $N(x)$ of which $n(x)$ are ionized. Assume that the donor current vanishes under stationary conditions. Then the donor current density is given by

$$0 = n e \mu_+ E - D_+ e \frac{\partial N}{\partial x},$$

---

[63] Since this paper was written, T. Hibi and K. Ishikawa have published a letter to the editor of the *Physical Review*, Vol. 87, Second Series, pp. 673-674, August 15, 1952 entitled "Spectral Dependence of Thermionic Emission with Activation from (Ba-Sr)O Cathodes over the Visible Region." Their results can be interpreted in terms of the model above. If such an interpretation is made, the result suggests that the barium and oxygen vacancy levels are separated by about 0.3 volt and that the traps lie at about 3 volts below the conduction band.

where μ_+ and D_+ are the donor mobility and diffusion constant, respectively, and E is the electric field. If electron diffusion is neglected, the electron current density is

$$j = n e \mu_- E,$$

where μ_- is also electron mobility. The two equations may be combined to yield

$$\frac{\partial N}{\partial x} = \frac{j}{D_+ e} \frac{\mu_+}{\mu_-} = \frac{j}{\mu_- kT}.$$

This integrates to

$$N = \frac{j}{\mu_- kT} (x + C),$$

where the integration constant C is to be determined from the condition that the total number of donors in the sample of length l is to be constant at a value $\overline{N}l$, where $\overline{N}$ is the average density of donors. When C is so determined, the result is

$$N = \overline{N} + \frac{j}{\mu_- kT} (x - l/2),$$

i.e., the donors are distributed linearly with distance with a slope which is proportional to the electron current density. As the current density is increased, the density at $x = o$ diminishes and reaches zero when

$$j = j_M = \frac{2 \mu_- kT \overline{N}}{l}.$$

Now the density of electrons in the conduction band is given by

$$n = \sqrt{\left(\frac{\psi}{2}\right)^2 + N\psi} - \frac{\psi}{2},$$

where $\psi = N_c e^{\frac{-\varepsilon}{kT}}$ in which ε is the position of the donors with respect to the bottom of the conduction band, expressed in terms of energy. Hence, the electron density vanishes when the donor density vanishes and the limiting current is

$$j_M = \frac{2\,kT}{e}\,\frac{\overline{N}\,e\,\mu_-}{l}.$$

When the current density approaches zero, the donor distribution becomes uniform and the conductance of the sample becomes

$$g = \frac{\overline{n}\,e\,\mu_-}{l},$$

where

$$\overline{n} = \sqrt{\left(\frac{\psi}{2}\right)^2 + \overline{N}\psi} - \frac{\psi}{2}.$$

It is interesting to apply the derived relations to an oxide cathode under the assumption that the current is determined solely by the resistance internal to the oxide. Let

$$\mu_- = 3\ \text{cm}^2\ \text{sec}^{-1}\ \text{volt}^{-1},$$

$$l = 5 \times 10^{-3}\ \text{centimeter},$$

$$g = 10^{-1}\ \text{mho}.$$

The latter is tantamount to the assumption of a well-activated cathode. Then

$$\overline{n} \approx 10^{15}\ \text{cm}^{-3}.$$

This density is high enough so that $\overline{N}$ exceeds $\psi/2$. Then

$$\overline{n} \approx \sqrt{\overline{N}\psi}.$$

Using DeVore's value for the energy gap (1.4 e.v.) gives

$$\overline{N} = 10^{18}\ \text{cm}^{-3}$$

at a temperature of 1000°K.

Then the limiting current is

$$j_M = 16\ \text{amperes}.$$

In the above computation, it was tacitly assumed that space charge plays no role. This cannot be the case. As the donor and electron densities fall in the depletion layer, electrons will begin to spill from the region of higher density into the region of lower density until the coulomb forces between electrons limit the process. Mott and Gurney[54] have considered a simple case of space-charge limitation. In the next section, their result will be applied to the oxide cathode.

b) *The Effect of Space Charge Within a Cathode on its Thermionic Emission.*

Mott and Gurney consider an insulator in contact with a metal. They show that, when the voltage across the insulator is substantial, electron diffusion may be neglected. Hence, the problem is to find a solution of the simultaneous equations

$$j = n\, e\mu_-\, E,$$

$$\frac{\partial E}{\partial x} = \frac{n\, e}{K_o},$$

in which K_o is the dielectric constant and the other symbols are as defined in the previous section. These equations are easily integrated to yield

$$n\, e = \sqrt{\frac{j K_o}{2\mu_-\, (x + C)}},$$

$$V = \sqrt{\frac{2j}{\mu_-\, K_o}}\, [(x + C)^{3/2} - C^{3/2}.],$$

where V is the potential at x, and C is an integration constant which is to be evaluated by matching the electron distributions in the insulator and metal at the contact. When

$$x \gg C = \frac{j\, K_o}{2\mu_-\, (n_0\, e)^2},$$

where n_0 is the electron density in the insulator at the contact, the relations above may be written

$$n e \approx \sqrt{\frac{j K_o}{2 \mu_- x}} ,$$

$$j \approx \frac{\mu_- K_o V^2}{2 x^3} .$$

To apply these relations to the depletion layer in an oxide cathode, it will be assumed that the depletion layer is an insulator of thickness S.

Let

$$K_o = 34,$$

$$\mu_- = 3,$$

$$n_o = 10^{15}.$$

The dielectric constant is that measured by Bever and Sproull,[61] the mobility is taken from Pell's paper,[53] and the electron density is that computed in the previous section. Then

$$\frac{j K_o}{2 \mu_- (ne)^2} \approx 10^{-5} j,$$

with j in amperes per square centimeter. The experimental evidence obtained in the amplifier experiments indicates that the thickness of the depletion layer is at least 10^{-4} centimeter for currents of the order of milliamperes. Hence, for any reasonable current density

$$S \gg C$$

and the approximate relations may be used. The current–voltage relation may be put in the form

$$R \equiv \frac{V}{j} \approx \sqrt{\frac{2 S^3}{\mu_- K_o j}} .$$

This relation says that the apparent resistance will vary as $j^{-1/2}$ if S remains constant. In the case of the oxide cathode, the amplifier experiments show that the thickness of the depletion layer increases with current. A similar behavior is exhibited by the simple model

discussed in the preceding section. Hence, if the current through the depletion layer is space-charge limited the resistance decreases somewhat more slowly than $j^{-1/2}$. In an earlier section, it was found that the cathode resistance of BaO coating varied as j^n, $-2/3 < n < -1/2$. The result suggests that space charge is playing a role. However, the evidence of breakdown introduces a possible competing process which decreases the exponent so that the result is not as convincing as could be desired.

In an earlier section it was noted that the emission equation of a semiconductor is

$$j = D\,n\,e \left(\frac{kT}{2\pi m} \right)^{1/2} e^{\frac{-\chi e}{kT}},$$

where n is the electron density at the emitting surface. If the current through a depletion layer near the emitting surface of the cathode is space-charge limited, the electron density at the surface is

$$n\,e \approx \sqrt{\frac{j\,K_o}{2\mu_- S}}.$$

When this relation is substituted in the emission equation, the result may be written

$$j = D^2 \left(\frac{kT}{2\pi m} \right) \frac{k_o}{2\mu S} e^{\frac{-2\chi e}{kT}} \equiv \frac{A^*}{S} e^{\frac{-2\chi e}{kT}}.$$

If Schottky effect is included, the relation becomes

$$j = \frac{A^*}{S} e^{\frac{-2\chi e}{kT} + \frac{2e\sqrt{eE}}{kT}}.$$

Hence, if a cathode has a depletion layer of constant thickness near the emitting surface and the current through this layer is space-charge limited, the apparent Richardson work function is twice the electron affinity and the apparent Schottky temperature is one half the cathode temperature. As pointed out before, the depletion layer thickness in a cathode increases with current. Therefore, the apparent work function will be somewhat greater than twice the electron affinity and the apparent Schottky temperature will be somewhat lower than one half the cathode temperature.

When compared with experimental data, this "emission equation" has much to recommend it:

1)   It indicates how it is possible to derive work functions of the order of 1 volt from Richardson plots when the known donor levels of BaO correspond to a work function of about 1.7 volts. It also suggests that the electron affinity of BaO cannot exceed 0.5 volt, a value somewhat lower than previous estimates.

2)   It indicates how Schottky plots with apparent temperatures ranging from $\frac{1}{3}$ to $\frac{1}{2}$ the actual cathode temperature arise.

3)   It suggests that the apparent work function is only indirectly connected with the latent heat of evaporation of electrons. If, as is customary, the latent heat is taken as the sum of the affinity and the energy gap between Fermi limit and the bottom of the conduction band, the latent heat is

$$\phi = \chi + \frac{kT}{e} \ln \frac{n}{N_c},$$

where N_c is the effective density of states in the conduction band. If the electron density is determined by the space-charge considerations under discussion, the latent heat is

$$\phi = \chi + \frac{kT}{e} \ln \frac{1}{N_c e} \sqrt{\frac{j^{K_o}}{2\mu_- S}}.$$

That the latent heat might be current dependent occasions no surprise on the part of one who has tried to measure it by direct means.

These considerations show that the donor depletion hypothesis with the current limited by space-charge considerations at high current densities, accounts in a qualitative way for many of the more prominent anomalous behaviors of the oxide cathode, and indicates orders of magnitudes which accord with experiment. While the computations are crude, the results encourage a view that a complete theory which may be compared with experiment on a quantitive basis will emerge soon.

CONCLUSION

The present paper has set forth the hypothesis that the oxide cathode is a semiconductor in which donors are mobile. The experiments which led to this view and the subsequent experiments intended to elucidate it have been described. The latter experiments have been

interpreted in terms of the donor depletion hypothesis, a corollary of the mobile donor hypothesis, with what success the reader may judge for himself.[64] Whatever his judgment, it is hoped that the writing of this paper will have served two major purposes,

1) The presentation of a considerable body of new experimental data,

2) the injection of new ideas into present thinking about oxide cathodes.

The paper has also sought to deduce a simple energy-level diagram of BaO which accords with experimental data at hand. The result must be regarded as tentative and subject to revision should new data not be encompassed by the model.

As is natural in any study of this kind, more questions are raised than are answered. Some of the questions raised have been noted in passing, others will be obvious to those working in the field. One of the major problems that requires attention is the difference between the BaO cathode and the mixed-oxide cathode. Some differences have been noted in the present paper, others are familiar, yet the distinctions are by no means clear enough so that the role of SrO or CaO in a mixed-oxide cathode can be regarded as understood. The role of reducing agents in the base metal of cathodes in' determining both cathode activity and life deserves further study. This problem has not been considered at all in the present paper which is devoted to far more elementary matters. Even this brief enumeration of unresolved problems makes it clear how far the art has surpassed the science.

---

[64] Recently, H. B. DeVore made a direct measurement of donor depletion at the emitting surface of a cathode. He annealed a cathode without anode voltage on the diode which includes the cathode and found the usual energy level structure by a photoemission measurement. He then annealed the cathode with anode voltage on the diode and found that the 1.4-volt threshold had shifted to about 1.6 volts.

Secondly, the writer wishes to express his gratitude to R. H. Plumlee who suggested the mass-spectrometer experiments and contributed so much to their execution. Without his cooperation, the spectrometer experiments could not have been carried out.

The writer also wishes to express his appreciation of the numerous discussions he has had with D. O. North and H. B. DeVore. Their critical comments on the writer's views have greatly clarified his thinking on the cathode problem.

Finally, the writer wishes to express his gratitude to Lloyd P. Smith of Cornell University who encouraged him to undertake a study of the oxide cathode. His constant advice and encouragement are responsible for whatever success the undertaking may have achieved.

DEVELOPMENT OF AN
IMPROVED GRAPHECHON STORAGE TUBE*†‡

By

W. T. DYALL,# G. R. FADNER,** AND M. D. HARSH#

Summary—The Graphechon is a developmental electrostatic charge-controlled storage tube having two electron guns arranged on a common axis, one on either side of the storage target. When this type of tube is used for scan conversion, registration of the reading and writing patterns requires that the reading and writing electron beams strike at right angles to the target at its center. An improved tube designed to fulfill this requirement by means of accurate alignment of the guns and the target is described. The new design also permits accurate mounting of the tube with respect to the scanning yokes.

GENERAL DESCRIPTION OF GRAPHECHON

THE Graphechon[1,2] is an electrostatic charge-controlled storage tube of the electron-beam type designed to store information, to convert information from one scanning system to another, and to provide output signals for a bright display. The improved Graphechon described in this paper has two electron guns arranged on a common axis, one on either side of the target. Because of the high capacitance of the target, it can provide as many as 600 reproductions of stored information before the signal-to-noise ratio goes below 20:1. A photograph of this developmental tube is shown in Figure 1.

The writing gun produces a high-velocity electron beam; the reading gun produces a medium-velocity electron beam. Each gun contains a thermionic cathode, a control grid (grid No. 1), an accelerating grid (grid No. 2), a focusing electrode (grid No. 3), and an accelerating and collecting electrode (grid No. 4). Grid No. 4 is in the form of a

[1] L. Pensak, "The Graphechon—A Picture Storage Tube," *RCA Review*, Vol. X, pp. 59-73, March, 1949.

[2] L. Pensak, "Picture Storage Tube," *Electronics*, Vol. 22, pp. 84-88, July, 1949.

wall coating adjacent to the target. Deflection of each beam is accomplished by the magnetic fields produced by external deflecting coils.

The target consists of a thin layer of insulating material deposited on an electron-transparent metallic conducting signal plate. The insulator acts as the dielectric for the capacitor formed between the signal plate and the area of the insulating side of the target bombarded by the reading beam. This capacitor is discharged by the writing beam and charged by the reading beam. Figure 2 shows a schematic arrangement of the Graphechon in operation.

When the high-velocity electron beam from the writing gun bombards the conducting signal plate of the target, it penetrates the signal plate and the insulator. This penetration induces a conducting path
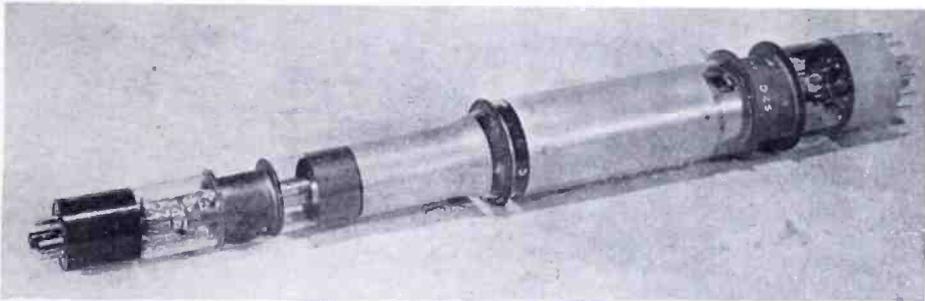

Fig. 1—Improved developmental Graphechon.

through the insulator,[3] as shown in Figure 2. Because of this conduction, the insulating surface discharges towards signal-plate potential where bombarded. When the writing beam is removed, the insulator regains its insulation. The discharging or writing characteristic[4] is a function of target capacitance, signal-plate potential, scanning speed, magnitude of writing-beam current, duration of writing-beam pulse, and repetition frequency of writing-beam pulse.

When the front surface of the target insulator is bombarded by the medium-velocity electron beam from the reading gun, secondary electrons are emitted and reach the collector (grid No. 4). The emission of electrons causes a current flow in the external circuit. A positive charge accumulates on the insulator which becomes increasingly positive with respect to the collector until a retarding field is built up and equilibrium established.

When equilibrium is reached, no further charging action occurs,

[3] L. Pensak, "Conductivity Induced by Electron Bombardment in Thin Insulating Films," *Phys. Rev.*, Vol. 75, pp. 472-478, February, 1949.

[4] A. H. Benner and L. M. Seeberger, "Graphechon Writing Characteristics," *RCA Review*, Vol. XII, pp. 230-250, June, 1951.

the number of secondaries which escape from the target is equal to the number of incident primaries, and no current flows in the target circuit. The time required to recharge the target to equilibrium is called the storage time. The charging or reading characteristic is a function of target capacitance, signal-plate potential, scanning speed, magnitude of reading-beam current, and the state of target discharge.

The change in potential of the insulator caused by bombardment by the writing beam upsets the equilibrium condition established by the reading beam. Further bombardment of the insulating surface by the reading beam charges the area under the beam in the direction
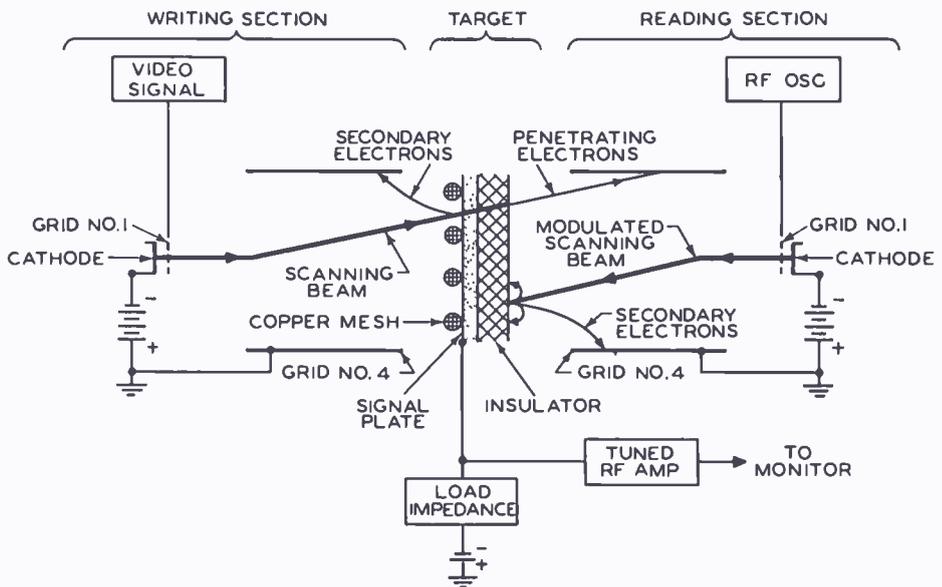
Fig. 2—Operation of the Graphechon.

which tends to re-establish equilibrium. The charging current in the target circuit is the signal current.

Bombardment of the target by the writing beam produces a flow of current in the target circuit which must be separated from the target current produced by the reading beam. The separation of the two components of target current may be accomplished by a time-sharing method, or by the use of radio-frequency modulation of the reading component in conjunction with a tuned output amplifier.

ALIGNMENT AND REGISTRATION

The Registration Problem

When a pattern such as a radar pattern containing position information is written on the target, and is then read out by television scan, the position information of the radar pips may contain errors

due to imperfect scanning by either beam. These errors may be called position errors, and are defined as the quotient of the distance between the desired spot position and the actual spot position, divided by the display diameter of the target. One objective of this study was to develop a tube in which the position error could be held to 0.5 per cent or less in scan-conversion applications. Accurate scan conversion with a minimum of misregistration is of particular importance in applications such as precision approach radar, airport surveillance radar, and target designator equipments.

Misregistration errors result from any or all of several contributing errors which may be uncorrelated. The largest single error is probably due to keystoning of the raster caused by slight misalignment of the guns. Other errors occur when the electron beam does not pass through the deflecting yoke perpendicular to the flux, or does not pass through the deflecting yoke on the yoke axis. Errors also result from variations in gun voltages, variations in centering currents, and from nonlinear deflecting flux.

It is extremely difficult, if not impossible, to separate the error caused by the tube from the error caused by the equipment. However, in order to achieve the required registration, all sources of error must be rigidly controlled. Even with a perfect Graphechon in which both the undeflected writing and reading beams strike normal to the target at its center, the requirement of a position error of less than 0.5 per cent is very difficult to meet because of difficulties with the associated equipment. If the associated equipment were perfect, the axes of the electron beams in a perfect tube would coincide with the axes of the deflecting coils. The beams would also be perpendicular to the deflecting flux. Furthermore, the flux would be of uniform density within the coils and zero outside of the coils, and have perfect linearity. There would be no errors caused by voltage variations.

Even in a perfect equipment, however, an imperfect tube may not allow the writing-beam axis, the reading-beam axis, the normal to the target center, and the deflecting-yoke axis to coincide. The largest error is the keystoning caused by the nonperpendicularity of the electron beams to the target. In the improved Graphechon discussed in this paper, lateral shift of the beams within the yokes is negligible. The plots in Figure 3 were calculated with the assumption that all other errors are negligible in comparison with the error due to keystoning. The results are, therefore, approximate, since other errors may add up to as much as one quarter of the keystoning error. If keystoning is assumed to be the only error, Figure 3 indicates the allowable beam displacements for various position errors provided the
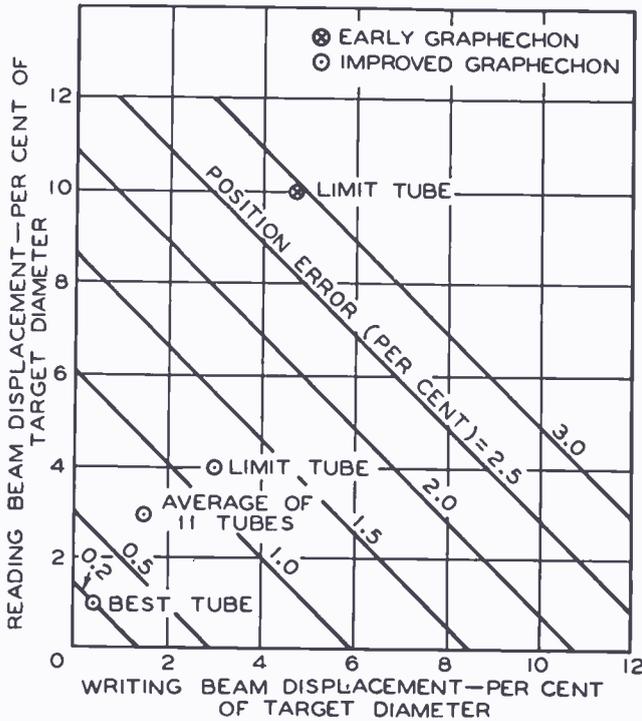
Fig. 3—Keystone position errors in a Graphechon.

target is not tilted. This information is for a tube in which the undeflected beams strike the target at points which are colinear with the target center, but are displaced from the target center in opposite directions, as shown in Figure 4. The allowable displacements for a position error of 0.5 per cent, the design objective, are also indicated.

For an early model Graphechon having undeflected beam displacements of five per cent and ten per cent for the writing gun and the reading gun, respectively, calculated keystone position error is about 2.8 per cent, as shown in Figure 3. In this tube, it is not likely that the beams were diametrically opposed, nor the target tilt negligible.

For an improved Graphechon having undeflected beam displacements of three per cent and four per cent respectively, calculated error is about 1.25 per cent under the same conditions, as plotted in Figure 3. As in the earlier model, the beams are not likely to be on opposite sides of the target center. The target tilt, however, is under better control. The average displacements of eleven of the improved tubes gave a corresponding position error of about 0.75 per cent. The best tube of
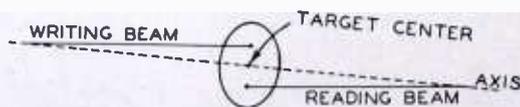
Fig. 4—Beam and target relationships for keystone-position-error plot of Figure 3.

this group gave a position error of only 0.2 per cent. These calculated points are plotted in Figure 3.

Reduction of Misregistration by Improved Tube Design

The developmental tube described in this paper was designed to decrease the position errors contributed by the Graphechon in a scan-converting system. In this new tube:

(1) The two undeflected electron beams strike the target very close to each other and close to the center of the target.

(2) The axis of each set of deflecting coils can be made to coincide very nearly with the corresponding electron-beam axis.

(3) The two undeflected electron beams strike the target at very nearly normal incidence.

Displacements of the undeflected beam from the center of the target have been greatly reduced. Previous model Graphechons had an undeflected writing-beam displacement of about 0.070 inch, or five per cent of the target diameter, while the reading-beam displacement was about 0.140 inch or ten per cent of the target diameter. Target tilt was not rigidly controlled. The present tube has a displacement of three per cent instead of five per cent for the writing gun, and four per cent instead of ten per cent for the reading gun. The axis of the beams has an accurate external reference for positioning the deflecting coils. The axis of the tube is within 0.010 inch of the beam axis. No accurate outside reference to the beam axis is ordinarily provided in electron-beam tubes. The tilt of the target is also held to a minimum during manufacture. The angle between the undeflected beams and the normal to the target is less than one degree.

The method of making the tube involves the fabrication of an envelope which is accurate both on the outside and on the inside and mounting the accurately made guns and target within the envelope. Thus, the envelope is also a jig which controls the positions of the guns and the target. The envelope is made of glass and metal sealed by radio-frequency induction heating. Two subassemblies are made first as shown in Figure 5. A gun holder with glass tubing sealed to either side forms each subassembly. After the first sealing operation, the inside surface of each gun holder is accurately lapped or honed to a tolerance of ± 0.00025 inch. The two subassemblies and the target holder are then placed in their respective positions on an accurately finished, water-cooled, sealing mandrel. This mandrel insures that the axes of the three individual parts will be coincident. After the final envelope seal at the target holder is made, the holder flanges are
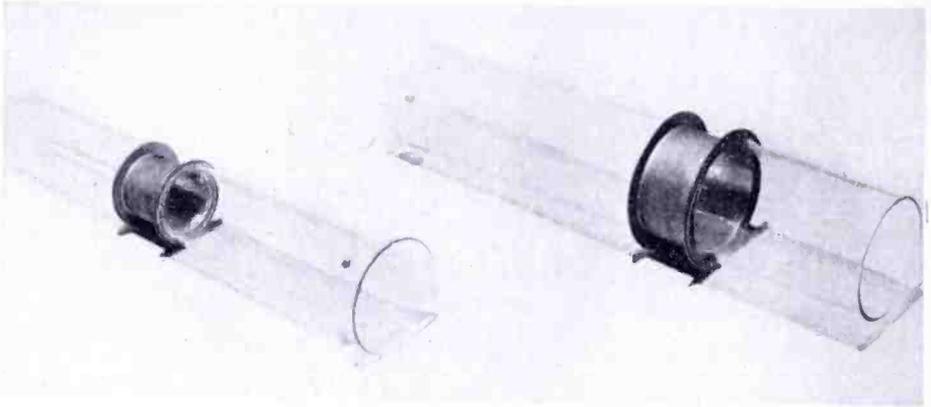
Fig. 5—Writing neck (left) and reading neck (right) of developmental
Graphechon.

ground to final dimensions. A mandrel similar to the sealing mandrel
is used to hold the envelope assembly for this operation.

The electron guns are conventional except for the mount spacers.
As shown in Figure 6, conventional spacers have been replaced by
metal cylinders brazed to the electrode cylinders on each gun. These
metal cylinders, or aligners, are finished by grinding after the brazing
operation. The tolerance here is also ± 0.00025 inch. The grinding
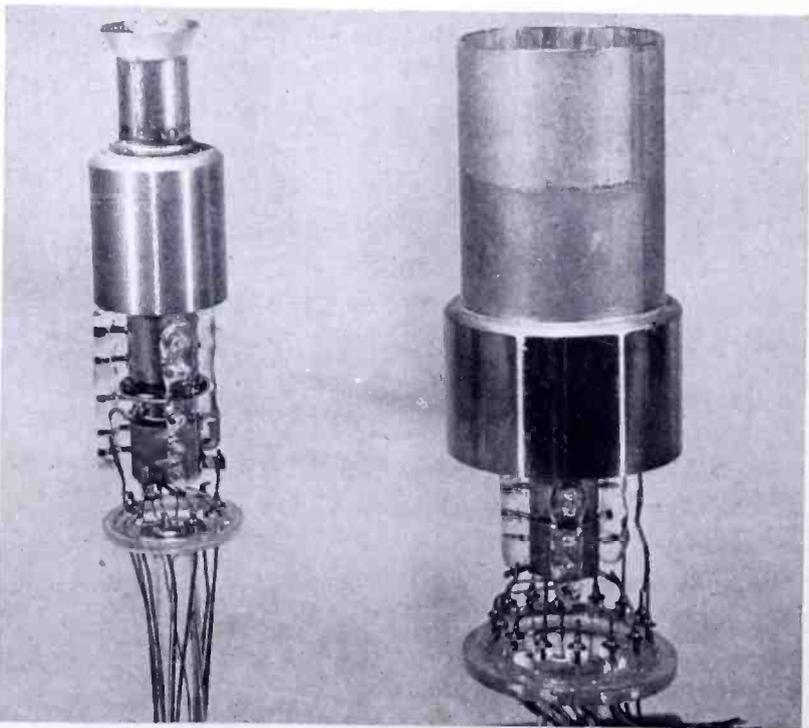
Fig. 6—Writing-gun assembly (left) and reading-gun assembly (right)
of developmental Graphechon.

provides, in addition to the correct diameter, that the axis of the outer surface of the aligner and the axis of the electrode cylinder will be very nearly coincident.

The assembly is completed by slipping the electron guns and the target into place. The accurately finished aligner is a close fit inside its corresponding holder. The fit of the aligner in the holder is the final controlling factor in determining the position of the beam axis with respect to the tube axis.

Undeflected Beam Displacement Measurement

The problem of measuring the distance from the center of the target to the landing point of the beam on the target must be solved by indirect means because the center of the target is not marked. The distance involved is of the order of 0.050 inch or less. First a way of marking the target center and then a way of measuring the distance to the beam spot were found.

The method is based on the simple geometric fact that the center of a circle is uniquely defined by the intersection of any two diameters. Four accurately spaced index lines are inscribed on the part of the target holder which supports the target. These lines are extended to define diameters during operation of the Graphechon. The extension is conveniently generated electrically by a variable-delay pulse. A standard television scanning system is used and the Graphechon signal output is indicated on a monitor kinescope. The marker pulse, at horizontal frequency, is mixed with the Graphechon video output signal and appears on the monitor as a straight vertical line. The Graphechon is rotated within the yokes, and the marker time delay is adjusted so as to superimpose two index marks and the marker line. The geometric center of the target now lies somewhere along the marker line. If the marker-line time delay is adjusted so that the line passes through the beam spot as shown in Figure 7, a photograph of the screen of the monitor kinescope, a measure of one coordinate results. The change in delay time can be converted to a measure of distance between beam spot and target center since the horizontal scanning speed is known.

The second coordinate of the spot to target-center distance is found by rotating the Graphechon 90 degrees about its axis and repeating the procedure.

This method assumes that no external magnetic fields act on the beam being measured. If fields are present, the effects may be cancelled by taking two readings for each coordinate with the Graphechon rotated 180 degrees between readings.

Magnetic Field Effects

If either beam in the Graphechon is acted upon by a magnetic field, accuracy will be lost. Either beam may be deflected as much as 8 per cent of the target diameter per gauss if the field is at right angles to the direction of the beam and acts in the region where the beam is moving slowly. Adequate shielding of the tube by high-permeability alloys is necessary to reduce the earth's field and other fixed fields to a satisfactorily low level within the tube. Since parts of the envelope and gun are highly magnetic, the tube must be degaussed before in-stallation. Residual magnetism of magnetic gun and envelope parts
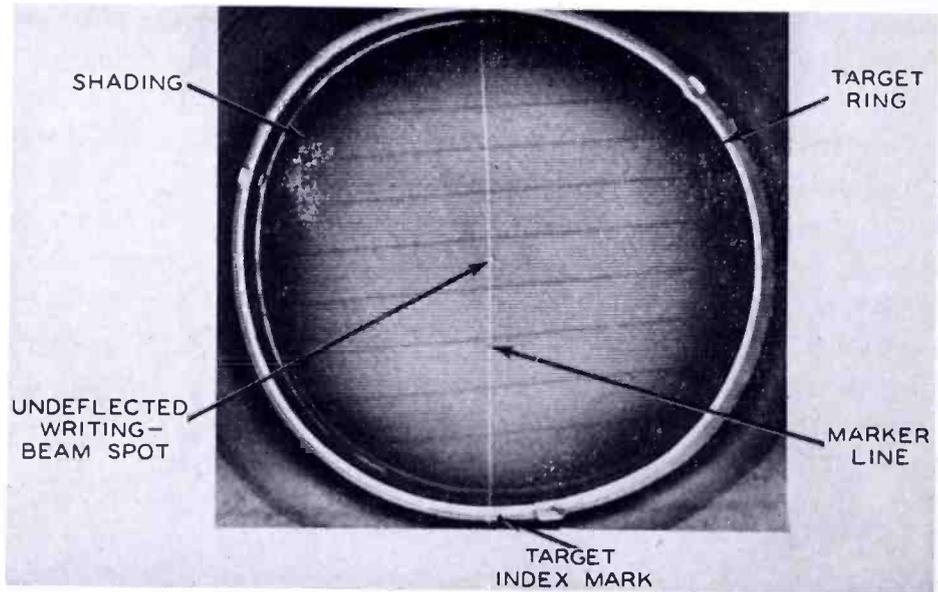
Fig. 7—Screen of monitor kinescope showing the vertical marker line pass-ing through the white spot made by the undeflected writing beam.

after degaussing in a 60-cycle field was measured with the aid of a low-velocity electron beam in a special cathode ray tube, and found to be approximately 0.03 gauss. The maximum beam-displacement error caused by a field of 0.03 gauss would be approximately 0.25 per cent of the full target diameter.

SIGNAL-TO-NOISE RATIO

Description of the Shading-Signal Effect

The signal output from a Graphechon has a nonuniform black level or background which causes a shading of the picture. As shown in Figures 7 and 8(b) the background is higher near the center of the target than it is near the edge. In addition, peak signal amplitude and signal storage are reduced near the edge. The shading effect results

from nonuniform redistribution of secondary electrons. These secondaries exist because the reading beam always generates the full number of secondaries determined by the nature of the surface and operating conditions. When the scanned area is negative, part or all of the secondaries can be collected by the bulb coating. The uncollected secondaries fall back on the target in different areas. The higher background level in the central part of the target results from the fact that more secondaries return near the center than near the edges as shown in Figure 9. The metallic target ring is normally operated at about 40 volts negative. The presence of this negative potential sets up a retarding field between the target and the collector near the outer edges of the target so that secondaries generated near the edge are attracted towards the central part of the target. This "rain" of
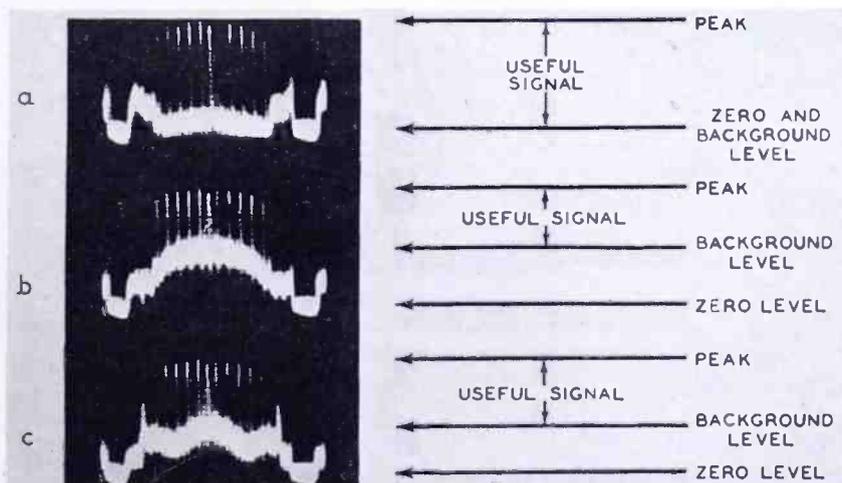
Fig. 8—Oscillograms of Graphechon signal output. (a) Shading-free target with shield-ring potential of 40 volts positive. (b) Target not having shield ring. (c) Shading-free target with shield-ring potential of 40 volts negative.

secondaries charges the surface negative, and therefore produces a background signal. Fringe fields from the deflecting yokes are undoubtedly present also. When the field is such that the beam is near the edge of the target, the field is, of course, in the right direction to cause secondaries leaving the target to turn towards the center of the target. Thus, in two ways, secondary electrons are forced towards the middle of the target.

The maximum current from a written signal is fixed by the potential of the target and by the beam current, and is independent of shading. The output signal is then the difference between the background signal and the peak signal. A reduction of the background shading, therefore, improves the signal-to-noise ratio.

Reduction of Shading Signal

A method of reducing the shading effect has been demonstrated. In this method, the electrostatic field of a shield ring, added to the target structure and operated at about 40 volts positive with respect to the collector, makes the background uniform over the entire target. The added shield ring is sealed to a mica ring and both are riveted to the target ring. A contact to the shield is brought out of the tube near the target holder.
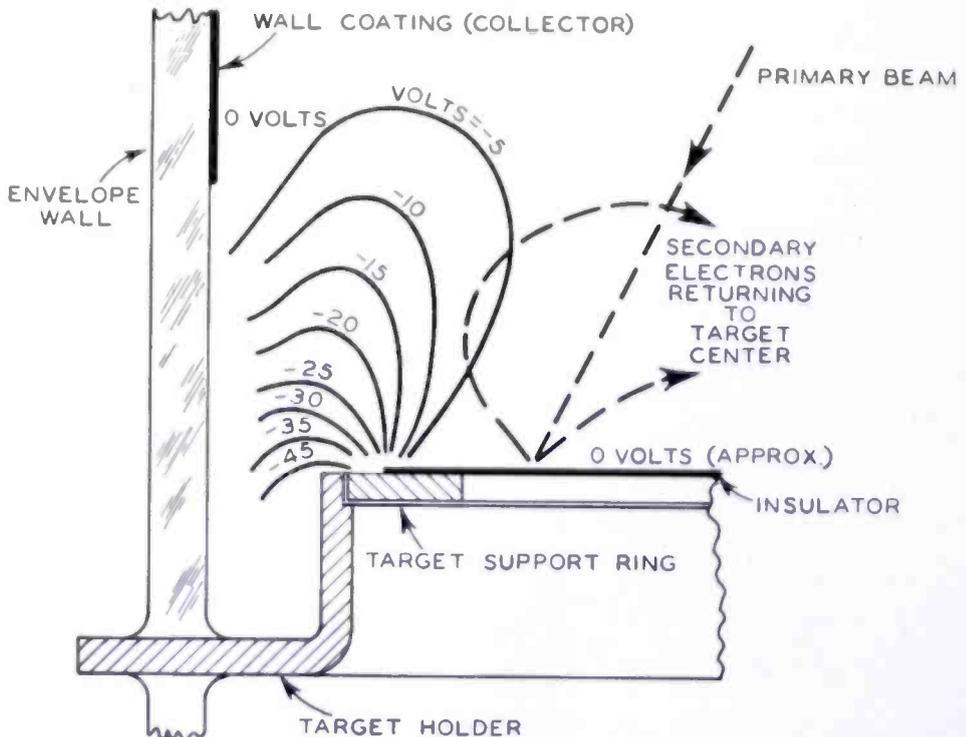

Fig. 9—Redistribution of secondary electrons causing shading effects in developmental Graphechon not having shield ring.

The oscillograms in Figure 8 show signal output amplitude as a function of the position of the reading beam for various operating conditions. Normal operating conditions were established and the shield-ring potential varied. Note in Figure 8(c) for a shield-ring potential of 40 volts negative, that the background is high at the center and at the edges. Figure 8(b) with the shield ring floating or at ground or collector potential, is typical of the characteristic for targets without the shield ring at normal operating voltages. When the shield-ring potential is adjusted to about 40 volts positive, the background is quite uniform over the entire target as shown in Figure 8(a). Further tests without radio-frequency modulation were made in which the output signal passed through a video amplifier. Results were

similar, except that the required values of shield-ring potential were different. A voltage of about five volts positive gave a uniform output for video operation.

The addition of this shield ring adds to the shunt capacitance of the target assembly. The target assembly without the shield ring has a shunt capacitance to ground of about 6 micromicrofarads. The shading-free target has a capacitance of about 60 micromicrofarads between the target and the shield ring. It is necessary, therefore, if the radio-frequency signal-separation method is used, to isolate the shield ring from associated wiring capacitance. A resistor of about one half megohm is recommended for use as the isolating impedance.

Incorporation of the shading-free target in the Graphechon gives an improvement by a factor of about two in the signal-to-noise ratio. The improved Graphechon has a signal-to-noise ratio of very close to 20 to 1 after a storage period of twenty seconds.

ACKNOWLEDGMENT

ATTENUATION OF WIRE HELICES
IN DIELECTRIC SUPPORTS*

By

R. W. PETER, J. A. RUETZ, AND A. B. OLSON

Research Department, RCA Laboratories Division,
Princeton, N. J.

Summary—Experimental results on the attenuation of a number of different dielectric-supported helices are presented. Of the various supports, one of fluted 707 glass yielded the lowest attenuation.

Helix attenuations as a function of frequency and phase velocity are given. The effects of such helix parameters as wire diameter, pitch, helix diameter, and material were studied.

INTRODUCTION

WITH the rapidly increasing importance of the traveling-wave tube as a microwave amplifier, the need for detailed engineering data regarding its components has grown. Most traveling-wave tubes of the low-voltage type use a helix as the delay line. The knowledge of its attenuation is important for tube design and the measurements presented here are intended to fill some gaps which exist in the available data.

Aside from the application in traveling-wave tubes, the helix has attained some importance as a directional antenna.[1,2] Its efficiency is dependent upon its attenuation. The results of this study, although directed towards the traveling-wave tube application, may also be useful for helix antenna design.

Several theoretical and experimental investigations of the helix attenuation have been made.[3-6] The experimental data is limited to

---

* Decimal Classification: R247.

[1] H. A. Wheeler, "A Helical Antenna for Circular Polarization," *Proc. I.R.E.*, Vol. 35, pp. 1484-1488, December, 1947.

[2] E. D. Smith, "Constructing Helical Antennas," *Electronics*, Vol. 23, p. 72, February, 1950.

[3] E. Lapostolle, "Les Phenomenes d'Interaction dans le Tube a Onde Progressive, Theorie et Verifications Experimentales," *Ann. Telecom.*, Vol. 3, pp. 265-290, August-September, 1948.

[4] M. Jessel and R. Wallauschek, "Etude Experimentale de la Propagation le long d'une Ligne a Retard en Forme d'Helice," *Ann. Telecom.*, Vol. 3, pp. 291-308, August-September, 1948.

[5] W. H. Surber and W. A. Craven, "Electro-Magnetic Wave Propagation Along a Uniform Helical Transmission Line," Unpublished Report, Princeton University, Department of Electrical Engineering, Tech. Rep. No. 1, June 15, 1948.

[6] W. A. Craven, "Dielectric and Conductor Attenuation of a Helical Wave Guide," Unpublished Report, Princeton University, Department of Electrical Engineering, Tech. Rep. No. 2, March 15, 1949.

single incidental examples which may show some general behavior of the attenuation but which cannot be used for extrapolation to other helix designs. The theoretical studies are not carried to a point where they can predict, even approximately, the experimentally found attenuation. The reason for this is the difficulty in describing accurately the field around a helix wire of finite thickness. This becomes even more difficult if the dielectric supporting material is taken into consideration.

It was felt desirable, therefore, to obtain empirical data on helices in different supports covering the whole range useful for low- and medium-power traveling-wave tubes, and to develop an approximate theory for the case of an unsupported helix.

A new theory based on a developed-helix model describes satisfactorily the dependence of the attenuation on all design parameters. It will be published separately.

MEASUREMENTS

The amplitude of a wave traveling along any uniform lossy transmission line decreases exponentially as exp. $(-\alpha z)$, and, therefore, the power decreases, since

$$P_2 = P_1 \, e^{-2 \alpha z}. \tag{1}$$

The attenuation constant, α, can be obtained by measuring input power, P_1, and output power, P_2, and the length of the line, z, and then making use of the relation

$$2\alpha = \frac{1}{z} \, 10 \log \frac{P_1}{P_2} \quad \text{(decibels per unit length)}. \tag{2}$$

Our helix attenuation measurements, obtained in the above manner, are shown in Figures 1 through 12. They cover the following range of helix specifications:

Helix outside diameter	0.100 to 0.250	inch
Wire length/helix length	13 to 23	
Corresponding beam voltage	1500 to 500	volts
Frequency	2600 to 3600	megacycles

The curves allow extrapolation outside of this range with good accuracy.

The helices were made of molybdenum and tungsten wire and were tested with and without silver plating. They were supported in precision-bore fused quartz tubing, in precision-bore and fluted 707 Corning glass tubing of the form shown in Figure 13, and on a flat block of polystyrene foam which did not add any measurable attenuation to the value obtained without support. The dimensions of the tested helices and supports are assembled in Table I. (The widths of the curves in Figures 1 through 8 represent the probable error.)

Table I—Dimensions of Tested Helices and Supports (in inches)

Helix Number	#1	#2	#3	#4
Helix Outside Diameter	.109 ± .001	.149 ± .001	.199 ± .001	.249 ± .001
Helix Wire Diameter	.007	.011	.012	.025
Support Inside Diameter	.112 ± .001	.152 ± .001	.202 ± .001	.252 ± .001
Quartz Tubing				
Outside Diameter	.175	.220	.250	.320
707 Tubing				
Outside Diameter	.190	.235	.270	.340
707 Fluted Tubing				
Outside Diameter (See Figure 13)	.250	.300	.360	.470

In Table II, the values of the surface resistivity, R_s, of different helix materials measured at 3000 megacycles are compared with the theoretical values which are computed from the direct-current resistivity, ρ:

$$R_s = \sqrt{\pi f \mu \rho}. \tag{3}$$

In the case of nonmagnetic conductors this becomes (in meter-kilogram-seconds units)

$$R_s = 2\pi \sqrt{\rho f \, 10^{-7}} \text{ ohms.} \tag{4}$$

The measured surface resistivities are quoted from Jessel and Wallauschek[4] and from measurements made by R. A. Braden of these laboratories. The measurements agree reasonably well with the theoretical values except for the cases of Jessel and Wallauschek's results with molybdenum and tungsten. For these, the experimental values
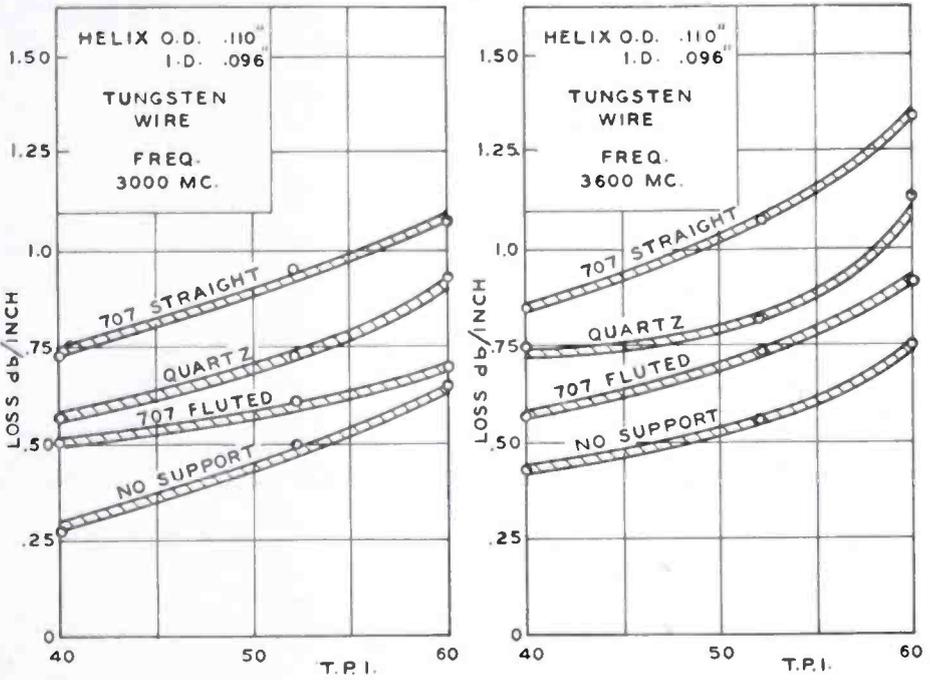
Fig. 1—Attenuation of tungsten-wire helix #1 measured
in different supports.
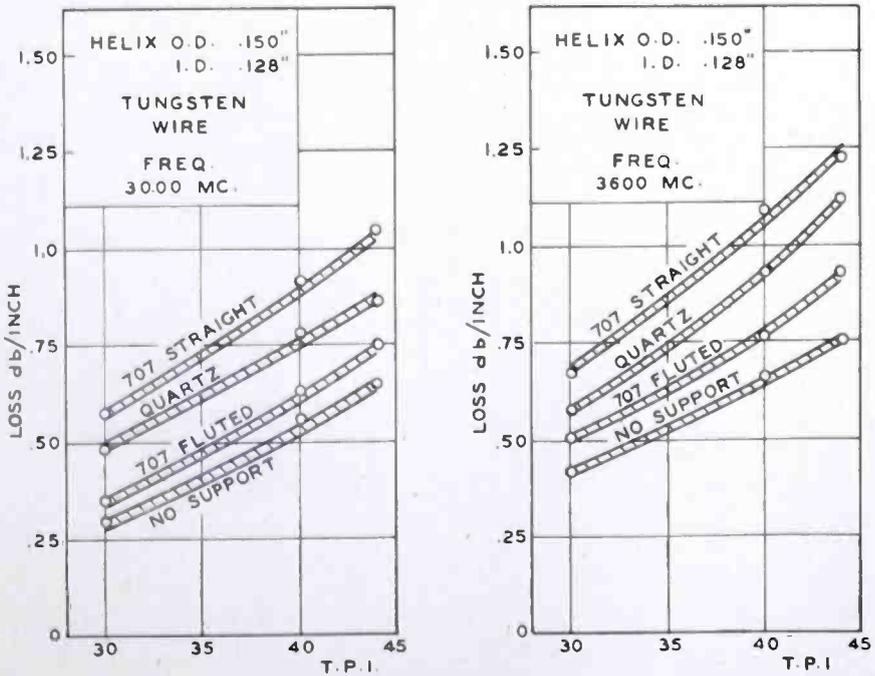
Fig. 2—Attenuation of tungsten-wire helix #2 measured
in different supports.
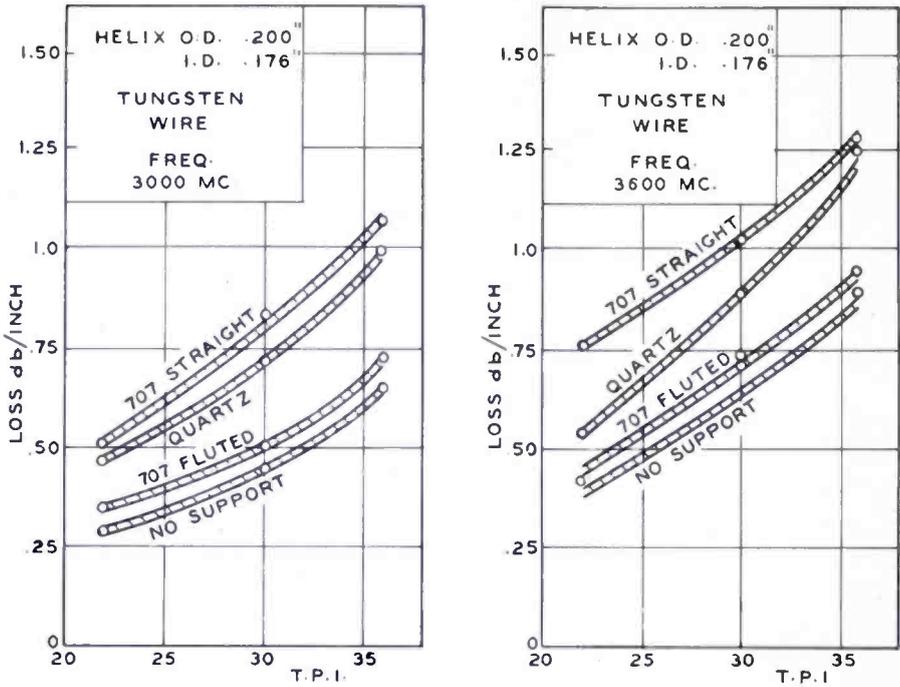
Fig. 3—Attenuation of tungsten-wire helix #3 measured
in different supports.
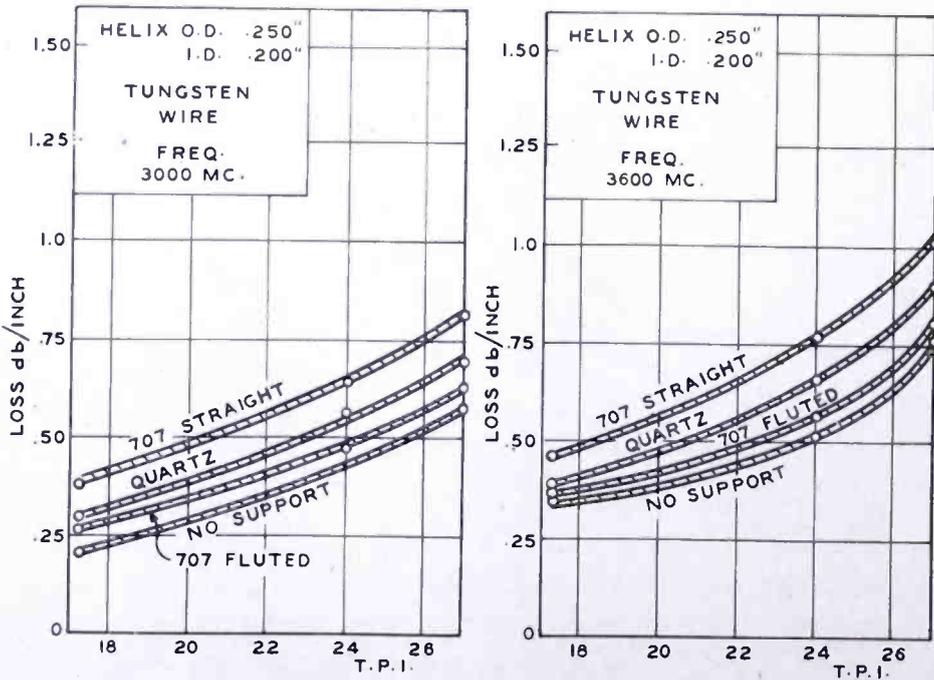
Fig. 4—Attenuation of tungsten-wire helix #4 measured
in different supports.
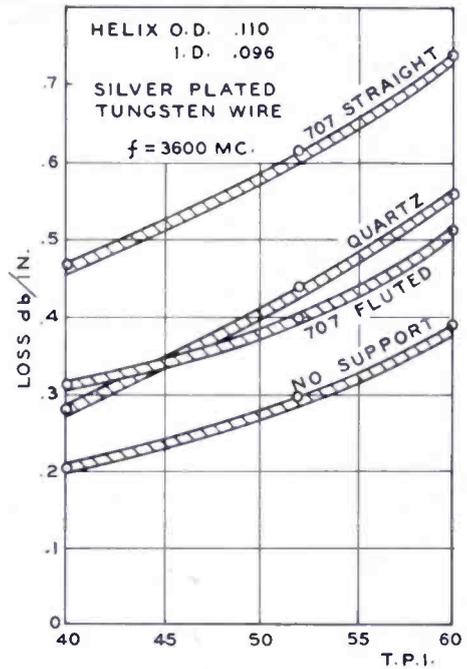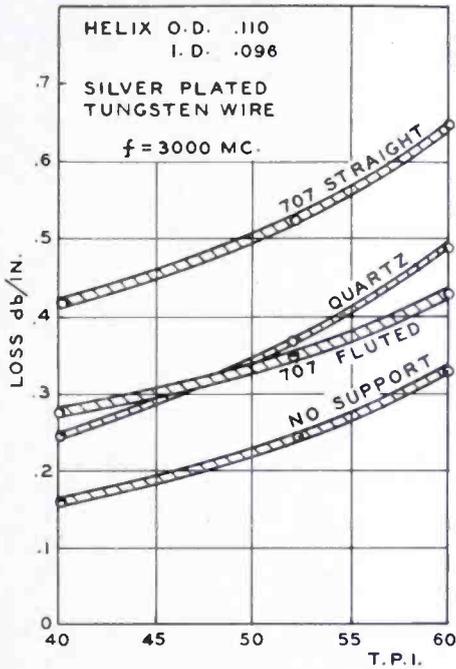
Fig. 5—Attenuation of silver-plated tungsten-wire helix #1 measured in different supports.
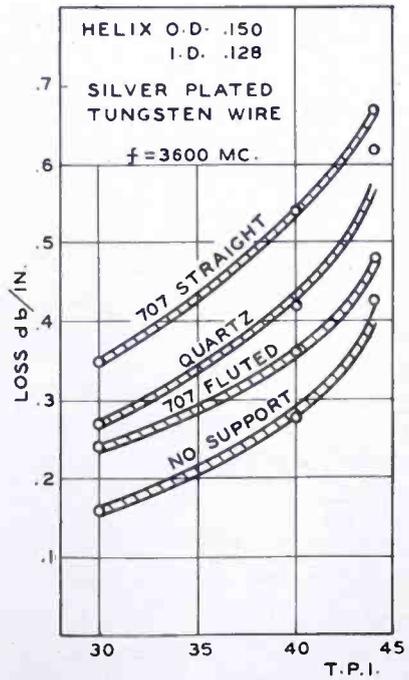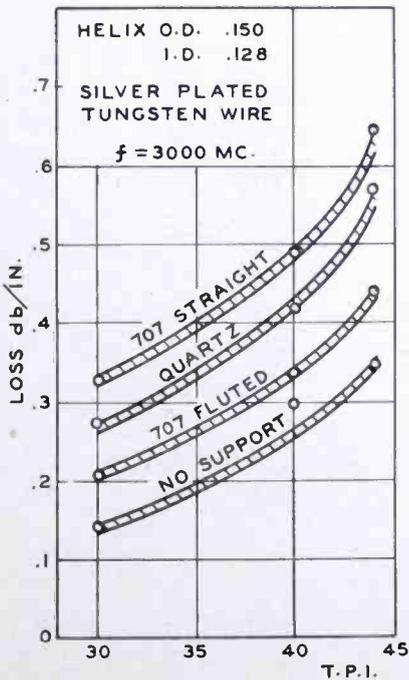

Fig. 6—Attenuation of silver-plated tungsten-wire helix #2 measured in different supports.
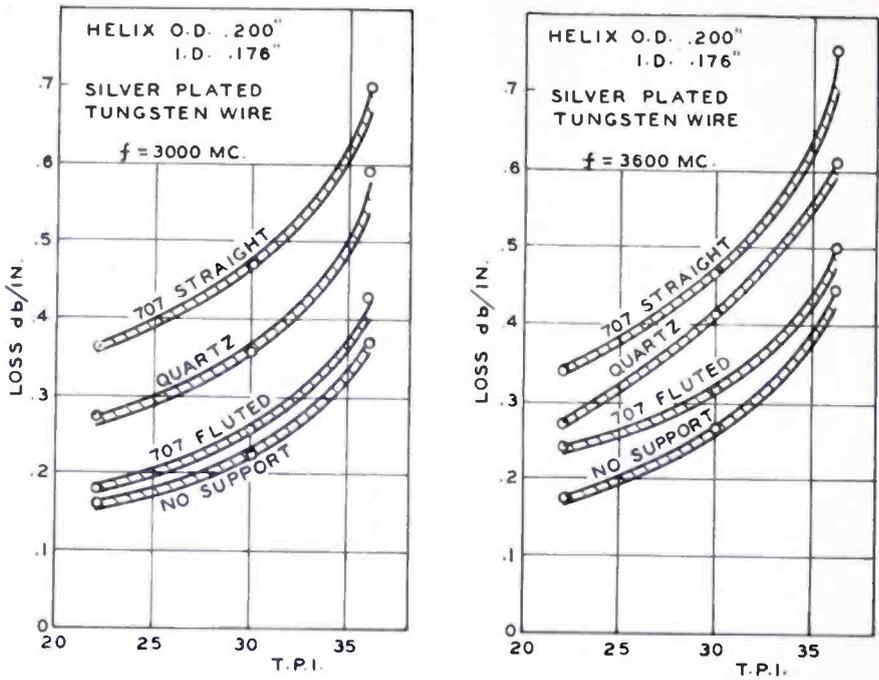
Fig. 7—Attenuation of silver-plated tungsten-wire helix #3
measured in different supports.
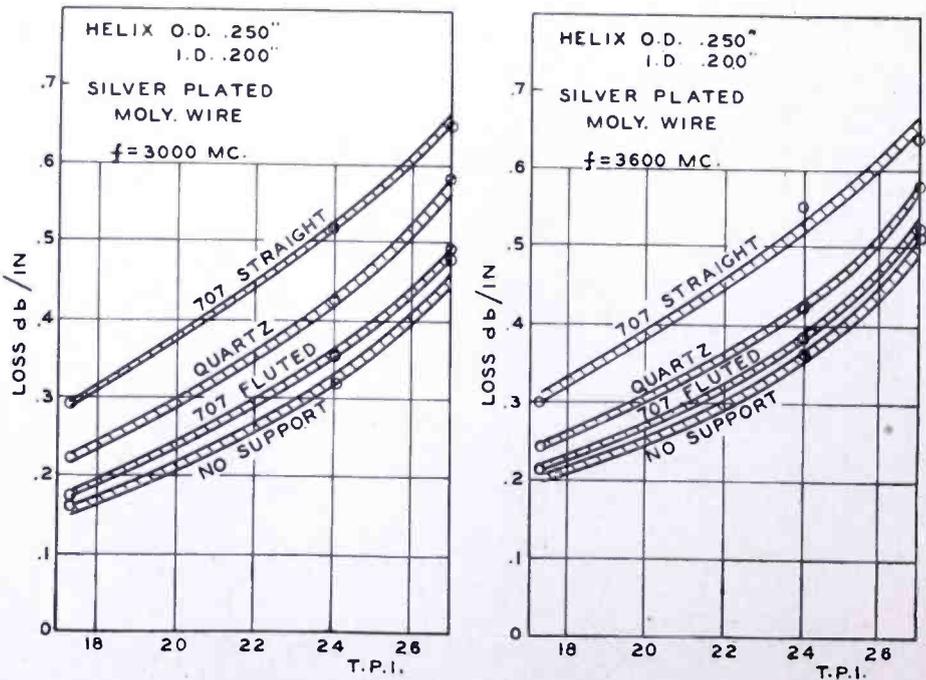
Fig. 8—Attenuation of silver-plated tungsten-wire helix #4
measured in different supports.

are about twice the computed ones. Braden's measurements are only 10 per cent high on the average.

Table II—Resistivity of Helix-Wire Materials

	Volume Resistivity (Ohm Meter)	Surface Resistivity at 3000 megacycles (Ohms)		
	(at 20° C.)	Theoretical	Measured (Jessel)	Measured (Braden)
Molybdenum	5.7×10^{-6}	0.0257	.050 ± 15%	0.027
Tungsten	5.6	0.0255	.057	0.026
Silver electrolytic deposit	1.64	0.0138	.021	.016-.018
Silver, polished	1.64	0.0138	.015	. . . .
Copper	1.72	0.0143	.019	0.016

In Table III, dielectric constants and power factors at 3000 megacycles are listed for quartz, and 707 and 774 Corning glasses. The first two of these were tested as helix supports.

Table III—Dielectric Constant and Loss of Materials Used as Helix Supports

Supporting Material	Dielectric Constant	Loss Tangent
Fused Quartz	3.80	0.0001
707 Glass	4.00	0.0019
774 Glass (Pyrex)	4.89	0.0089
Ceramic "AlSiMag 243"	5.75	0.002

Figures 1 through 8 show consistently that the lossiest support of the materials tested is 707 precision-bore tubing. Quartz, as might be expected, has a lower loss. It is interesting to see, however, that properly designed fluted 707 tubing of the form shown in Figure 13 is better than precision-bore quartz tubing in spite of its being a much lossier dielectric.

In traveling-wave tubes most commonly used, the value of $\sigma = (2\pi a/\lambda)(2\pi a/p)$ lies above $\sigma = 1.5$ ($2a$ = helix diameter, p = helix pitch, λ = wave length). The dimensions A, B, and C in Figure 13 of the fluted-glass-tube cross section were chosen, therefore, such that the dielectric attenuation would be much reduced for helices with $\sigma \geq 1.5$.

The dielectric loss of a helix surrounded by a concentric layer of lossy dielectric material can be computed. The loss in the supporting flutes, however, can only be estimated. The shape of the flutes must satisfy the additional condition that the mandrel on which the tubing is shrunk be removable after the shrinking process.

The cross section of the fluted-glass support finally selected (Figure 13) has the following characteristic dimensions:

$$A/B = 1.33,$$

$$B/C = 1.2 - 1.3. \qquad (5)$$

The attenuation of helices supported in this fluted 707 glass tubing is considerably less than in precision-bore quartz tubing as long as $\sigma > 1.5$ as seen in Figures 1-8. It becomes larger only when σ is much smaller than 1.5 as in the case of Figure 5.

In Figure 9, the average attenuation of all unplated helices measured above is plotted versus

$$\cot \psi = \frac{2\pi a}{p} = \frac{\text{wire length}}{\text{axial helix length}}. \qquad (6)$$

The striking result is that α seems to be practically independent of wire and helix diameters and a function only of the developed wire length.

The spread of the attenuation values of the same helices after silverplating became much larger, as seen in Figure 10. This is probably due to inhomogeneous surface condition caused by the electrolytic deposit. Attenuation measurements on helices with the same pitch, p, and the same mean diameter, $2a$, but wound of different wire size, d, show (see Figure 11) that there is a broad minimum around

$$\frac{d}{p} = \frac{1}{3}. \qquad (7)$$

If the wire gets thinner, the surface resistance increases; if the wires of successive turns come closer and closer together, the current carrying area of the circumference shrinks and the resistance also increases. Between these extremes of very small wire size and close approach of neighboring wires, a flat minimum exists.

These measurements were taken at different frequencies, f. The curves in Figure 12 show a linear dependence of the helix attenu-

|	2a/d	2a	d	MATERIAL
○	9.0	.225"	.025"	MOLY
▲	15.6	.188	.012	TUNGSTEN
◇	12.5	.139	.011	TUNGSTEN
●	14.7	.103	.007	TUNGSTEN

2a = MEAN HELIX DIA.
d = WIRE DIA.
p = HELIX PITCH
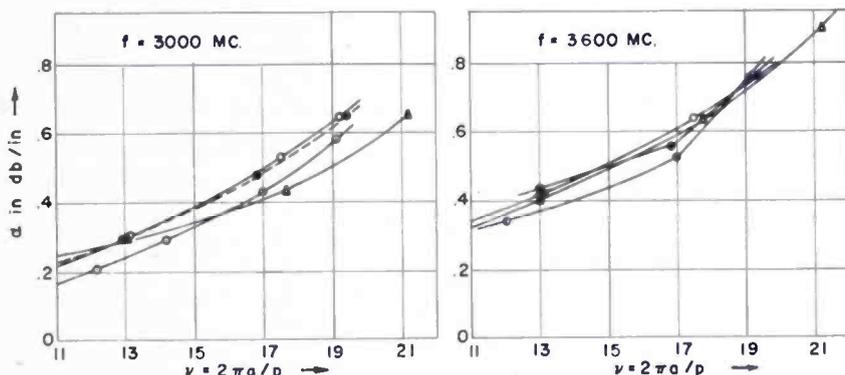
Fig. 9—Attenuation coefficient of unsupported tungsten helices as a function of the ratio, ν, between wire length and helix length.

ation on the frequency. The periodic deviations of α from a straight line increased with increasing relative wire-diameter-to-pitch ratio indicating periodic nonuniformity in the spacing between wires. The helix with 0.020-inch wire was wound with an improved winding technique. The periodic changes in the pitch of the helix with $d = 0.015$-inch wire were measured with a microscope and found to be less than $\pm$ 2.5 per cent.

	2a/d	2a	d	MATERIAL
●	9.0	.225"	.025"	SILVER ON Mo
▲	15.6	.188	.012	SILVER ON W
○	12.5	.139	.011	SILVER ON W
●	14.7	.103	.007	SILVER ON W

2a = MEAN HELIX DIA.
d = WIRE DIA.
p = HELIX PITCH
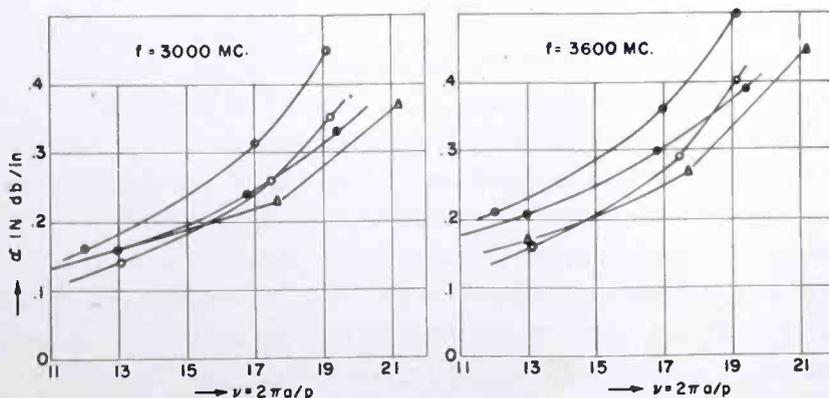
Fig. 10—Attenuation coefficient of unsupported silver-plated tungsten helices as a function of the ratio, ν, between wire length and helix length.

MEASURING PROCEDURE

The helix attenuation was obtained by measuring the insertion loss, L, and dividing it by the helix length, z, according to Equation (2). The insertion loss was measured by the substitution method, i.e., by comparison with a calibrated variable attenuator. Figure 14a shows the test arrangement schematically. The helix undergoing test is matched to rectangular wave guides on both ends by means of a straight helix antenna of adjustable length and a quarter-wave choke as shown in Figure 15. The test section AB is isolated by two matched 14-decibel
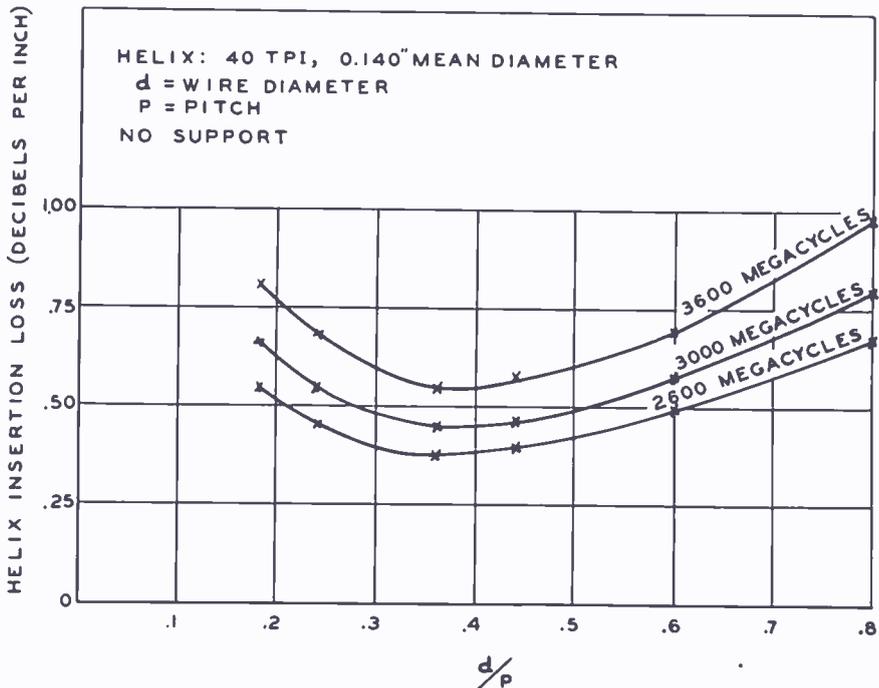
Fig. 11—Attenuation of helices with the same pitch and mean diameter as
a function of the wire diameter.

wave guide attenuators from the signal generator on one side, and from the crystal detector on the other side.

The measuring procedure adopted was as follows: First the helix was matched to both wave guide branches with the two standing-wave machines by interchanging generator and detector. The calibrated attenuator on the signal generator was then set to give a convenient reading on the output of the receiver. The reading of the attenuator was noted. The test section, AB, was then replaced by a short circuit as shown in Figure 14b and the signal power was reset to give the same reading on the detector as before. The difference between the two attenuator readings gave the total helix insertion loss:

$$L_0 = 2L_1 + L_2 + L_3 + L \quad \text{(decibels)}, \tag{8}$$

from which the helix attenuation was obtained:

$$2\alpha = \frac{1}{z}(L_0 - 2L_1 - L_2 - L_3) \quad \text{(decibels per inch)}. \tag{9}$$
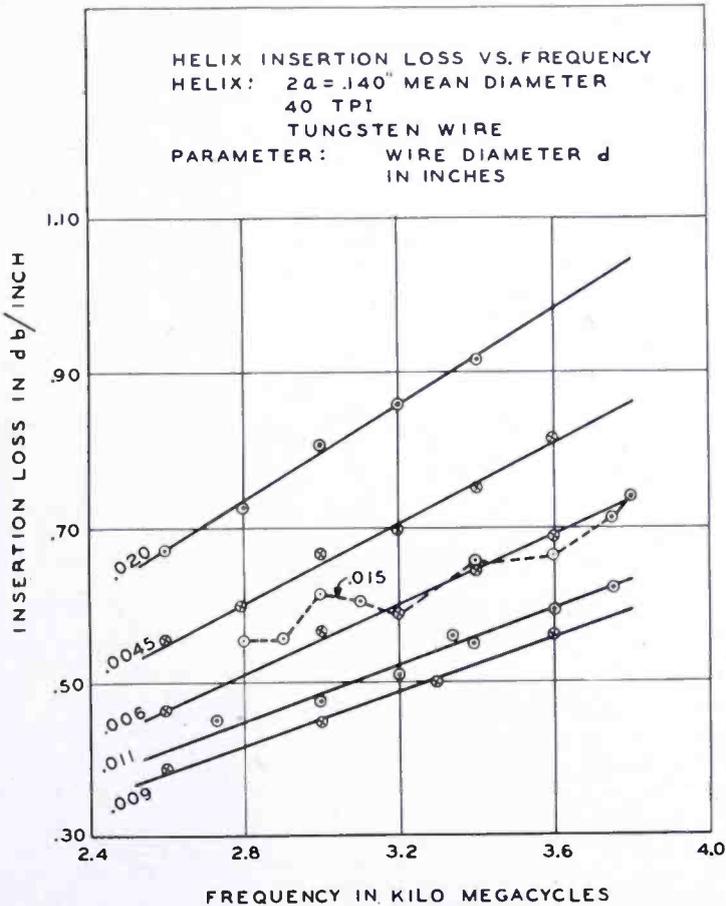
Fig. 12—Helix attenuation as a function of frequency for various wire sizes.

The wave guide loss was measured to be $2L_1 = 0.2$ decibel. The two reflection losses, L_2 and L_3, can be computed from the measured residual standing-wave ratios, η_2 and η_3, in the two arms, under the assumption that the whole reflected power is lost. This can be safely assumed, as the voltage-standing-wave ratio was always kept well below $\eta = 1.5$, so that double-reflected power is negligible. Some often used values of the reflection loss,

$$L_r = 10 \log \frac{P^+}{P^+ - P^-} = 10 \log \frac{(\eta + 1)^2}{4\eta}, \tag{10}$$

are listed in Table IV.

Table IV—Reflection Loss versus Voltage-Standing-Wave-Ratio

Voltage-Standing-Wave Ratio, η	Reflection Loss, L_r
1.1	0.02 decibel
1.2	0.04
1.3	0.08
1.4	0.13
1.5	0.18
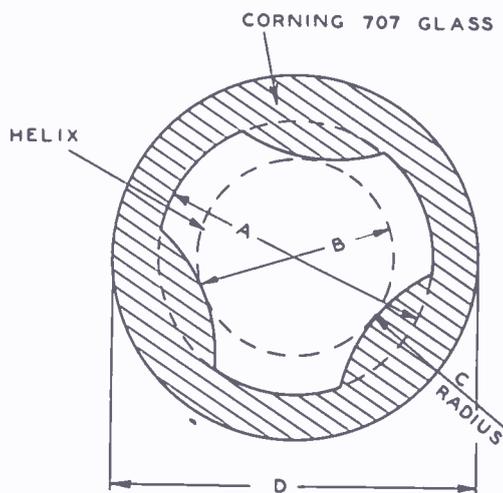
HELIX O.D	A	B	C	D
.110	.150	.112	.094	.250
.150	.200	.152	.125	.300
.200	.270	.202	.156	.360
.250	.335	.252	.193	.470

NOTE: DIMS. IN INCHES

Fig. 13—Design and dimensions of fluted 707 glass helix support.

For an assumed case of $\eta_2 = \eta_3 = 1.35$ and a helix length $z = 10$ inches, the influence of the reflection loss on the attenuation, 2α, is

$$\frac{1}{z} (L_2 + L_3) = 0.02 \text{ decibel per inch.} \tag{11}$$

ACCURACY OF MEASUREMENTS

The absolute accuracy, given by the systematic errors, is essentially dependent upon the calibrated attenuator of the signal generator. According to a comparison with a precision attenuator, we found that its absolute accuracy is well within the accuracy with which the
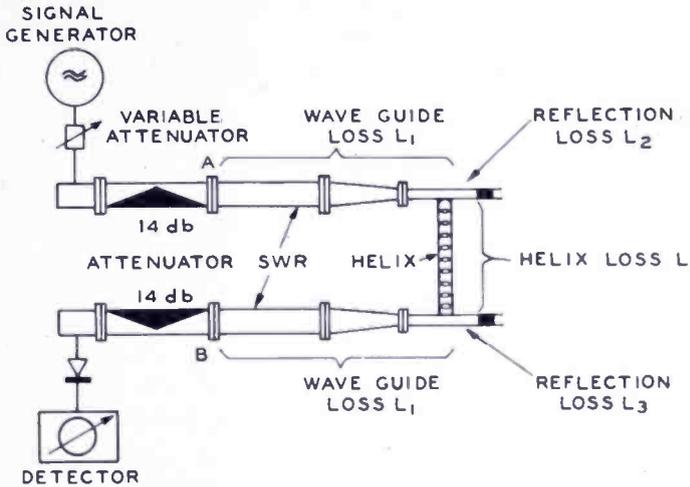
Fig. 14a—Test arrangement for measuring the attenuation of a helix.
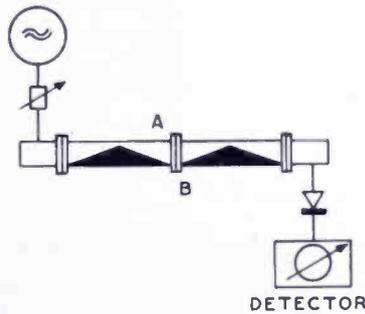

Fig. 14b—Test Arrangement for calibration.
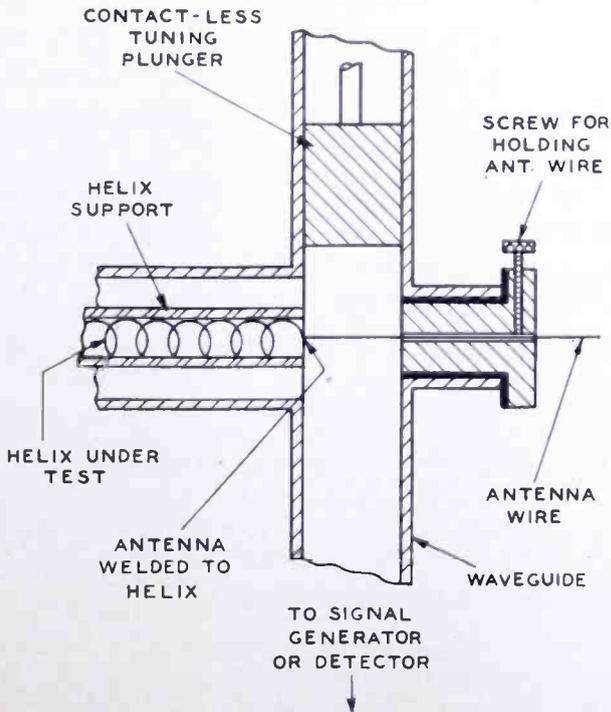
Fig. 15—Details of the wave-guide-to-helix transformer with adjustable antenna and tuning plunger.

insertion loss measurements could be repeated. The probable error evaluated from a series of repeated measurements was about

$$\Delta L = \pm \, 0.08 \ \text{decibel}. \tag{12}$$

This causes a probable error in the attenuation of a 10-inch-long helix of

$$\Delta \alpha = \pm \, 0.008 \ \text{decibel}. \tag{13}$$

Inhomogeneities in the helix can act as an additional cause of systematic errors, increasing the helix insertion loss by internal reflections along the helix. This effect is most serious at large ratios of d/p. Figure 12 shows how periodic variations in the helix pitch of less than $\pm \, 2.5$ per cent increase the attenuation at certain frequencies (see sample with 0.015-inch wire diameter). The effect was eliminated by improving the helix winding technique (see sample with 0.020-inch wire diameter).

Conclusions

Attenuation curves for dielectric-supported helices are presented covering the whole construction range useful for medium- and low-power traveling-wave tubes.

The helix attenuation increases linearly with the frequency and slightly more than linearly with the ratio of free-space to phase velocity. It has a very flat minimum at a wire-diameter-to-pitch ratio of $\frac{1}{3}$ and varies with the square root of the resistance coefficient of the metal which forms the helix surface.

Of the measured dielectric supports, 707 precision-bore glass tubing showed the highest loss. Quartz precision-bore tubing is better, and fluted 707 glass tubing causes the lowest loss, as it supports the helix in three points of the circumference only. This is a remarkable result, as 707 has a power factor, at 3000 megacycles, of twelve times that of quartz.

RCA TECHNICAL PAPERS†

Third Quarter, 1952

Any request for copies of papers listed herein should be
addressed to the publication to which credited."

"Maximum Coverage for VHF-UHF TV," F. W. Smith, *Electronics* (July) 1952

"New UHF-TV Antenna, Part 1—Construction and Performance Details of TFU-24B UHF Antenna," O. O. Fiet, *FM and Tele.* (July) 1952

"New UHF-TV Antenna, Part 2—TFU-24B Horizontal and Vertical Radiation Characteristics," O. O. Fiet, *FM and Tele.* (August) 1952

"A Note on the Design of Constant-Resistance Cathode-Ray Deflection Circuits," R. C. Webb, *RCA Review* (September) 1952

"Parallel-Tuned Circuit Periodically Switched to a Direct-Current Source," L. J. Giacoletto, *RCA Review* (September) 1952

"Plural Electron Scattering and Its Influence on Electron Diffraction Patterns," S. G. Ellis, *Phys. Rev.* (September) 1952

"Protecting Sensitive Current Meters," L. J. Giacoletto, *Electronics* (July) 1952

"Specimen Charging in the Electron Microscope and Some Observations on the Size of Polystyrene Latex Particles," S. G. Ellis, *Jour. Appl. Phys.* (July) 1952

"Survey of Transistor Development, Part I." B. N. Slade, *Rad. and Tele. News* (September) 1952

"A Time-Division Multiplex Terminal," O. E. Dow, *RCA Review* (September) 1952

"Tone-Burst Generator Checks A-F Transients." M. C. Kidd, *Electronics* (July) 1952

"A Transistor Curve Tracer," G. B. Herzog, R. D. Lohman, and J. Kurshan, *RCA Industry Service Laboratory Bulletin LB-882* (September 30) 1952

"Transistor Oscillators," E. A. Oser, R. O. Endres, and R. P. Moore, Jr., *RCA Review* (September) 1952

"Transistor Trigger Circuits," A. W. Lo, *RCA Industry Service Laboratory Bulletin LB-875* (August 11) 1952

"TV Engineering Requirements for FCC Applications," I. Newton, *Broadcast News* (July-August) 1952

"Two New Photomultipliers for Scintillation Counting," M. H. Greenblatt, M. W. Green, P. W. Davidson, and G. A. Morton, *Nucleonics* (August) 1952

"Ultraviolet Television Microscopy," V. K. Zworykin, L. E. Flory, and R. E. Shrader, *Electronics* (September) 1952

"Universal Design Curves for Tone-Control Circuits (Part I)," M. B. Knight, *Rad. and Tele. News* (July) 1952

"Universal Design Curves for Tone-Control Circuits (Part II)," M. B. Knight, *Rad. and Tele. News* (August) 1952

"Universal Design Curves for Tone-Control Circuits, (Part III)," M. B. Knight, *Rad. and Tele. News* (September) 1952

"Use of the Flying-Spot Scanner to Study Photosensitive Surfaces,". J. I. Pantchechnikoff, S. Lasof, J. Kurshan, and A. R. Moore, *Rev. Sci. Instr.* (September) 1952

"Video Test Signal Generator," H. Borkan, W. C. Morrison, and J. G. Reddeck, *Electronics* (September) 1952

"The Walkie-Pushie-Lookie Television Camera," J. E. Burrell, *Tele-Tech* (September) 1952

"WO-56—A 7-inch Oscilloscope for TV Servicing," M. J. Ackerman and R. D. Scheldorf, *RCA Rad. and Tele. Serv. News* (August-September) 1952

"The 3-Gun Shadow-Mask Color Kinescope," H. B. Law, *Elec. Eng.* (August) 1952

AUTHORS

GEORGE H. BROWN received the B.S. degree at the University of Wisconsin in 1930; the degree of M.S. in 1931; the Ph.D. degree in 1933; and his professional degree of E.E. in 1942. From 1930 until 1933 he was a Research Fellow in the Electrical Engineering Department at the University of Wisconsin, and from 1933 to 1942 he was in the Research Division of the RCA Manufacturing Company at Camden, N. J. Since 1942, he has been at RCA Laboratories Division, Princeton, N. J. Dr. Brown is a Member of Sigma Xi, the American Institute of Electrical Engineers, New York Academy of Sciences, and a Fellow of the Institute of Radio Engineers, and the American Institute of Electrical Engineers.

HENRY B. DEVORE received the B.S. degree in physics in 1926 and the M.S. degree in 1927 from Pennsylvania State College and the Ph.D. degree in 1934 from the California Institute of Technology. From 1927 to 1931, he was employed at the DuPont Experimental Station. He joined the research division of RCA Manufacturing Co. at Harrison, N. J. in 1934, transferring to RCA Laboratories Division at Princeton, N. J., in 1942, where he worked on the development of television pick-up tubes and on microwave antenna problems. From 1945 to 1947, he was associated with Remington Rand, Inc. Since 1947, he has been at RCA Laboratories Division, Princeton, N. J., engaged in fundamental research on solids. Dr. DeVore is a Member of Sigma Xi and the American Physical Society and a Senior Member of the Institute of Radio Engineers.

WILLIAM T. DYALL received the B. S. degree from Iowa Wesleyan College in 1943, and the M. S. degree in Physics from the Massachusetts Institute of Technology in 1948. In 1943 he was a teaching fellow and graduate student in Physics at the University of Wisconsin and at M.I.T. From 1943 to 1946, he was in the U. S. Naval Reserve on active duty as an Electronics Officer both afloat and ashore, and now holds the rank of Lieutenant, USNR. From 1946 to 1948, Mr. Dyall was a graduate student at M.I.T. and a part-time staff member of the M.I.T. Research Laboratory of Electronics. Since 1948, he has been employed by the Tube Department of RCA at Lancaster, Pa. He has been engaged in advanced development and product design engineering for cathode-ray tubes and storage tubes, and is now Supervising Engineer in the Tube Development Shop. Mr. Dyall is a Member of the American Physical Society, and a Senior Member of the Institute of Radio Engineers.

GLENN R. FADNER, JR. received the B. S. degree from Northwestern University in 1950. In 1944 and 1945, he was in the U. S. Army Air Corps. He received training in electrically operated remote-control turret systems. In 1950 he joined the Tube Department of RCA at Lancaster, Pa., where he was engaged in development of processing and fabrication methods for storage tubes, and product design and application engineering for phototubes. Mr. Fadner left RCA in October 1952 to join the Electrolux Corporation.

M. DUFFIELD HARSH received the degree of B. S. in Electrical Engineering in 1950 from Drexel Institute of Technology. Since 1950, he has been employed by the Tube Department of RCA at Lancaster, Pa. He has been engaged in power tube application engineering, and advanced development and product design engineering for storage tubes. Mr. Harsh is an Associate Member of the Institute of Radio Engineers, a Member of Tau Beta Pi, and a Member of Eta Kappa Nu.

LEON S. NERGAARD received the B.S. degree in Electrical Engineering from the University of Minnesota in 1927, the M.S. degree from Union College in 1930, and the Ph.D. degree from the University of Minnesota in 1935. From 1927 to 1930, he was in the research laboratory and vacuum-tube engineering department of the General Electric Company; from 1930 to 1933 a teaching assistant in the department of physics at the University of Minnesota; from 1933 to 1942 in the research and development laboratory of the RCA Manufacturing Company; and since 1942 at the RCA Laboratories Division in Princeton, N. J. He is a Member of Sigma Xi, the American Physical Society, the American Association for the Advancement of Science, and a Fellow of the Institute of Radio Engineers.

ARTHUR B. OLSON received the B. S. degree in Physics in 1949 from the University of Minnesota and the M. S. degree in 1950 from the same university. He joined RCA Laboratories Division in Princeton, N. J. in 1950, leaving in 1952 to join the Engineering Research Associates in St. Paul, Minn. as a Physicist. Mr. Olson is a Member of Phi Beta Kappa.

ROLF W. PETER (See RCA Review, Volume XIII, No. 3, September 1952, p. 421.

JOHN A. RUETZ received the B. S. and M. S. degrees in Electrical Engineering from the University of Michigan in 1949 and 1950, respectively. From 1944-1946 he served as an electronic technician in the U. S. Navy. In 1950, he joined the RCA Laboratories Division, Princeton, N. J., where he is now engaged in work on microwave amplifiers. Mr. Ruetz is a Member of the Institute of Radio Engineers.

OAKLEY M. WOODWARD (See *RCA Review*, Volume XIII, No. 2, June 1952, p. 262.